FUNCTIONAL LYMPHATIC CHANGES AND THE IMMUNE RESPONSE DURING LYMPHEDEMA DEVELOPMENT

A Dissertation
Presented to
The Academic Faculty

By

Matthew Cribb

In Partial Fulfillment
of the Requirements for the Degree
Doctor of Philosophy in the
George W. Woodruff School of Mechnical Engineering
Bioengineering

Georgia Institute of Technology

December 2021

FUNCTIONAL LYMPHATIC CHANGES AND THE IMMUNE RESPONSE DURING LYMPHEDEMA DEVELOPMENT

Thesis committee:

Dr. J. Brandon Dixon, Advisor
School of Mechanical Engineering
Georgia Institute of Technology

Dr. Rudolph Gleason
School of Mechanical Engineering
Georgia Institute of Technology

Dr. Krishnendu Roy
School of Biomedical Engineering
Georgia Institute of Technology

Dr. Mark Nicolls
School of Medicine
Stanford University

Dr. Susan Thomas
School of Mechanical Engineering
Georgia Institute of Technology

Date approved: December 1, 2021

ACKNOWLEDGMENTS

I would like to thank all of my family, especially my mother and father, for their support of my pursuit of a PhD. Unfortunately my father passed away in 2013 before I had even begun my PhD, but they instilled a love of knowledge, learning, and experimentation in me from a very young age. They are also both graduates of Georgia Tech, which influenced me in my choice of college and will now lead to my third degree from Georgia Tech. I would also like to thank my grandparents, my sister, my uncles and aunts, and my stepfather for all of their support as well.

I also have to thank my labmates over the past 6 years, as they have been both great coworkers and friends. Their support, willingness to help, and desire to discuss scientific problems encouraged and motivated me throughout my time in graduate school. In addition to their scientific assistance, our random discussions and hangouts outside of lab were a source of levity and fun.

My advisor, Dr. Brandon Dixon, has also been a great supporter of my scientific goals. His assistance and advice proved instrumental in earning an F31 fellowship through the NIH and publishing the multiple papers that make up this thesis. He was also very willing to support my travel to various conferences as I ended up attending 8 conferences during my time in the lab. I would also to thank all of the funding sources, collaborators, and core managers that have made this thesis possible.

TABLE OF CONTENTS

LIST OF FIGURES

LIST OF ACRONYMS

APCs antigen-presenting cells

DCs dendritic cells

dLN draining lymph node

dLNs draining lymph nodes

ECM extracellular matrix

FGF fibroblast growth factor

HA hyaluronic acid

iNOS inducible nitric oxide synthase

LECs lymphatic endothelial cells

LMCs lymphatic muscle cells

LN lymph node

LNs lymph nodes

LTB_4 Leukotriene B_4

MMP-2 matrix metalloproteinase 2

MMP-9 matrix metalloproteinase 9

MRI magnetic resonance imaging

mTOR mammalian target of rapamycin

NIR near-infrared

NP nanoparticle

NPs nanoparticles

OCT optical coherence tomography

PEG polyethylene glycol

S1P Sphingosine 1-phosphate

SSMs subcapsular sinus macrophages

TCR T-cell receptor

VEGFA vascular endothelial growth factor A

VEGFC vascular endothelial growth factor C

VEGFR3 vascular endothelial growth factor receptor 3

SUMMARY

The lymphatic system serves important roles in fluid balance and immune system regulation within the body. Through both passive and active transport of fluid, the lymphatic network transports interstitial fluid back into the circulatory system. When the lymphatic system fails, that excess fluid can no longer be properly transported back into the circulation. This leads to a disease called lymphedema, which manifests as swelling of distal limbs and normally occurs following injury to the lymphatic network. The mechanisms of lymphedema development are not completely understood, but the immune response is known to play an important role in lymphedema pathogenesis. The main goal of this thesis is to investigate both the functional response of the intact lymphatic vasculature and changes in leukocyte populations within dLNs during lymphedema progression.

In the first aim, we used near-infrared (NIR) imaging techniques to quantify changes in lymphatic function *in vivo* following induction of lymphedema in mice using a novel lymphedema model. We specifically investigated the effect of two potential therapeutic mechanisms, antagonism of LTB_4 production and deletion of epsin, on lymphatic function following lymphedema surgery. Further *in vivo* and *ex vivo* analysis was performed to elucidate potential mechanisms regulating the effect of LTB_4 on lymphatic contractile function. In the second aim, we used flow cytometry to investigate changes in leukocyte populations within dLNs during acute lymphedema progression. Our novel lymphedema model leaves a pair of intact collecting lymphatic vessels on one side of the mouse tail while other tail lymphatics are ligated, allowing for analysis of the immune response within dLNs experiencing differences in drainage. Further analysis using a nanoparticle delivery system was used to quantify differences in particle uptake between dLNs as lymphedema progressed. The effect of LTB_4 antagonism on the immune response was also elucidated. Overall, this work furthers understanding of the mechanisms driving lymphedema pathogenesis, by combining comprehensive analysis of changes in lymphatic contractile function *in vivo* and

ex vivo with investigation of changes in the immune response within dLNs.

CHAPTER 1
INTRODUCTION AND BACKGROUND

1.1 General Background

1.1.1 Lymphatic System

The lymphatic system is an extensive system of vessels that transports fluid from interstitial spaces throughout the body back to the circulatory system. It serves important functions in maintenance of fluid balance within tissues, regulation of immune system function, and lipid absorption and transport. A hierarchy of vessels makes up the lymphatic system. Blind-ended initial lymphatic capillaries respond to interstitial pressure changes and take in fluid from interstitial spaces. This fluid, now lymph, then travels through pre-collectors, which are characterized by sparse basement membrane and lymphatic muscle coverage. Finally the collecting lymphatic vessels, which have a basement membrane and complete lymphatic muscle coverage, intrinsically contract to transport lymph against a hydrostatic pressure gradient back through the thoracic duct into the circulatory system. This recycling of extravasated fluid from blood capillaries along with other interstitial proteins through lymphatics maintains fluid homeostasis in the extremities.

Lymphatics serve essential roles in almost all organs within the body. Recent studies have surprisingly shown the presence of a meningeal lymphatic system within the brain which importantly functions to remove excess cerebrospinal fluid and also transports immune cells within the brain [1–5]. Another report has revealed the important role that lymphatic endothelial cells (LECs) have in guiding and promoting heart development and repair [6]. These studies have shown the ubiquitous importance of lymphatics in healthy organ and tissue function.

Lymphatics play an important role in the transport of immune cells and regulation of

immune responses. Lymph nodes, which stage immune responses and are home to a variety of immune cells, form along the lymphatic system and appear throughout the body. Leukocytes within the lymph nodes, mainly T and B cells, are exposed to lymph draining from the interstitium, which may carry antigens or migrating antigen-presenting cells (APCs) that initiate a response. APCs may include macrophages or dendritic cells (DCs) which take up antigen at sites of injury or inflammation, activate in response to inflammatory signals, and migrate to nearby dLNs. The T cells or B cells, present in predefined zones within the lymph node structure, may be activated by APCs and begin to proliferate, mature, and produce antibodies.

Both during development and in the context of injury or inflammation, lymphatics grow and develop through a process called lymphangiogenesis. The most important growth factor in lymphangiogenesis, vascular endothelial growth factor C (VEGFC), binds to vascular endothelial growth factor receptor 3 (VEGFR3) and initiates growth and migration of LECs [7–11]. As lymphatics respond to VEGFC stimulation, various proteinases such as matrix metalloproteinase 2 (MMP-2) and matrix metalloproteinase 9 (MMP-9) are produced to disrupt the extracellular matrix and allow for expansion of the existing lymphatics [12–14]. Other growth factors including vascular endothelial growth factor A (VEGFA) and fibroblast growth factor (FGF) have also been shown to mediate lymphangiogenesis in various contexts [15, 16].

In vitro methods have been used extensively to characterize the mechanisms driving lymphangiogenesis both in development and following injury [17]. Tisse culture of LECs has revealed various mechanisms driving lymphangiogenesis, including detailed analysis of the VEGFC-VEGFR3 axis along with the lymphangiogenic potential of various inflammatory cytokines and proteins. These studies have allowed for isolated analysis of the response of LECs to various factors, but are unable to replicate the extracellular environment along with other cells (such as lymphatic muscle cells (LMCs)) which influence lymphatic growth and function. Matrigel has been used as a substrate for tissue culture of LECs to

mimic the extracellular matrix network, but it lacks customization and has limited potential for therapeutic applications[18–20]. Multiple bioengineered scaffolds, including hydrogels developed from polyethylene glycol (PEG), hyaluronic acid (HA), and alginate, have been developed to improve control over the mechanical properties of the scaffold and to potentially serve as scaffolds for therapeutic lymphangiogenesis [21–23]. A recent study has also shown the potential of PEG hydrogels to encapsulate excised lymphatic collecting vessels (which include LECs, LMCs, and some extracellular tissue) and support lymphangiogenesis from these vessels [24].

Multiple methods have been used to visualize and quantify lymphatic function *in vivo*, including lymphoscintigraphy, lymphangiography, magnetic resonance imaging (MRI), optical coherence tomography (OCT), and fluorescent tracers [25–29]. The choice of imaging method depends on the temporal and spatial resolution needed for a particular experiment. Lymphoscintigraphy, lymphangiography, MRI, and OCT provide ample spatial information regarding lymphatic uptake and function while sacrificing temporal resolution. The use of fluorescent tracers allows for imaging at high temporal resolution but most wavelengths of visible light are unable to penetrate through skin and visualize lymphatics with sufficient spatial resolution. Using tracers that fluoresce at NIR wavelengths allows for sufficient depth penetration through tissue to visualize superficial lymphatics. NIR imaging has thus been used extensively to visualize lymphatic pumping *in vivo*, allowing for real-time analysis of lymphatic contractile function [30–33].

1.1.2 Lymphatics and the Immune System

Lymphatic vessels serve as an important route of transport for immune cells migrating from various tissues to dLNs and eventually to the blood circulation. Afferent lymphatic vessels transport lymph and immune cells from tissue to LNs while efferent lymphatics take lymph exiting from the LNs through the thoracic duct and back into the circulation. Most leukocytes, including T and B cells, DCs, neutrophils, monocytes, and macrophages,

are trafficked through lymphatics either naively or in inflammatory states. One of the most important proteins regulating this migration is CCR7, which is highly expressed on many leukocyte subsets and binds to its ligand CCL21 which is expressed on LECs [34]. Multiple studies have shown that CCR7 deletion results in a lack of migration of leukocytes to dLNs and impaired immune responses [35, 36]. Sphingosine 1-phosphate (S1P) has also been shown to regulate T cell migration into lymphatics in tissue, revealing the complex mechanisms driving leukocyte migration to dLNs [37].

Intravital imaging has revealed that T cells crawl along initial lymphatics at slow velocities after entering the lymphatic network and then increase velocity as they enter the bulk lymph flow within collecting lymphatics [38]. Interestingly, DCs periodically interact with T cells within lymphatics, primarily in the initial capillaries where T cell movement is slow. This interaction involves antigen presentation from DCs to T cells and activation of T cells and the length of this interaction may depend on antigen availability [39]. These studies have shown that the lymphatic network itself can host interactions between immune cells in a similar fashion to immune cell activation normally observed within LNs.

LECs have also been shown to have many roles in archiving and presenting antigen to lymphocytes [40–44]. LECs store antigen following infection which is then uptaken by DCs and presented to T cells [42]. Additionally, LECs can directly present antigen to CD8+ T cells via cross-presentation on MHC-I molecules, initiating a memory T cell response which helps to ward off future infection [40]. Within the lymph node, LECs also maintain subcapsular sinus macrophages (SSMs) through production of CSF-1, assisting the capability of these cells to respond to exogenous antigen and initiate immune responses [45]. This direct influence on the immune response via LEC interaction with various leukocytes shows the important role that lymphatics play in modulating the immune system.

The lymphatic network within the lymph node (LN) is made up of multiple different LEC subtypes which each serve varied functions within the structure of the LN. A recent study by Takeda et al. identified six unique LEC subsets which correspond to certain re-

gions within the LN, such as the subcapsular and medullary sinuses [46]. These different subtypes also have different functions, as medullary sinus LECs were specifically shown to mediate neturophil adhesion via CD209. The variety of LECs within the LNs suggests that the lymphatic network's mediation of the immune response is complex and multi-varied [47].

1.1.3 Lymphedema

Lymphedema is a debilitating disease which occurs due to lymphatic failure. Primary lymphedema occurs due to genetic mutations which result in the development of non-functional lymphatics, while secondary lymphedema occurs following injury to the lymphatic system, such as lymph node removal during breast cancer surgery or blockage of lymphatic flow via parasitic worms that cause lymphatic filariasis [48, 49]. Lymphedema is characterized by extensive swelling of the affected limb, dermal thickening, adipose deposition, tissue fibrosis, and susceptibility to infection. The progressive worsening of these symptoms can lead to great discomfort and difficulty in regaining normal use of the affected limb [50]. In developed countries such as the United States breast cancer-related lymphedema, which occurs following damage to the lymphatic system through lymph node removal, radiation, and chemotherapy, is the most common form of secondary lymphedema and affects roughly 20% of breast cancer survivors [50–52].

Primary lymphedema is often driven by mutations of genes controlling lymphatic development and growth (such as VEGFR3, SOX18, and FOXC2) [53]. VEGFC-VEGFR3 signaling activates both the RAS\MAPK and the PI3K\AKT signaling pathways, and these mutations can lead to lymphatic insufficiency (lymphedema) or uncontrollable growth of lymphatic tissue (lymphatic malformations). Rapamycin (sirolimus) is an inhibitor of mammalian target of rapamycin (mTOR) (signaling molecule downstream of PI3K) and has been used clinically with some success for the treatment of lymphatic malformations [54]. The success of rapamycin indicates that pharmacotherapeutic agents have potential to

improve outcomes in lymphatic diseases, possibly even in secondary lymphedema where the causative mechanism is not clear.

The pathogenesis of lymphedema is incompletely understood, but advancements have been made in studying the response of the lymphatic network following injury. It is well known that lymphangiogenesis occurs following lymphatic injury, as VEGFC secreted by both immune cells and stromal cells induces lymphatic growth and proliferation [55–58]. However, these new lymphatic branches are often dysfunctional and leaky in the context of lymphedema, exacerbating the leakage of fluid out of the lymphatics into the interstitium [12, 59, 60]. Multiple studies have attempted to use VEGFC therapy to induce lymphangiogenesis in lymphedema in order to improve the drainage capability of the injured lymphatic network [61–65]. These studies have shown some success in reducing swelling, but this form of therapy also increases growth of dysfunctional lymphatics which can reduce the therapeutic potential of VEGFC. A recent study has implicated PTEN, a downstream inhibitor of VEGFC signaling, as a potential target to increase lymphangiogenesis without inducing off-target inflammation-induced effects and while improving the junctional stability of the growing lymphatic network [66].

The Immune Response in Wound Healing

The immune response during wound healing has been extensively studied, with particular focus on elucidating the multiple mechanisms through which immune cells regulate the tissue microenvironment during healing. The wound healing process normally consists of hemostasis, inflammation, proliferation, and remodeling [67]. Neutrophils are the first responders to the wound, responding to DAMPs (damage-associated molecular patterns) and initiating the immune response. Macrophages are recruited by chemokines released by neutrophils, and engulf cell debris and apoptotic neutrophils [68]. Macrophages have been classically classified as either M1 (pro-inflammatory) or M2 (anti-inflammatory) subtypes. However, more recent work has found that macrophages often express diverse func-

tions that are not fully encompassed by either classification [68, 69]. M1 macrophages are known to release pro-inflammatory stimuli, such as cytokines (IL-1 and TNF-α) along with growth factors (VEGFA and VEGFC). These macrophages aid in activating the adaptive immune response while additionally promoting angiogenesis and lymphangiogenesis. M2 macrophages secrete cytokines such as IL-4 and IL-10, which promote resolution of the immune response and stabilization of the epithelium and blood and lymphatic networks. Macrophages also interact with epithelial cells and fibroblasts at the wound to promote reepithelialization and skin repair [69]. Monocytes play an important role in the wound healing response, differentiating to macrophages and DCs at the wound site. DCs capture antigen at the site of the wound and migrate back to the dLNs, presenting antigen to T cells within the dLNs and activating the adaptive immune response. These initial responders of the innate immune system drive many changes in the extracellular matrix (ECM) and wound microenvironment that assist in the process of healing.

T cells are also known to play a role in the wound healing process. A particularly important subset of T cells are $\gamma\delta$ resident dendritic epidermal T cells, which reside in the epidermis and respond quickly following a wound [70]. The T-cell receptor (TCR) diversity of $\gamma\delta$ T cells is particularly limited, as these resident epidermal T cells all express the same TCR. This homogeneity allows these T cells to uniformly respond to damage signals released by keratinocytes following a wound [70]. Following activation, these cells produce growth factors and TNF-α which help accelerate wound closure and reepithelialization [70]. In addition to these skin-resident T cells, regulatory T cells activated in dLNs and recruited to the wound site also help regeneration and repair during healing [71]. Regulatory T cells importantly modulate the function of macrophages and neutrophils, preventing excess inflammation and inducing secretion of anti-inflammatory cytokines and stabilizing growth factors [71]. A study by Wang et al showed that the presence of CD4+ T cells at the wound helped to reduce scarring and promote wound healing [72]. CD8+ cytotoxic T cells alone did not significantly improve healing, however some studies have shown that CD4+ T

cells can also have cytotoxic effector function, revealing the diversity of T cell responses in inflammation [72, 73]. Another study revealed that CD4+ T cells improve healing following myocardial infarction, indicating the broad importance of T cells in the wound healing immune response [74]. Many aspects of the complicated interplay between leukocytes and the wound microenvironment during healing have been elucidated through various studies, however recent improvements in transcriptomics and sequencing have revealed increased complexity even within various leukocyte populations.

The Immune Response in Lymphedema

Recent research has highlighted the role the immune response plays in driving many aspects of lymphedema pathology. Various studies have shown that immune cells such as macrophages, dendritic cells, and T cells infiltrate lymphedematous skin, both in human samples and a variety of animal lymphedema models [59, 75–79]. Macrophages and T cells specifically have been shown to produce enzymes (inducible nitric oxide synthase (iNOS)), growth factors (VEGFC) and cytokines (TNF-α, IL-4, IL-13) which affect lymphatic function and regulate lymphangiogenesis [59, 60, 75, 76, 80]. CD4+ T cells have been shown to play a major role in lymphedema pathogenesis through regulation of VEGFC secretion by macrophages, activation of DCs at sites of lymphatic injury, and fibrogenesis [75–77].

T Cells

T cells, specifically CD4+ T helper cells, have been shown to regulate lymphedema pathogenesis through production of cytokines that influence lymphatic function and fibrogenesis. Avraham et al showed that lymphedematous tissue is characterized by both Th1 (CD4+ IFN-γ+) and Th2 (CD4+ IL-13+ IL-4+) responses, and that knockout of CD4+ T cells in a mouse model reduced lymphedema and accompanying fibrosis [75]. Interestingly, depletion of CD8+ cytotoxic T cells did not result in reduced lymphedema, suggesting that mechanisms driving lymphedema development are specific to the action of CD4+ T helper

cells [77]. Depletion of CD4+ T cells drastically reduced fibrosis as quantified via histological analysis of Scar index, type I collagen, and the collagen I/III ratio [77].

Interestingly, regulatory T cells (Tregs) (CD4+ CD25+ FoxP3+) are also increased in lymphedematous tissue but depletion of these cells worsens the disease [77, 81]. In fact, depletion of Tregs resulted in greatly increased inflammatory cytokine expression, including IFN-γ, IL-4, IL-13, TGFb1, and TNF-α [81]. Increasing Treg populations through both IL-2 antibody mediated expansion and therapeutic transfer reversed the characteristics of lymphedema, suggesting that anti-inflammatory approaches may have utility as potential treatments for lymphedema [81]. A study by Nores et al has extended these results by showing that Tregs drive abnormal adaptive immune responses following lymphatic injury, and deletion of FoxP3+ Tregs can reverse some of these impaired responses [82].

B Cells

Few studies have investigated B cells and humoral immunity in the context of lymphedema development. Thomas et al showed that humoral immunity is impaired in a genetic mouse model where dermal lymphatics are completely ablated [83]. The lack of drainage to dLNs resulted in reduced B cell responses to immunization, while T cell responses were delayed but not significantly smaller [83]. The previously mentioned study by Nores et al investigating the immunosuppressive effects of Tregs also showed that Tregs modulated antibody production following lymphatic injury. Deletion of FoxP3 was sufficient to restore antibody production to normal levels, indicating the interactions that various leukocyte populations have during lymphedema progression [82]. Zampell et al showed that B cells are not significantly increased in lymphedematous skin, so it is likely that most B cell functions are regulated within dLNs following lymphatic injury [77]. Further study is needed to better understand the response of B cells within dLNs during lymphedema development and functional changes that may occur within the B cell population.

Macrophages and Monocytes

Macrophages are known to significantly regulate inflammation via secretion of various cytokines and proteins, including VEGFC, TNF-α, IL-1, IL-6, IL-8, and IL-12 [59, 84–87]. During lymphedema development, macrophages migrate to the site of lymphatic injury and begin to produce these molecules which drive changes in lymphatic morphology, function, and fibrosis. Ogata et al showed that macrophages significantly upregulate VEGFC following lymphatic blockage, and this increase in VEGFC production results in lymphangiogenesis of leaky, nonfunctional lymphatic vessels [59]. Interestingly, their results also revealed that CD4+ T cells, mainly Th1 and Th17 subtypes, modulated VEGFC secretion by macrophages via production of IFN-γ and IL-17 [59]. Another study showed that macrophages in lymphedematous tissue are mainly anti-inflammatory M2 macrophages, and depletion of these macrophages using a CD11b-DTR genetic mouse model actually increased fibrosis and swelling [78]. Other reports have also shown the prevalance of M2 macrophages within lymphedematous tissue [79]. The importance of macrophages in driving tissue-level changes during inflammation and following lymphatic injury are well established, however the function of macrophages within the dLNs during lymphedema progression is not fully understood. Given the function of LN macrophages during viral infection, it is possible that similar mechanisms occur during the inflammation characterizing lymphedema progression [88].

Similarly to macrophages, monocytes have also been shown to increase in lymphedematous tissue as swelling and fibrosis develop [77, 79]. Differentiation of monocytes to macrophages or DCs within tissues is one important mechanism of monocyte function which likely affects the immune response in lymphedema [89–91]. Recent research has elucidated a role for long-lived monocytes in trafficking to LNs and presenting antigen to initiate adaptive immunity [92, 93]. Monocytes may initiate these same responses during lymphedema development, but these mechanisms have not been fully investigated.

Dendritic Cells

Multiple studies have shown that dendritic cells are increased in lymphedematous tissue [76, 77]. Nores et al showed that DCs are activated at sites of lymphatic injury, migrate to dLNs and activate T cell responses (primarily CD4+ helper T cells) which then exit the LNs and migrate to tissue where they initiate fibrogenesis and excessive lymphangiogenesis [76]. Several studies have showed that loss of dermal lymphatics decreases DC migration to dLNs, suggesting that intact lymphatic pathways are necessary for mobilization of DCs to LNs along with subsequent CD4+ T cell activation [83, 94]. Given that significant swelling and fibrosis driven by CD4+ T cells is apparent in lymphedema models where all lymphatic pathways are ablated, it is likely that multiple pathways for T cell activation by DCs are involved in the progression of lymphedema.

Neutrophils

Neutrophils are the initial responders to inflammatory stimuli, clearing foreign particles and antigen at the frontline of the innate immune system. In lymphedema, multiple studies have shown increased neutrophil accumulation at sites of lymphatic injury [77, 79]. Multiple reports have also investigated neutrophils within the LNs in the context of inflammation [95–98]. Hampton et al report that neutrophils migrate to dLNs and initiate lymphocyte proliferation following bacterial infection [99]. Interestingly, a study by Castell et al reveals that neutrophils modulate CD4+ T cell activation following inflammation [100]. Other work has shown that neutrophils reduce humoral immunity in LNs following bacterial infection [98]. The mechanisms through which neutrophils influence the immune response during lymphedema progression are not well understood, but the importance of neutrophil interactions with lymphocytes and subsequent modulation of adaptive immunity suggest that these mechanisms may also be involved in lymphedema pathology.

Anti-Inflammatory Therapy for Lymphedema Treatment

Additionally, various anti-inflammatory therapies have shown promise in treating lymphedema. Tacrolimus, an immunosuppressive drug which inhibits calcineurin and downstream IL-2 production, has been used as a topical treatment for lymphedema in mice and reduced tail swelling, immune infiltration, and improved lymphatic function following lymphedema induction [101]. FTY720, a sphingosine-1-phosphate (S1P) receptor modulator which prevents lymphocyte egress from lymph nodes, has also been shown to treat lymphedema in mice [76]. Adoptive transfer of regulatory T cells also reduced swelling in a mouse lymphedema model [81]. These studies show that targeting the inflammatory mechanisms of lymphedema development is a promising strategy for the development of lymphedema therapies.

Lymphatic Functional Response During Lymphedema

Other studies have investigated the functional response of collecting lymphatic vessels during lymphedema. Modi et al showed that lymphatic pumping pressure, a measure of the ability of a collecting lymphatic vessel chain to pump against an applied pressure, is reduced in lymphedema patients [26]. Unno et al also found that patients with leg lymphedema exhibited lower pumping pressure compared to healthy patients [102]. In a sheep model of lymphatic ligation which did not result in tissue swelling, a vessel left intact remodeled and pumped with increased contractile frequency and force generation in the weeks following ligation of a parallel collecting vessel[103]. These studies have begun to make the connection between changes in lymphatic function induced by lymphatic injury.

Interestingly, changes in collecting lymphatic vessel morphology have been observed in both clinical lymphedema and animal models. Mihara et al showed that collecting lymphatic vessel morphology varied in patients with different stages of disease (from stage 0 to stage 3), with progressive sclerosis of collecting lymphatics observed in more severe lymphedema (stage 2 and 3) [104]. Another study by Ogata et al investigated how smooth

muscle cells surrounding lymphatic collecting vessels were affected during lymphedema, revealing thickening of the vessel wall and increased smooth muscle actin (SMA) expression within the vessel wall in lymphedema patients [105]. These experiments have shown that lymphedema development is characterized by remodeling of collecting lymphatic vessels, with severe lymphedema resulting in complete sclerosis and dysfunction.

Computational models of lymphatic pumping have also shaped our understanding of the response of lymphatic collecting vessels during lymphedema development. Caulk et al developed a model of lymphatic response to force using data from biaxial active and passive behavior of lymphatics [106]. This model was then coupled with a lumped parameter model describing lymphatic flow to begin to describe remodeling of collecting lymphatic vessels in the context of forces simulating the lymphedema microenvironment [107]. Razavi et al used a similar approach to describe the capacity of a chain of lymphangions to pump against an adverse pressure gradient, which was verified using *in vivo* measurements of lymphatic pumping pressure [108]. Other approaches have also been used to model lymphatic contraction and the interaction between the fluid within the collecting lymphatic vessel and the vessel itself [109]. These models have helped to expand understanding of the mechanisms driving loss of lymphatic contractile activity during lymphedema.

1.2 Specific Aims

1.2.1 Specific Aim 1: Investigating Lymphatic System Contractile Function During Lymphedema Development Using *in vivo* and *in vitro* Methodologies

Lymphedema is a disease characterized by lymphatic dysfunction, but the mechanisms leading to the dysfunction of the intact lymphatic vasculature following lymphatic injury are unclear. Pro-lymphangiogenic approaches are potential therapies for lymphedema, but the functional response of the lymphatic system following pro-lymphangiogenic therapy has been understudied. Given the necessity of active lymphatic contraction to properly drain lymph from the extremities, both the growth of new lymphatic vessels and the proper

function of the lymphatic network are needed to reverse the fluid buildup that occurs during lymphedema.

In this aim, we hypothesize that lymphatic contractile function of the intact lymphatic vasculature decreases as lymphedema progresses, and that this decrease in function correlates with an increase in swelling of the affected limb. Additionally, we hypothesize that two different pro-lymphangiogenic pathways (antagonism of LTB_4 production and inhibition of epsin function), also increase function in the intact lymphatic vasculature during lymphedema progression. We aim to measure these changes in function using *in vivo* NIR imaging, and *ex vivo* imaging of isolated contracting lymphatic collecting vessels.

1.2.2 Specific Aim 2: The Kinetics of Lymphatic Dysfunction and Leukocyte Expansion in the Draining Lymph Node in a Mouse Model of Lymphedema

The immune response has been heavily implicated in lymphedema development. Leukocytes, primarily T cells (both CD4+ helper T cells and CD25+ regulatory T cells) and macrophages, have been shown to promote fibrosis, produce inhibitory cytokines, and induce aberrant lymphangiogenesis. However, it is not well understood how immune cells respond in lymph nodes draining the site of lymphatic injury during lymphedema progression. Additionally, LTB_4 is known to act as a chemoattractant, but its role in modulating the immune response during lymphedema progression is not well characterized.

In this aim, we hypothesize that leukocytes will expand in dLNs following lymphedema induction. In our model, where we leave an intact lymphatic collecting vessel during surgery to induce lymphedema, we expect that the LN draining the intact lymphatic vessel (intact vessel dLN) will experience more leukocyte expansion than the non-draining LN (injured vessel dLN). Additionally, we expect that LTB_4 antagonism via bestatin will reduce the immune response in the intact vessel dLN, increase drainage to the intact vessel dLN, and decrease tail swelling following single vessel ligation surgery.

CHAPTER 2
INVESTIGATING LYMPHATIC SYSTEM CONTRACTILE FUNCTION DURING LYMPHEDEMA DEVELOPMENT USING *IN VIVO* AND *IN VITRO* METHODOLOGIES (AIM 1)

[1]

2.1 Overview

Lymphedema is a disease characterized by lymphatic failure, however it is unclear how lymphatic function changes in the intact lymphatic vasculature during lymphedema progression. Previous work has suggested that lymphatic function is lost during lymphedema progression [26, 102]. However, the mechanisms driving these changes in lymphatic function are not well understood. Using a novel lymphedema model which leaves a pair of intact collecting lymphatic vessels while inducing lymphedema progression via ligation of the rest of the lymphatic network of the mouse tail, we aim to better understand the progressive loss of lymphatic function. Additionally, we use this model to test the potential beneficial effects of previously described therapeutic pathways on lymphatic contractile function. We show that LTB_4 antagonism via bestatin and epsin inhibition via a genetic mouse model both improve lymphatic function during lymphedema progression. We then attempted to more directly show the mechanism through which LTB_4 may affect lymphatic function. *Ex vivo* and *in vivo* methods of measuring lymphatic function are used to directly test the effect of LTB_4 and 5-LO signaling on collecting lymphatic vessel contractile function. Our results suggest that the benefits of LTB_4 antagonsim on lymphatic function are likely not due to the direct effect of LTB_4 or 5-LO signaling metabolites on lymphatic function. This indicates that an indirect mechanism of LTB_4, potentially through its effect on

[1] Adapted from Weiler at al [110] and Tian et al [111]

immune cells, mediates its effect on lymphatic function. Our work shows that therapeutic pro-lymphangiogenic pathways may also be targeted to increase lymphatic function during lymphedema progression.

2.2 Motivation and Background

Lymphedema is a debilitating disease characterized by extensive swelling of the affected limb, tissue fibrosis, and increased susceptibility to infection [50]. Lymphedema can occur following injury to the lymphatic system (such as lymph node removal during breast cancer surgery), but only manifests in roughly 20% of breast cancer survivors and can present even up to 5-10 years following the initial surgery [50]. It is thought that lymphatic failure occurs gradually during lymphedema progression, with previous studies showing that lymphatic pumping capacity is lower in lymphedematous limbs compared to normal limbs [26, 102]. However, it is unclear how changes in mechanical forces and the inflammatory microenvironment affect lymphatic contractile transport during the progression of lymphedema.

A variety of animal models are currently used to simulate lymphedema, including lymph node removal, lymphatic ligation, and the commonly used mouse tail lymphedema model [76, 79, 103, 112]. In the mouse tail lymphedema model, all lymphatics surrounding the tail are ligated, including both the initial and collecting lymphatic vessel networks. This loss of lymphatic drainage capacity, induced by complete blockage of lymphatic flow, quickly results in acute swelling of the tail. One benefit of this model is the rapid swelling that occurs following the initial surgery, as other models such as lymph node removal result in minimal swelling. The swollen tail tissue also recapitulates many of the histological hallmarks of lymphedema, including dermal thickening and lymphatic hyperplasia [79]. However, this swelling naturally resolves 2-3 months following the surgery, showing that the full extent of clinical lymphedema is not captured by the model. Additionally, the complete loss of lymphatic drainage is not representative of clinical lymphedema, where

intact lymphatic pathways remain following initial damage to the lymphatic system (often through lymph node removal). A better lymphedema model is needed which retains the swelling response observed following complete lymphatic blockage, but retains intact lymphatic pathways.

In our work, we have developed a model we call the single vessel ligation lymphedema model, which involves ligating one pair of collecting vessels and the majority of initial lymphatics surrounding the tail, while leaving the other pair of collecting vessels intact. Using this model, we have shown that lymphatic contractile function in the intact collecting vessel decreases as lymphedema progresses [110]. This progressive loss of lymphatic function sheds light on the response of the intact lymphatic vessel network following lymph node removal which eventually leads to secondary lymphedema. Further questions remain, including how changes in function of the intact vessel relate to differences in swelling between individuals, and investigation of the mechanisms driving the observed change in lymphatic function. Our model also allows for measurement of changes in lymphatic function in the context of various potential treatments for lymphedema.

Lymphangiogenic therapy has been studied and tested extensively as a potential treatment for lymphedema [61–65]. Many of these studies have focused on the potential of VEGFC as a master regulator of lymphangiogenesis, and have attempted to directly target the VEGFC-VEGFR3 axis through direct injection of VEGFC protein, use of adenoviruses with VEGFC DNA, or VEGFC mRNA approaches. These methods which attempt to directly modulate VEGFC have seen some success, but challenges remain given potential off-target effects of exogenous VEGFC. Recent research has implicated two indirect pathways which affect lymphangiogenesis in the context of lymphedema. LTB_4, a metabolite of arachidonic acid, has been shown to be increased in lymphedematous skin and has a bimodal effect on lymphangiogenesis. At the high concentrations observed in lymphedema, LTB_4 is anti-lymphangiogenic while at lower concentrations it is pro-lymphangiogenic [111]. Epsins are proteins involved in degradation of ubiquinated cell surface proteins

[113–115]. Epsins have been shown to regulate endocytosis of ubiquinated EGF receptors and depleting epsins reduces tumor growth due to upregulation of VEGF signaling [116, 117]. Deletion of epsins has been shown to increase lymphangiogenesis in the context of diabetes and lymphedema through increased cell surface expression of VEGFR3 [118]. The lymphangiogenic mechanisms of these molecular pathways in the context of lymphedema have been investigated, but the effect of modulating these pathways on lymphatic contractile function has not been studied. Given the importance of both increasing lymphangiogenesis and function of the intact lymphatic vasculature in order to potentially treat lymphedema, further analysis of any functional changes induced by these mechanisms is needed.

This aim presents an investigation of lymphatic function in the context of lymphedema development, both through *in vivo* imaging of lymphatic function and *ex vivo* testing of isolated lymphatic vessel function. First, we report the relationship between lymphatic function and tail swelling in the single vessel ligation lymphedema model. We then describe how various potential therapeutic molecular mechanisms, specifically LTB_4 and epsins, modulate lymphatic function both in naive mice and during lymphedema progression. Our findings show that lymphatic function and swelling are correlated as lymphedema develops in our model. Additionally, we show that both antagonism of LTB_4 using the drug bestatin and deletion of epsins via a genetic mouse model improve lymphatic function as measured by NIR imaging following single vessel ligation surgery but not in naive mice. Further analysis of the effect of LTB_4 on lymphatic function, through exogenous application to isolated lymphatic vessels and upregulation of the 5-LO pathway *in vivo* using an adenovirus, suggest that an increase in 5-LO and LTB_4 alone is not sufficient to reduce lymphatic function.

2.3 Methods

2.3.1 Experimental Design

Bestatin treatment following double vessel ligation: NIR imaging was performed presurgery and at 24 days following surgery. Bestatin was injected intraperitoneally daily starting on day 3. Saline Control (n=4), Bestatin (n = 3). **Bestatin treatment in naive mice:** NIR imaging was performed prior to beginning injections and then at weeks 1, 2, 3, and 4 following initial imaging. Bestatin was injected intraperitoneally daily following initial imaging. Saline Control (n=4), Bestatin (n=4). **Bestatin treatment following single vessel ligation:** NIR imaging was performed presurgery and at weeks 1, 2, 4, and 6 following surgery. Bestatin was injected intraperitoneally daily starting on day 3. Saline Control (1W: n=11, 2W: n=11, 4W: n=7, 6W: n=7), Bestatin (1W: n=9, 2W: n=9, 4W: n=5, 6W: n=5). **Testing effect of exogenous LTB_4 on *ex vivo* lymphatic contractile function:** Collecting lymphatic vessels were isolated from mouse flanks and cannulated within isolated vessel chambers for testing. Varying concentrations of LTB_4 or vehicle control (ethanol) were added to the vessel bath and the functional contractile response of the vessel was recorded. LTB_4 (n=4), Ethanol (n=3). **Testing effect of lyopholized or evaporated LTB_4 on *ex vivo lymphatic contractile function*:** Ethanol was removed from LTB_4 solution through lyopholization or evaporation under argon prior to addition of the LTB_4 solution to the vessel bath. LTB_4 was resuspended in PBS. Lyopholized LTB_4 (n=3), Evaporated LTB_4 (n=5), PBS (n=4). ***In vivo* treatment with AdLOX5 or AdGFP adenoviruses:** AdLOX5 or AdGFP adenovirus was injected intradermally into the tail and sacral LNs were harvested 2-3 weeks following injection. AdGFP (n=8), AdALOX5 (n=4). NIR imaging was used to quantify contractile lymphatic function in mice injected with AdLOX5 or AdGFP adenoviruses. AdGFP (n=5), AdALOX5 (n=6). **NIR imaging following epsin deletion:** Mice were injected with tamoxifen intraperitoneally to induce deltion of epsin in LECs. NIR imaging was used to quantify lymphatic function prior to epsin deletion and at days

10 and 21 following deletion. Control (n=4), Epsin LEC-iDKO (n=4). **Single vessel ligation following epsin deletion:** NIR imaging was performed presurgery and at weeks 1, 2, 4, 6, 8, and 10 following surgery. Tamoxifen injection and epsin deletion occurred prior to surgery. Control (n=9), Epsin LEC-iDKO (n=13).

2.3.2 Immunohistochemistry

Tail sections were harvested at two weeks following lymphatic injury in the dominant vessel ligation group. Tail sections were also harvested at two weeks in mice that underwent double vessel ligation. Tissues were harvested distal and proximal to the site of injury. These tissues were fixed in 10% neutral-buffered formalin, embedded in paraffin, and 5 µm sections were sliced for immunohistochemical analysis. For immunofluorescent staining, sections were treated with sodium citrate in a 90 °C water bath for antigen retrieval. Non-specific binding was blocked with 20% goat serum, 1% bovine serum albumin (BSA) and 79% PBS for one hour at room temperature. Sections were then incubated overnight at 4 °C with a hamster monoclonal anti-podoplanin (1:100, ab11936) primary antibody from Abcam (Cambridge, MA). Sections were then incubated with a corresponding secondary antibody (1:200, A21110) from Thermo Fisher Scientific for four hours at room temperature. A Zeiss LSM 700 confocal microscope was used to image slides after staining, and analysis was performed on high-powered sections (20×) with at least 6 high-powered fields (hpf) per animal.

2.3.3 NIR functional imaging

NIR lymphatic imaging was performed according to previously published methods. Briefly, 10 µL of LI-COR IRDye 800CW PEG (LI-COR Biosciences, Nebraska, USA) was injected intradermally into the tip of the tail for fluorescence imaging (the fluorophore was reconstituted according to manufacturer instructions for lymphatic imaging). An injection volume of 10 µL was chosen based upon past success in rodent models, so as to not overload the

lymphatics with unnecessary fluid volume while at the same time providing enough tracer for sufficient detection. The injection was given at an entry angle of approximately 10 degrees to an approximate depth of 1 mm to specifically target the lymphatic vasculature. Care was taken to position the injection as close to the midline of the tail as possible to avoid favoring one collecting vessel over the other. Images were taken with a customized imaging system consisting of a Shutter Instruments Lambda LS Xenon arc lamp, an Olympus MVX-ZB10 microscope, a 769 nm bandpass excitation filter (49 nm full-width half maximum, FWHM), an 832 nm bandpass emission filter (45 nm FWHM), and an 801.5 nm longpass dichroic mirror. Images were acquired with a Photometrics Evolve Delta 512 EM-CCD. The field of view was centered on the mouse's tail 7 cm downstream (towards the base of the tail) from the injection site at the tip of tail. This location ensured that only the downstream collecting lymphatics would be visualized. The small volume of fluid injection and the use of NIR to enhance tissue penetration ensures that only fluorescence in the deeper collecting lymphatics is visible downstream of the injection site. The animals were imaged continuously from the time of injection until 20 minutes post-injection with a 50 ms exposure time and a frame rate of 10 fps. Analysis of NIR functional metrics was performed during the steady-state period ranging from 5–20 minutes after injection, as defined previously. NIR functional measurements included a combination of previously reported metrics and newly developed metrics for this model. Packet frequency, emptying rate, and pumping pressure were measured and recorded as previously published. To measure lymphatic pumping pressure, a pressure cuff was placed around the tail, 6 cm from the tip of the tail. The pressure was increased to 80 mmHg, held for 5 minutes, decreased down to 55 mmHg, and lowered to 0 mmHg in increments of 2.5 mmHg for 5 seconds at each pressure. Fluorescence intensity in the collecting vessel distal to the cuff was measured, and lymphatic pumping pressure was quantified as the pressure in the cuff when intensity was halfway between its minimum and maximum value as flow resumed past the cuff. Transport time was used to determine the identity of the dominant and nondominant

collector, but was not used during time-course analysis of lymphatic function. Packet velocity was also not used for functional analysis because the dynamics of mouse contractile function, especially in the diseased cases, prevented reliable velocity measurements.

2.3.4 Surgical Lymphedema Model

We used the single vessel ligation model of lymphedema developed in our lab where a pair of collecting vessels on one side of the mouse tail were left intact while the remaining dermal initial lymphatics and collecting vessels were ligated and cauterized [110]. Eight-week-old male and female C57Bl/6 mice (Charles River Laboratories, Wilmington, MA, USA) were used for this study according to procedures approved by the Georgia Institute of Technology IACUC Review Board (Protocol # A100293 approved on 6 March 2019). All animals were first anesthetized using inhaled isoflurane (5% induction, 2% maintenance). All animals received incisions 1.6 cm from the base of the animal spanning 80–90% of the circumference of the tail with particular care to standardize the incisions as much as possible. All incisions were cauterized to prevent bleeding and fluid leakage. After the surgical procedures, both collecting vessels were checked with NIR imaging to ensure they were either severed or remained intact as appropriate. Previously, our group characterized the lymphatic physiology of the tail as having a dominant and a nondominant collecting vessel [33]. All surgeries done in this study involved ligation and cauterization of the dominant collecting vessel.

2.3.5 Bestatin Treatment

Bestatin treatment started at three days after surgery, as a previous study showed that beneficial effects of bestatin treatment were dependent on starting the treatment at this time [111]. To make bestatin stock, bestatin (Cayman Chemical, Ann Arbor, MI, USA) was first dissolved in DMSO at a 4 mg/mL concentration. Aliquots of 100 µL of this solution were stored in -20 °C. Aliquots were diluted with 900 µL of sterile saline per aliquot prior to in-

jection. This bestatin solution was then administered through daily intraperitoneal injection at a concentration of 2 mg/kg. The control group received daily intraperitoneal injections of equivalent volumes of sterile saline without DMSO.

2.3.6 Isolated lymphatic vessel preparation

Mice were euthanized with CO2 gas and then flank lymphatic vessels were harvested. First, the skin was cut open along the midline of the ventral side of the mouse and pulled away from the flank to reveal the lymphatics under the skin. The fascia and adipose tissue was cut away to reveal the flank lymphatics running parallel to the flank artery. A roughly 0.5 cm section of the collecting lymphatic vessel was removed from the tissue and cleaned of remaining connective tissue. During the isolation, the area was kept moist with DPBS. The vessel was then cannulated onto micropipettes within a isolated vessel chamber (Living System Instrumentation, St Albans, VT; CH-1). Sutures were used to tie the vessel onto the pipettes while taking care not to twist the vessel. The vessel system was then filled with either PSS adjusted to a pH of 7.4 at 37°C or DMEM/F12 (ThermoFisher Scientific; 11039047).

2.3.7 *Ex vivo* experimental setup

A previously described *ex vivo* perfusion system was used to control the average transmural pressure of fluid within the isolated lymphatic vessel [119]. After the lymphatic vessel had been cannulated within an isolated vessel chamber, the chamber was connected to the perfusion system. Three-way valves connected to pressure transducers allowed for measurement of pressure within the system on either side of the vessel. For our protocol, a pressure step program was first used to acclimate the isolated vessel and allow it to begin contracting. Average transmural pressure was held at 1, 3, 5, and 7 cmH2O for 3 minutes at each pressure before returning to 3 cmH2O. Further analysis of lymphatic response to LTB_4 was performed at a consistent 3 cmH2O transmural pressure. Video of the contracting

lymphatic vessel was taken with a guppyPRO camera and a custom LabVIEW program was used for diameter tracing in real time. Baseline lymphatic contraction was taken for 15 minutes at 3 cmH2O and LTB_4 or vehicle control was then added to the bath in increasing concentrations (150 nM, 750 nM, and 1500 nM). Lymphatic contraction was then imaged again for 15 minutes at each concentration.

For lyopholization of ethanol from the LTB_4 solution, 50 µL of LTB_4 solution was frozen at -80°C and then placed in a Labconco Freezone Freeze Dry System overnight. Following lyopholization, the LTB_4 was reconstituted in PBS and added to the vessel bath. For evaporation of ethanol, 50 µL of LTB_4 solution was exposed to a stream of argon while evaporation of the ethanol occurred. The LTB_4 was then reconstituted in PBS and added to the vessel bath.

2.3.8 Adenovirus treatment *in vitro*

HVLECs were cultured on 6 well plates, with 1 mL of a 50 µg/mL collagen I solution in 0.1% acetic acid used to coat the well prior to seeding. EBM (with 20% FBS, 1% PSA, and 1% Glutamax) was used as media. One day after seeding, either GFP or ALOX5 adenovirus (Vector Biolabs) was added with fresh EBM at an MOI of 200 or 250. Cells were exposed to the virus for 1-4 days and media was then changed. After one week of culture, cells were either imaged for changes in GFP expression or harvested for RNA extraction for qPCR.

2.3.9 qPCR

RNA was extracted from culture HVLECs using the procedure outlined in the RNeasy Mini Kit Handbook (Qiagen). Following RNA extraction, reverse transcription was used to produce cDNA. The Applied Biosystems High Capacity Reverse Transcription kit (4368814, Thermo-Fisher Scientific) was used for reverse transcription. 13.2 µL of RNA from each sample was added to 2 µL of 10x RT Buffer, 0.8 µL of 25x dNTP, 2 µL of 10x RT Primer, 1 µL of RNase Inhibitor, and 1 µL of RT enzyme. An Applied Biosystems Thermal Cycler

was used to run the desired temperature sequence: 25°C (10 min), 37°C (120 min), 85°C (5 min), and 4°C hold. Following reverse transcription, the Applied Biosystems Step One Plus Real Time PCR System was used for qPCR of the cDNA.

2.3.10 Flow cytometry

Both the sacral LNs, which drain fluid from the tail, were harvested when mice were euthanized. The LNs were stored in a 1 mg/mL Collagenase D solution (Sigma-Aldrich, St. Louis, MO, USA) and incubated at 37 °C for 1 h for disassociation. We then pushed the LNs through a 70 µm cell strainer to create a single cell suspension. A CD16/32 antibody blocking solution (Tonbo Biosciences, San Diego, CA, USA) was added for 5 min on ice. After spinning down for 5 min at 350xg and decanting the liquid, Zombie Aqua live/dead solution (BioLegend, San Diego, CA, USA) was added at room temperature for 30 min. Following a wash step, multiple antibodies conjugated to fluorophores were added to the suspensions for 30 min on ice. The antibodies used were APC anti-mouse F4/80 (1:40), APC/Cyanine7 anti-mouse Ly6G (1:100), Brilliant Violet 421 anti-mouse/human CD11b (1:33), Brilliant Violet 605 anti-mouse CD3 (1:40), Brilliant Violet 711 anti-mouse CD64 (1:40), Brilliant Violet 785 anti-mouse CD19 (1:40), PE anti-mouse I-A/I-E (1:40), PE/Cy7 anti-mouse CD206 (MMR) (1:50), and PerCP anti-mouse CD11c (1:40) (Bio-Legend, San Diego, CA, USA). After labeling with antibodies, cells were fixed in a solution made up of 50% Fixation Buffer (BioLegend, San Diego, CA, USA) and 50% PBS for 20 minutes at room temperature. Cells were then suspended in Intracellular Staining Perm Wash Buffer (1X)(BioLegend, San Diego, CA, USA) and then stained with a Alexa Fluor 488 anti-mouse GFP antibody (1:20)(BioLegend, San Diego, CA, USA) for 20 minutes at room temperature. The stained cells were then stored in Cell Staining Buffer (BioLegend, San Diego, CA, USA) for analysis. A BD Fortessa Flow Cytometer was used to run the samples. UltraComp eBeads (Thermo Fisher Scientific, Waltham, MA, USA) were used for single-stain compensation controls. BD FACSDiva was used to record results and FlowJo

was used for all analysis of results.

2.3.11 Adenovirus treatment *in vivo*

Mice were injected intradermally at the tip of the tail with either 20 µL of GFP or ALOX5 adenovirus (Vector Biolabs) at a PFU of $1.2 * 10^9$. The AdGFP adenovirus was supplied at $1.2 * 10^{11}$ PFU/mL and 10 µL of this solution was mixed with 10 µL of sterile saline for each injection. The AdLOX5 adenovirus was supplied at $5.0 * 10^{10}$ PFU/mL and 20 µL of this solution was used for each injection. NIR imaging was performed 24 hrs prior to adenovirus injection for baseline function, and at days 4, 7, and 14 following injection. All adenovirus injections were performed in a fume hood and mice injected with adenovirus were housed and handled using ABSL-2 precautions.

2.3.12 Epsin LEC-iDKO mice

$Epn1^{fl/fl}/Epn2^{-/-}/Prox1-Cre-ER^{T2}$ (LEC-iDKO) mice were generated by crossing $Epn1^{fl/fl}/Epn2^{-/-}$ mice with $Prox1 - Cre - ER^{T2}$ mice. Adult LEC-iDKO mice on an epsin 2–null background were selectively ablated of epsin 1 in LECs by administering 4-hydroxytamoxifen at 8 to 10 weeks of age. Littermates without $Prox1 - Cre - ER^{T2}$ were used as controls. Genetic background was verified in all animals using PCR.

2.4 Results

2.4.1 Single vessel ligation lymphedema model mimics histological hallmarks of clinical lymphedema

Tail sections were harvested at two weeks following lymphatic injury in the dominant vessel ligation group. Tail sections were also harvested at two weeks in mice that underwent double vessel ligation. Sections were harvested distal and proximal to the site of injury. These sections were paraffin-embedded and sliced for immunohistochemical analysis. Immunohistochemistry (IHC) was used to stain for podoplanin, a lymphatic marker

(Figure 2.1A-D). Sections distal to the wound in the double vessel ligation group showed significantly increased lymphatic vessel area and perimeter compared to sections proximal to the wound in both the single and double vessel ligation groups (Figure 2.1E,F). However, sections distal to the wound in the double vessel ligation group showed no differences in lymphatic vessel area and perimeter compared to sections distal to the wound in the single vessel ligation group. These results show that the single vessel ligation lymphedema model mimics the histopathological response seen in clinical lymphedema, specifically lymphatic hyperplasia, at the timepoint of peak swelling.

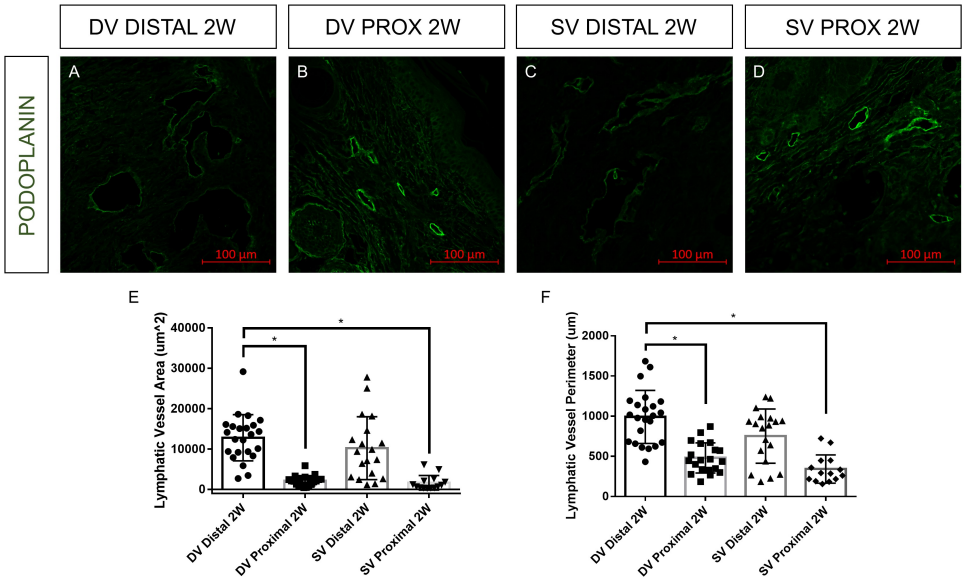

Figure 2.1: Single and double vessel lymphatic ligation result in lymphatic hyperplasia following surgery. (A–D) Mouse tail sections harvested distal and proximal to the site of lymphatic injury at two weeks following surgery were stained for podoplanin to determine lymphatic vessel area and perimeter. Lymphatic vessel area and perimeter in double vessel (DV) distal sections at two weeks were significantly increased compared to DV proximal sections at two weeks and single vessel (SV) proximal sections at two weeks. There was no significant difference between SV and DV distal sections at two weeks. (E,F) Quantification of lymphatic vessel area and perimeter from sections shown in (A–D) (n = 2 per group, at least 6 hpf per section).

2.4.2 Lymphatic dysfunction as measured by packet transport correlates with increased swelling under a variety of conditions

The surgical model of lymphedema proposed here results in a differential swelling response due to the collecting vessel that is left intact. In order to test whether the extent of swelling correlated with lymphatic function as measured by NIR fluorescence imaging, a heterogeneous group of mice were included in this study. This heterogeneity included variation in gender, strain (BALB/c and C57BL/6), and diet (chow and high fat). To compare mice with little swelling to those with significant swelling, two groups were categorized: mice with less than 20 percent increase in maximum circumference and those with more than 20 percent increase in maximum circumference. In humans, lymphedema is often characterized as a difference of 10 percent in volume between limbs; since this mouse model of lymphedema results in larger relative swelling, 20 percent was chosen as the threshold. As a point of reference, swelling in the double ligation model is typically around a 40–50 percent increase in max circumference at the peak of swelling. Mice that swelled greater than 20 percent at any timepoint over the course of the ten-week study showed significantly different swelling responses in the week after surgery compared to mice that never swelled greater than 20 percent (Figure 2.2A), suggesting that it is either the surgery itself or the immediate response to surgery that drives the severity of swelling in this animal model. This difference in swelling response was not significant in later weeks. There was a significant difference in lymphatic pumping pressure between the two swelling groups ($p = 0.0069$), suggesting differences in lymphatic function correlate with changes in swelling Figure 2.2B). Using the 20 percent swelling threshold, it was found that swelling negatively correlated with packet transport in mice with increased swelling ($n = 14$, $p = 0.045$), while there was no correlation between swelling and packet transport in mice with less swelling (Figure 2.3A). It was also found that swelling did not correlate with packet frequency in mice with increased swelling, while there was a negative correlation between swelling and frequency in mice with less swelling ($n = 4$, $p = 0.046$) (Figure 2.3B). Although it is diffi-

cult to say whether the swelling response leads to lymphatic dysfunction or these decreases in lymphatic function drive swelling, these results show that the extent of swelling severity is closely tied to changes in lymphatic function. The differences in the effect of swelling on packet frequency and packet transport show that changes in packet frequency do not necessarily reflect changes in overall transport capacity.

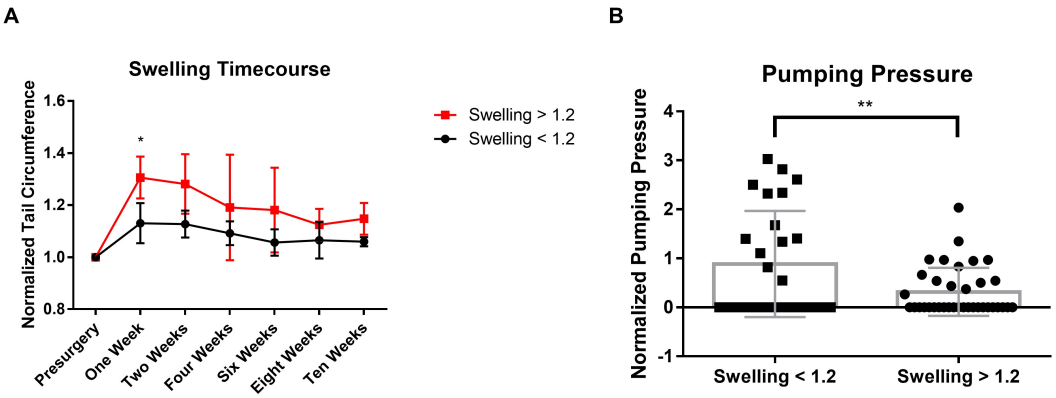

Figure 2.2: Lymphatic pumping dysfunction is maintained after significant swelling. (A) Plot shows the normalized tail circumference measured over ten weeks postsurgery between the two different swelling classifications. There is a significant difference in swelling between the two groups at one-week postsurgery (p = 0.0013). (B) Plot shows normalized pumping pressure compared between two different swelling classifications (less than or greater than 20% swelling). The normalized pumping pressure measured in mice with less than 20% swelling is shown to be significantly higher than in mice with greater than 20% swelling (p = 0.0069). Values are normalized to presurgery baseline. $^{*}(p < 0.05),^{**}(p < 0.01)$.

2.4.3 LTB_4 antagonism leads to improved tail anatomy and better lymphatic clearance

To evaluate the effects of LTB_4 antagonism on mouse tail lymphatic anatomy and function, we compared bestatin-treated groups with saline-treated lymphatic ablation surgery controls. We quantified lymphatic function using a novel technology integrating a NIR

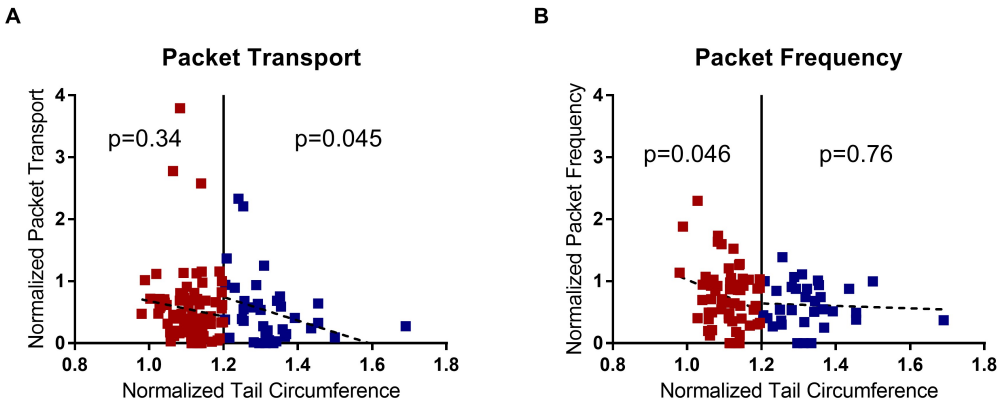

Figure 2.3: Lymphatic collecting vessel function negatively correlates with swelling. (A,B) Plots show the correlation between normalized tail circumference and normalized packet transport (A) or normalized packet frequency (B) for two different swelling classifications (less than or greater than 20% swelling). Values are normalized to presurgery baseline. Data where swelling is less than 20% is shown in red while data where swelling is greater than 20% is shown in blue. There is a significant negative correlation between normalized packet transport and tail circumference when swelling is greater than 20% (A: R^2 = 0.11, p = 0.045), and a significant negative correlation between normalized packet frequency and tail circumference when swelling is less than 20% (B: R^2 = 0.07, p = 0.046).

imaging system with a controlled pressure cuff to modulate lymph flow (11, 12). In the bestatin-treated mice, NIR identified lymph flow successfully passed beyond the surgical wound and filled the proximal lymphatic collectors, whereas minimal NIR transportation was seen in the saline-treated lymphedema animals (Figure 2.4A, B). Extravasation of Evans Blue dye proximal to the wound indicated increased permeability of the lymphatics in the saline-treated group, which was attenuated by bestatin therapy (Figure 2.4C). These results support the restorative effects of bestatin therapy after injury.

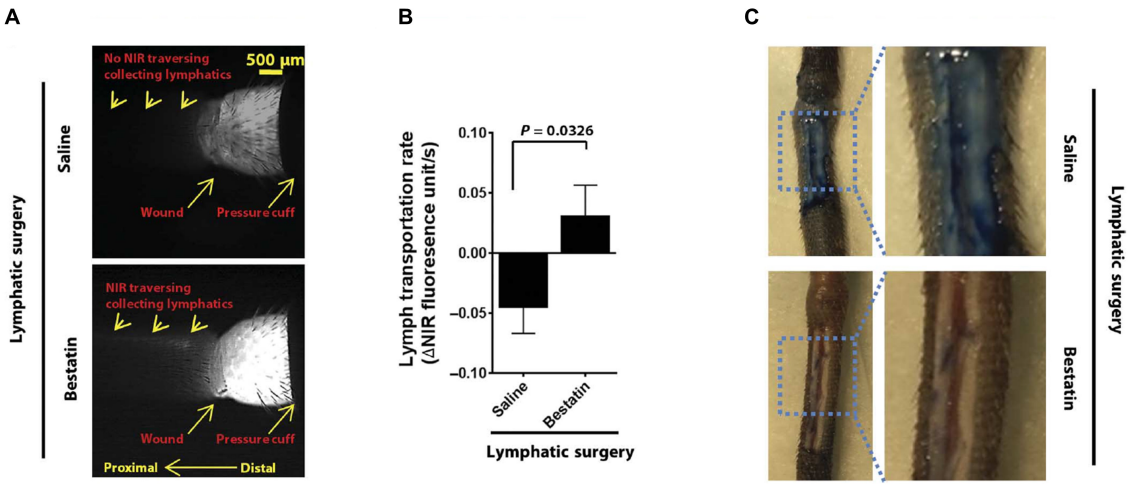

Figure 2.4: Bestatin treatment improves tail anatomy and restores lymphatic function. (A) Representative still photographs captured by a NIR imaging system with a controlled pressure cuff. The collecting lymphatic function was tracked by imaging the transportation of a NIR dye in the vessels. Collecting lymphatics and the surgical wound are marked. Direction of lymph flow from the distal to the proximal part of the mouse tail is indicated. Scale bar, 500 mm; n =3.(B) Trafficking ability of collecting lymphatics as quantified by the rate of NIR packet movement; n = 3; data are presented as means and SEM, Mann-Whitney test. (C) Representative images showing extravasation of Evans Blue dye from the lymphatics distal to the wound in the saline-treated mouse tail after lymphatic surgery; n = 3.

2.4.4 LTB_4 antagonism does not affect lymphatic contractile function in naive mice

Given the effects that LTB_4 antagonism via bestatin had on lymphatic function in the double vessel ligation model, we were interested in determining if LTB_4 antagonism affected lymphatic function in naive mice. Mice were injected with bestatin using the previously described methods and were treated daily for four weeks. Using NIR imaging to quantify lymphatic functional metrics, we found that lymphatic contractile frequency, amplitude, and transport were unchanged during bestatin treatment (Figure 2.5A-C). These results suggest that the beneficial effect of bestatin treatment on lymphatic function in the double vessel ligation model was likely due to the high levels of LTB_4 found in lymphedema.

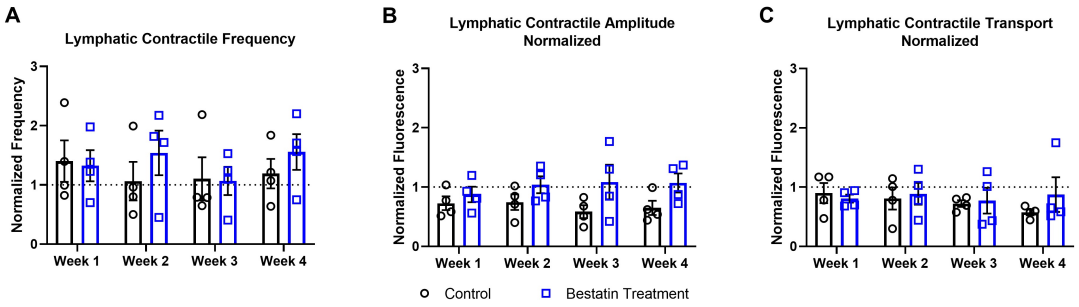

Figure 2.5: Bestatin treatment does not affect lymphatic pumping in naive mice. Plots show lymphatic functional metrics measured by NIR imaging during four weeks of daily bestatin treatment or saline control. These metrics includ (A) lymphatic contractile frequency, (B) lymphatic contractile amplitude normalized to intensity, and (C) lymphatic contractile transport normalized to intensity. Saline Control (n=4), Bestatin (n=4).

2.4.5 LTB_4 antagonism improves lymphatic contractile function following single vessel ligation

To determine how lymphatic pump function is altered due to bestatin treatment during lymphedema progression when a lymphatic outflow pathway is still intact, we used NIR imaging techniques that have been previously described [32, 33, 110, 120]. At 1W, 2W, 4W, and 6W following surgery to induce lymphedema, we injected a 20 kDa PEG molecule conjugated to an 800IR CW NHS ester dye (LI-COR Biotechnology, Lincoln, NE, USA)

intradermally into the mouse tail. Bestatin treatment started three days after surgery and continued daily until the 6W timepoint. As the active contractions from lymphatic pumping create intensity fluctuations, movement of these "packets" that are reflective of the vessel stroke volume can be quantified using live NIR imaging. In so doing, we found that lymphatic function as determined by measuring the lymphatic contractile transport of the tracer normalized to the presurgery baseline was significantly increased at 2W in bestatin-treated mice compared to the saline group (Figure 2.6A), an effect that was lost after 4W. Other metrics, including lymphatic contractile frequency, amplitude, and pumping pressure showed no significant change in bestatin-treated mice compared to the saline group (Figure 2.6B-D).

2.4.6 LTB_4 does not affect *ev xivo* pumping function of isolated lymphatic collecting vessels

Given the beneficial effects of LTB_4 antagonism on lymphatic contractile function *in vivo* in various lymphedema models, we were interested in determining if LTB_4 directly affected lymphatic contraction. To test this, we isolated lymphatic collecting vessels from the mouse flank and cannulated the vessels on 75 µm-100 µm diameter pipettes in a specialized vessel isolation chamber (Living System Instrumentation, St Albans, VT; CH-1). The chamber was then connected to a pressure control system that allowed for precise control of the fluid pressure within the isolated vessel. Baseline contractile function at a transmural pressure of 3 cmH2O was quantified via video captured at 10 frames per second. LTB_4 was then added exogenously to the vessel bath in increasing concentrations (150 nM, 750 nM, and 1500 nM) and video was captured for 15 minutes at each concentration. Equal volumes of ethanol were used as a vehicle control as LTB_4 was supplied in an ethanol solution. Compared to vehicle control, LTB_4 had no effect on frequency of contraction or fractional pump flow while ethanol significantly reduced contraction amplitude and ejection fraction compared to LTB_4 at the highest concentrations (Figure 2.7A-D), suggesting that LTB_4 may

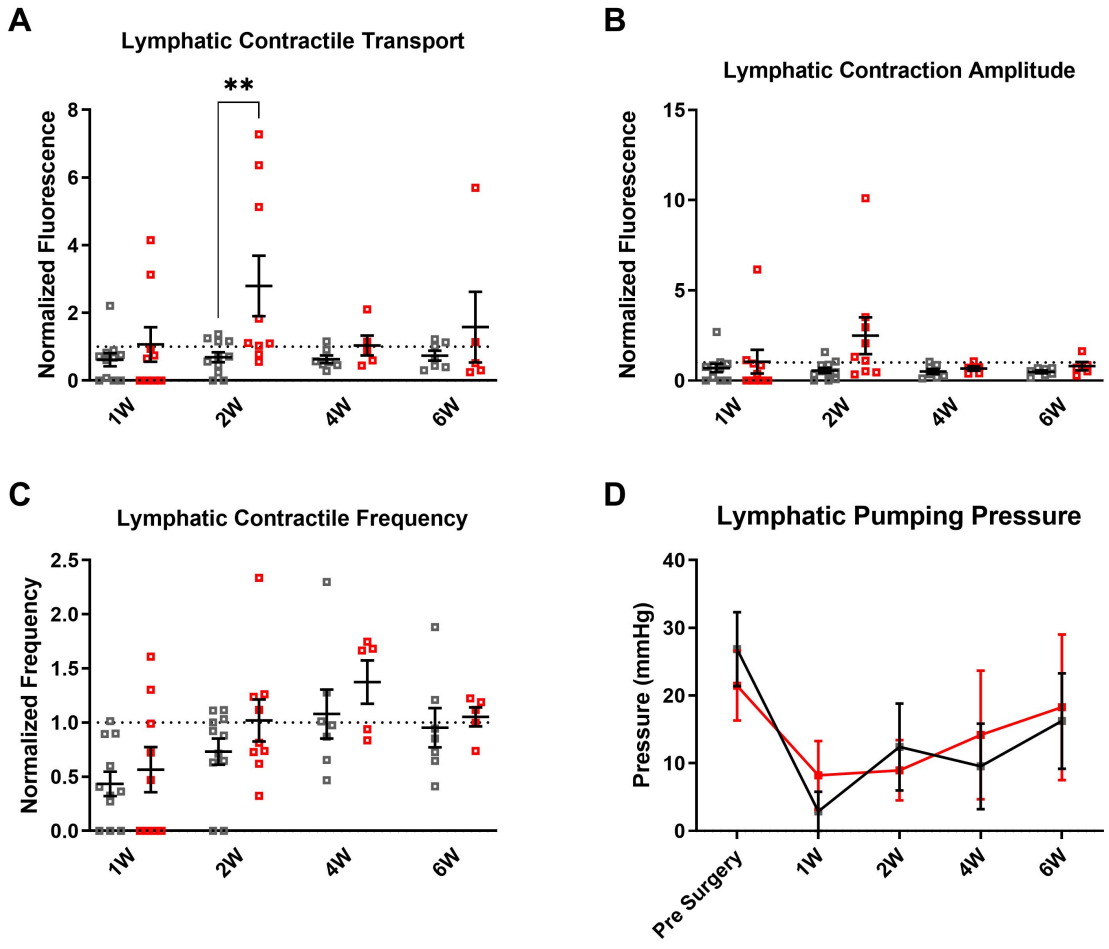

Figure 2.6: Bestatin treatment increases lymphatic contractile transport during lymphedema development. (A) Lymphatic contractile transport, (B) lymphatic contractile amplitude, (C) lymphatic contractile frequency, and (D) lymphatic pumping pressure measured from NIR imaging of in vivo lymphatic collecting vessel contraction at 1W, 2W, 4W, 6W timepoints. A mixed-effects model with Šídák's multiple comparisons was used to compare between treatments for each timepoint. Saline Control: 1W (n = 11), 2W (n = 11), 4W (n = 7), 6W (n = 7); Bestatin: 1W (n = 9), 2W (n = 9), 4W (n = 5), 6W (n = 5). $^{*}(p < 0.05),^{**}(p < 0.01)$.

actually mitigate the negative effects of ethanol on lymphatic contractility. This was an unexpected result, as we had expected LTB_4 to decrease lymphatic function at high concentrations given our observed *in vivo* effects of LTB_4 antagonism. To isolate the effects of LTB_4 from those of ethanol, we attempted to remove ethanol from the LTB_4 solution through two different methods; freezing the solution and lyopholizing the ethanol, and evaporation of the ethanol under argon. The lyopholized or evaporated LTB_4 was then suspended in PBS and added to the vessel bath at the highest previously tested concentration, 1500 nM. Neither lyopholized nor evaporated LTB_4 affected lymphatic function (frequency, amplitude, ejection fraction, or fractional pump flow) compared to PBS alone (Figure 2.8A-D). Taken together, these experiments suggest that LTB_4 alone does not significantly modulate lymphatic contractile function.

2.4.7 5-LO overexpression via adenovirus injection does not affect lymphatic contractile function *in vivo*

To further determine if the 5-LO pathway of arachidonic acid metabolism was involved in regulating lymphatic contraction, we aimed to overexpress 5-LO *in vivo* through use of an adenovirus designed to transduce cells with the ALOX5 (5-LO) gene. To first determine the efficacy of the adenovirus, we tested two adenovirus constructs on HVLECs *in vitro*. The control adenovirus vector, designed to induce GFP expression in target cells, significantly increased GFP expression in cultured HVLECs at an MOI of 250 (Figure 2.9A-B). The AdLOX5 adenovirus did not induce fluorescent protein expression, so we used qPCR to measure the expression of the ALOX5 gene within the treated HVLECs. Cultured HVLECs treated with AdLOX5 adenovirus at an MOI of 200 showed significant increase in ALOX5 gene expression (Figure 2.9C). These results showed that transduction by the adenovirus constructs was effective. We then injected mice intradermally in the tail with either the AdGFP or AdLOX5 adenovirus at 10^9 PFU. To measure the transduction efficiency of the virus *in vivo*, we harvested sacral lymph nodes from treated mice two weeks after injection

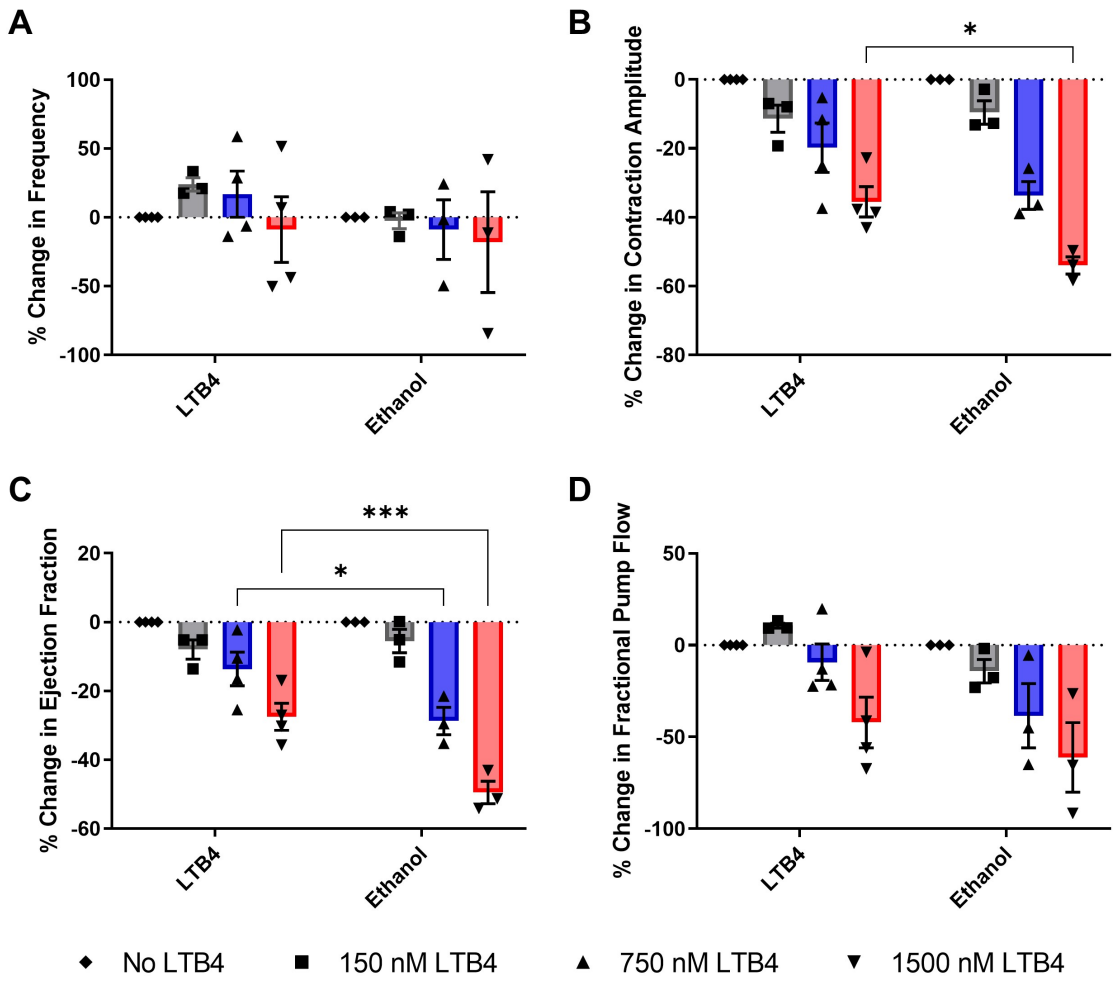

Figure 2.7: Exogenous LTB_4 does not affect contractile function of isolated lymphatic collecting vessels. Lymphatic functional metrics were quantified from videos of isolated lymphatic collecting vessels contracting while held at a transmural pressure of 3 cmH2O. Increasing concentrations of LTB_4 were added to the vessel bath (150 nM, 750 nM, and 1500 nM). Metrics shown here as a percent change from baseline at the tested concentrations for (A) contraction frequency, (B) contraction amplitude, (C) ejection fraction, and (D) fractional pump flow. LTB_4 (n = 4), Ethanol (n = 3). $^{*}(p < 0.05), ^{***}(p < 0.001)$.

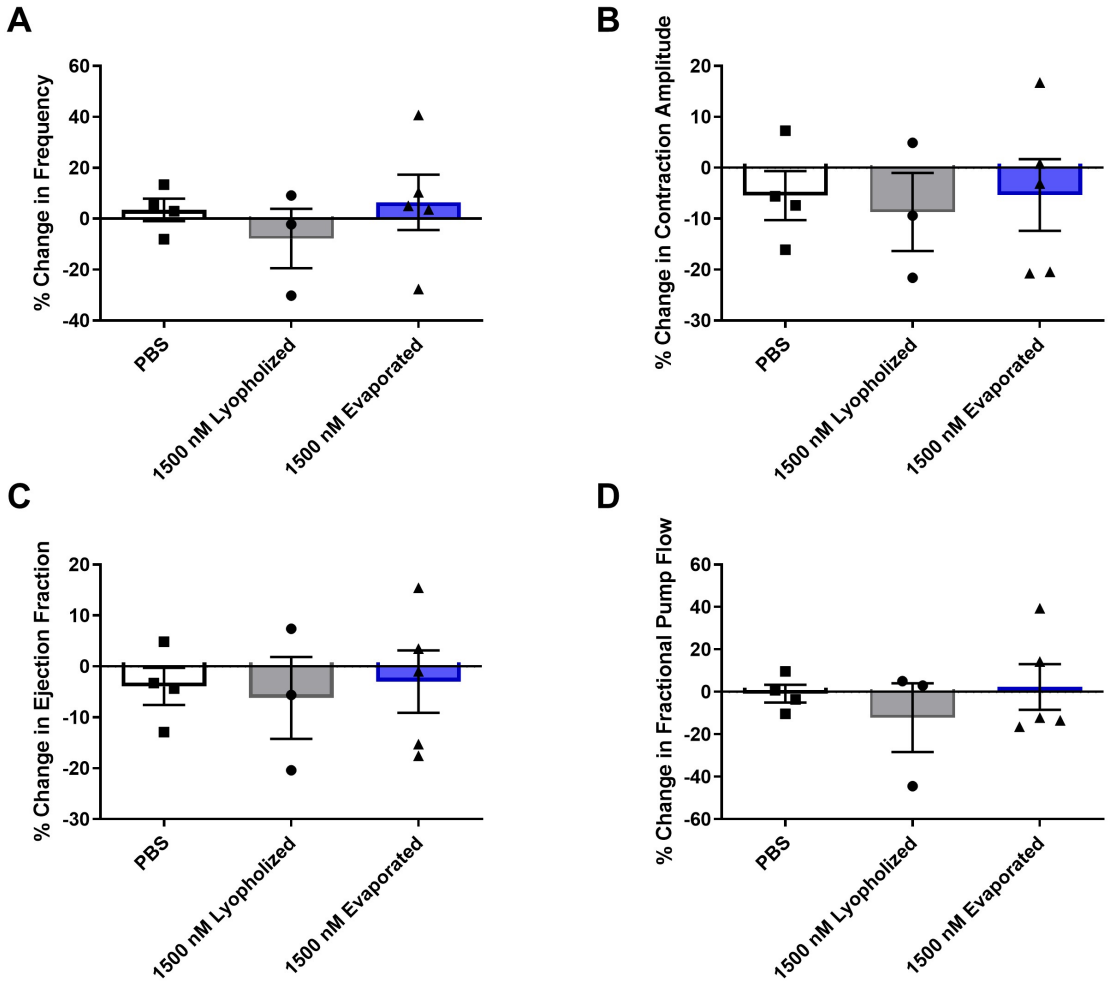

Figure 2.8: LTB_4 does not affect contractile function of isolated lymphatic collecting vessels following removal of ethanol via lyopholization or evaporation. Ethanol was removed from the LTB_4 solution via either lyopholization or evaporation. The remaining LTB_4 was then resuspended in PBS and added to the vessel bath at a concentration of 1500 nM. Lymphatic functional metrics shown here as a percent change from baseline at the tested concentrations for (A) contraction frequency, (B) contraction amplitude, (C) ejection fraction, and (D) fractional pump flow. PBS (n = 4), Lyopholized (n = 3), Evaporated (n = 5).

and used flow cytometry to measure GFP expression of various leukocytes within the LNs. We expected that the virus and the accompanying GFP transduction signal would end up within the LNs as it would passively drain to lymph nodes through lymphatics along with active transport via APCs that took up the virus. We found that B cells (CD19+) and myeloid cells (CD3- CD19-) showed significant GFP expression in mice treated with the AdGFP adenovirus compared to the AdLOX5 adenovirus, while T cells (CD3+) showed no significant differences between the treatment groups (Figure 2.9D-E). This result matched our hypothesis, as myeloid cells and B cells are known to directly interact with antigen (in this case the adenovirus), while the T cells are activated by APCs. Taken together, our *in vitro* and *in vivo* tests of the adenovirus show its effectiveness in transducing cells with the desired ALOX5 gene.

We then aimed to measure lymphatic contractile function *in vivo* following injection of the ALOX5 adenovirus. One day prior to intradermal injection of the GFP or ALOX5 adenovirus, we used NIR imaging as described previously to measure lymphatic function. Function was then measured on day 4, 7 and 14 following adenovirus injection. The quantified metrics of lymphatic function (contractile frequency, amplitude, and transport) showed no differences between GFP and ALOX5 adenovirus-treated mice, suggesting that overexpression of 5-LO is insufficient to significantly modulate lymphatic function (Figure 2.10A-C). Combined with our previous *in vitro* experiments, we conclude that increased 5-LO expression (and in turn, increased LTB_4) does not directly affect lymphatic function.

2.4.8 5-LO overexpression via adenovirus injection does not affect immune response within dLNs

Given the known chemoattractive role of LTB_4 for neutrophils and T cells, we were interested in determining if upregulation of 5-LO via adenovirus injection would influence the immune response within the dLNs [121, 122]. To quantify leukocyte populations within the

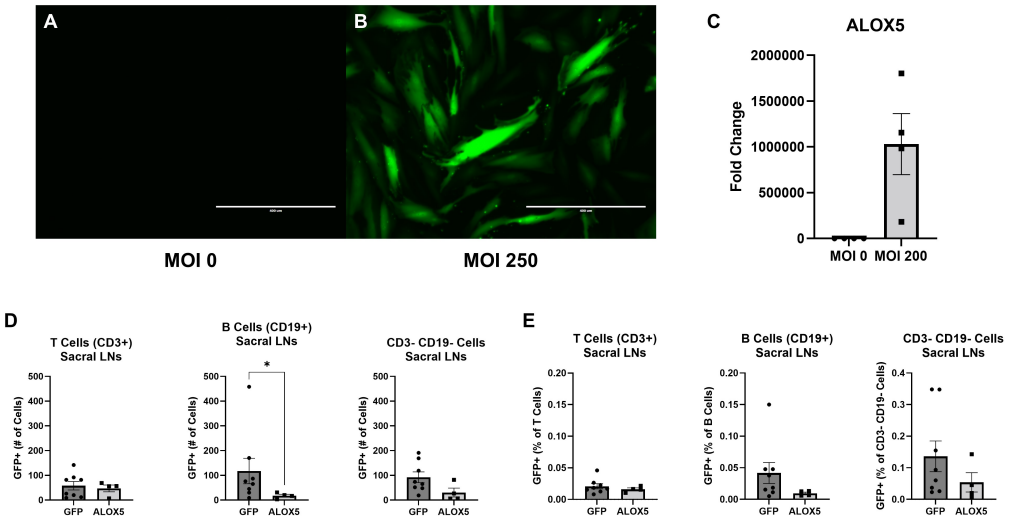

Figure 2.9: Adenovirus treatment induces GFP and ALOX5 expression *in vitro* and *in vivo*. Cultured HVLECs were treated with either GFP or ALOX5 adenovirus. GFP expression of HVLECs treated with GFP adenovirus at (A) MOI = 0 or (B) MOI = 250. (C) Fold change of ALOX5 gene as measured by qPCR from HVLECs treated with ALOX5 adenovirus at an MOI = 200. GFP or ALOX5 adenovirus was injected intradermally into the mouse tail at a PFU of 10^9 and sacral LNs were harvested for flow cytometry. (D) Number of GFP+ cells for T cells (CD3+), B cells (CD19+), and myeloid cells (CD3- CD19-). (E) % of parent cells which are GFP+ for T cells (CD3+), B cells (CD19+), and myeloid cells (CD3- CD19-). GFP (n=8), ALOX5 (n=4).

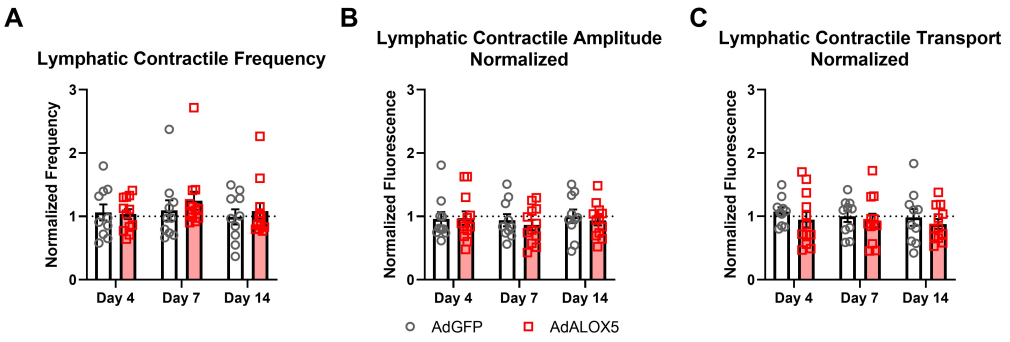

Figure 2.10: Overexpression of 5-LO *in vivo* via ALOX5 adenovirus treatment does not affect lymphatic contractile function. NIR imaging was used to measure lymphatic contractile function in mice treated with either GFP or ALOX5 adenovirus. (A) Contractile frequency, (B) contractile amplitude, and (C) contractile transport were all quantified at days 4, 7, and 14 following adenovirus injection and normalized to baseline function. GFP (n=5), ALOX5 (n=6).

dLNs, we used flow cytometry to identify T cells (CD3+), B cells (CD19+), CD11b+ cells, monocytes (CD11b+ CD64+), macrophages (CD11b+ F480+), M1 macrophages (CD11b+ F480+ MHCII+), dendritic cells (CD11c+ MHCII+), and neutrophils (CD11b+ Ly6G+). We observed no change in the frequencies of these cells within dLNs following AdALOX5 injection compare to the control AdGFP vector (Figure 2.11). This data suggests that up-regulation of 5-LO *in vivo* on its own does not alter the immune composition of LNs.

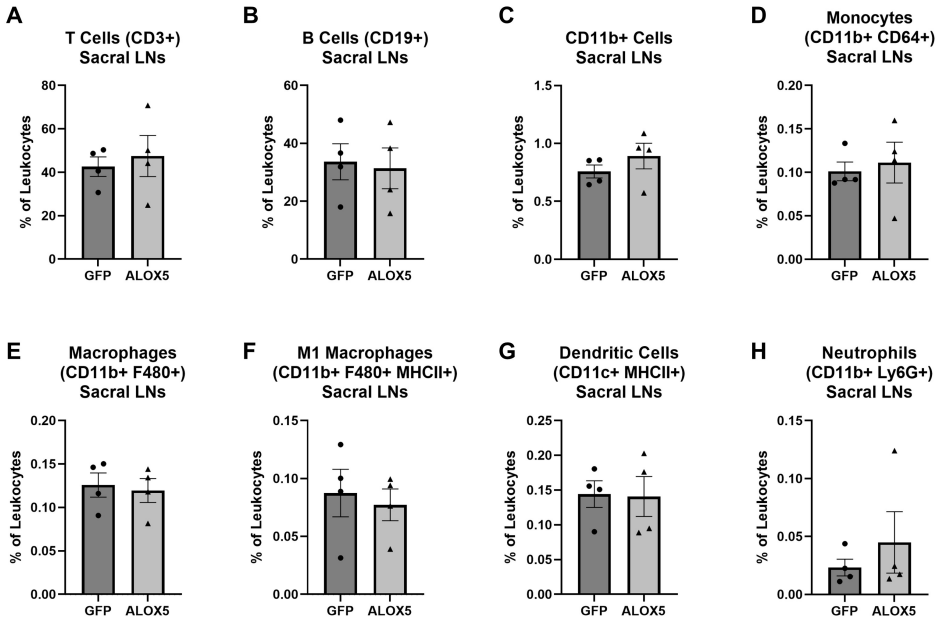

Figure 2.11: Overexpression of 5-LO *in vivo* via ALOX5 adenovirus treatment does not affect immune response in dLNs. Flow cytometry was used to analyze leukocyte populations within dLNs. (A) T cell, (B) B cell, (C) CD11b+ cell, (D) monocyte, (E) macrophage, (F) M1 macrophage, (G) dendritic cell, and (H) neutrophil frequencies of total leukocytes within dLNs at 3 weeks after intradermal adenovirus injection. GFP (n=4), ALOX5 (n=4).

2.4.9 Epsin LEC-iDKO mice do not have altered lymphatic contractile function

Following our studies testing the effect of LTB_4 and the 5-LO signaling pathway on lymphatic function, we aimed to extend these results by investigating how postnatal epsin depletion, a known pro-lymphangiogenic mechanism, would affect lymphatic function *in vivo*. A previous study by Wu et al has shown that postnatal epsin deletion increases

lymphangiogenesis through reduction of VEGFR3 degradation [118]. As prenatal epsin deletion results in the development of abnormal lymphatic valves, inducible deletion of epsin postnatally was necessary to investigate how epsin deletion may influence the lymphatic response naively and in the context of injury [123]. To determine how epsins may be involved in regulating lymphatic function, an inducible genetic knockout mouse model designed to specifically delete epsins in LECs was used. This mouse model was created by crossing $Prox1-Cre-ER^{T2}$ mice with $Epn1^{fl/fl}/Epn2^{-/-}$ mice. Adult $Epn1^{fl/fl}/Epn2^{-/-}/Prox1-Cre-ER^{T2}$ (Epsin LEC-iDKO) mice were treated with tamoxifen at 8-10 weeks of age to selectively delete epsin 1 in LECs (epsin 2 was already constitutively deleted). Following tamoxifen treatment, NIR imaging was used to measure function of the lymphatic vessels in the tail. Function was measured prior to tamoxifen injection, and at days 10 and 21 following treatment. Lymphatic contractile frequency, amplitude, and transport normalized to baseline function were not significantly changed following tamoxifen treatment (Figure 2.12A-C), suggesting that epsins are dispensable for normal lymphatic function in naive mice.

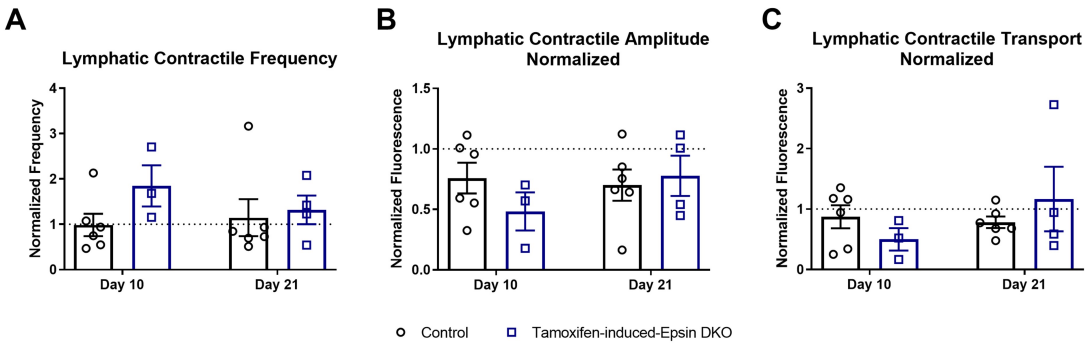

Figure 2.12: Lymphatic contractile function is unchanged in Epsin LEC-iDKO mice. NIR imaging was used to quantify (A) lymphatic contractile frequency, (B) amplitude, and (C) transport normalized to baseline function at days 10 and 21 following tamoxifen treatment.

2.4.10 Epsin LEC-iDKO mice have improved lymphatic contractile function following single vessel ligation surgery

To determine if epsins are involved in regulating lymphatic function in the context of lymphatic injury and disease remodeling, we investigated changes in lymphatic function *in vivo* following single vessel ligation surgery to induce lymphedema in Epsin LEC-iDKO mice. NIR imaging was used to measure function of the intact lymphatic collecting vessels at 1,2,4,6,8, and 10 weeks following surgery. Using a mixed-effects statistical model, we found that lymphatic contractile transport normalized to pre-surgery function was significantly increased in Epsin LEC-iDKO mice compared to control mice ($p = 0.0495$). Additionally, the interaction between time and transport was also significantly different in Epsin LEC-iDKO mice, suggesting that the change in transport over time is different between the two groups ($p = 0.0359$). There was also a significant difference for the interaction between time and lymphatic contractile amplitude normalized to pre-surgery function ($p = 0.0432$). Lymphatic contractile frequency showed no differences between Epsin LEC-iDKO and control mice. When specific timepoints were analyzed, transport was significantly increased 4 weeks after surgery in Epsin LEC-iDKO mice. Other metrics (frequency, amplitude) were not significantly changed at any specific timepoint (Figure 2.13A-C). This data suggests that epsin deletion increases function in the intact collecting lymphatic vessels as remodeling occurs following lymphatic injury. The increase in amplitude and transport while frequency is unchanged also indicates that epsin deletion during lymphedema improves the overall pumping capacity of the lymphatics without affecting the frequency of contraction.

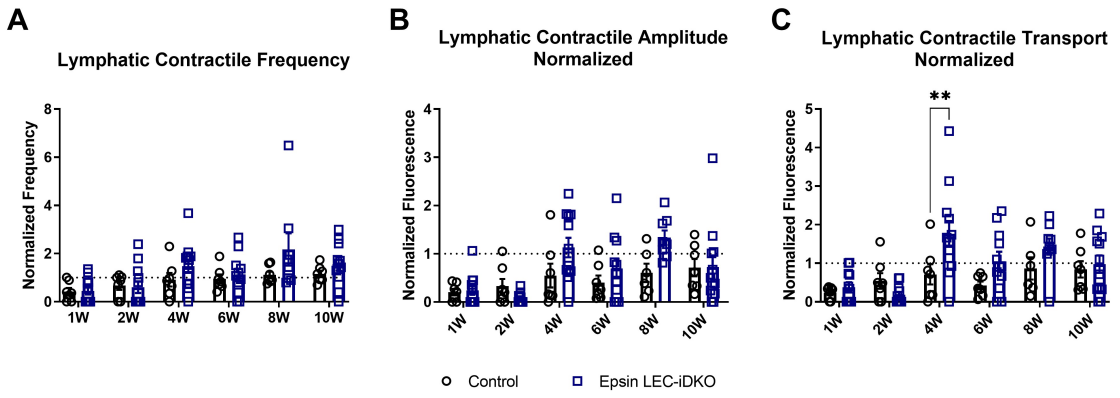

Figure 2.13: Epsin LEC-iDKO mice exhibit increased lymphatic contractile function following single vessel ligation surgery. NIR imaging was used to quantify (A) lymphatic contractile frequency, (B) amplitude, and (C) transport normalized to baseline function at 1,2,4,6,8, and 10 weeks following single vessel ligation surgery. Control (n=9), Epsin LEC-iDKO (n=13).

2.5 Discussion and Future Work

2.5.1 Loss of lymphatic function in lymphedema correlated with swelling

Changes in lymphatic function during lymphedema progression have been previously reported, both in various animal models and in humans. In animal models, these changes have primarily been reported in the context of full lymphatic ablation, leaving no intact functional collecting vessels. Thus, the lack of lymphatic function in these models is unsurprising as this is an intended consequence of the surgery to induce lymphedema. In humans, lymphatic function has primarily been measured in patients who have already developed lymphedema. These patients often have dysfunctional and tortuous lymphatic vessels, and lymphatic pumping pressure in lymphedematous limbs has also been reported to be decreased compared to healthy individuals [26, 102, 124]. A previous study has also indicated that higher baseline lymphatic pumping pressure may predispose patients to eventual lymphedema development following lymph node removal to treat breast cancer [125]. Our data suggests that swelling progression is linked with the measured loss of contractile function in the intact collecting lymphatics following single vessel ligation. This

loss of lymphatic function is shown through chronic reduction in both lymphatic contractile transport and pumping pressure.

2.5.2 LTB_4 antagonism improves lymphatic function in lymphedema, but increased LTB_4 or 5-LO signaling alone does not affect lymphatic function

Antagonizing LTB_4 production via bestatin has been shown to reduce swelling in the double vessel ligation mouse tail lymphedema model [111]. These beneficial effects have been mainly attributed to the pro-lymphangiogenic mechanism of reducing LTB_4 concentration in lymphedematous tissue. Our work adds to these results by showing that bestatin treatment increases lymphatic contractile function, both in the double vessel and single vessel ligation lymphedema models. Importantly, full ligation of the mouse tail lymphatic network is not necessary to observe the beneficial effects of LTB_4 antagonism on lymphatic function. Additionally, LTB_4 antagonism does not improve lymphatic function in naive mice, indicating that increased LTB_4 concentration in lymphedema at least partially reduces lymphatic function. These results suggest that LTB_4 modulates lymphatic function in the context of lymphedema, either through direct action on collecting lymphatic vessels or through some other indirect action.

Given the observed increase in lymphatic function following bestatin treatment in the context of lymphedema, we aimed to determine if there was a direct effect of LTB_4 on lymphatic contractile function. We expected that high concentrations of LTB_4 would inhibit lymphatic contraction *ex vivo*. Through testing various concentrations of LTB_4 on isolated mouse lymphatic collecting vessels, we found that LTB_4 actually reduced lymphatic function less than vehicle control at the highest concentration (1500 nM). The vehicle control (ethanol) reduced lymphatic function by itself, so we attempted to remove ethanol from the LTB_4 solution to isolate the effect of LTB_4. Two methods, lyopholization and evaporation under argon, were used to remove ethanol from the solution. The resuspended LTB_4 showed no effect on lymphatic contraction compared to PBS control when added di-

rectly to the vessel bath of contracting isolated lymphatic collecting vessels. These results were surprising to us, given that LTB_4 antagonism had successfully increased lymphatic function *in vivo* in the context of lymphedema, where LTB_4 concentration is high. Given that exogenous LTB_4 did not directly effect lymphatic function *ex vivo*, we suspected that LTB_4 modulated lymphatic function through an indirect mechanism, potentially mediated by immune cells.

We overexpressed the 5-LO gene *in vivo* through use of the AdALOX5 adenovirus in order to determine if increased 5-LO signaling (upstream of LTB_4 production) was sufficient to modulate lymphatic contractile function. We hypothesized that up-regulation of 5-LO signaling would decrease lymphatic function *in vivo*, most likely through an indirect immune cell-mediated mechanism given the fact that LTB_4 did not affect function in isolated lymphatic vessels. However, injection of the AdALOX5 adenovirus into the mouse tail did not change lymphatic function in the tail compared to a control GFP adenovirus over two weeks following injection. The combined *ex vivo* and *in vivo* data suggest that increasing 5-LO signaling or LTB_4 concentration alone is not sufficient to significantly affect lymphatic function. The beneficial effects of LTB_4 antagonism on lymphatic function in the context of lymphedema are thus likely a product of the unique lymphedema microenvironment rather than an effect solely mediated through LTB_4. Further study is needed to better understand the mechanisms driving loss of lymphatic function during lymphedema progression, both mechanical changes induced through tissue remodeling and immune cell-mediated changes induced through secretion of various cytokines and tissue factors.

2.5.3 Postnatal epsin deletion improves lymphatic function only in the context of lymphatic injury

Our study of LTB_4 indicated that a potential lymphedema therapy predicated on its pro-lymphangiogenic mechanism may also improve lymphatic function. We extended this finding by analyzing changes in lymphatic function in the context of another pro-lymphangiogenic

therapy, inhibition of epsin signaling. To completely inhibit epsin signaling, we used a inducible lymphatic-specific epsin depletion genetic mouse model. This approach allowed us to deplete epsin via tamoxifen injection in adult mice, removing any potential negative effects of epsin depletion in prenatal mice on lymphatic development. Previous work has shown that depleting epsins in the context of diabetes improves lymphangiogenesis through its regulation of VEGFR3 degradation [118]. Here, we show that epsin depletion improves lymphatic function following single vessel ligation surgery, but not in naive mice. This result adds to our bestatin data in showing that pro-lymphangiogenic mechanisms may also have a beneficial effect on lymphatic contractile function in the context of disease. Epsins are involved in degradation of many ubiquinated cell surface proteins, so the exact mechanism through which epsin depletion affects lymphatic function still needs to be elucidated. Previous experiments have shown that activation of VEGFR3 does affect lymphatic function, suggesting that the regulation of VEGFR3 degradation by epsins may be one potential mechanism modulating lymphatic function [126, 127]. Further study can elucidate cellular mechanisms and signaling pathways involved in modulating the functional response of lymphatic collecting vessels.

2.5.4 Conclusion

Using NIR imaging techniques, we were able to measure how lymphatic contractile function changed during lymphedema progression and correlate these functional changes with the swelling response. The single vessel ligation model provided a more clinically relevant platform to both investigate changes in the intact lymphatic vasculature during lymphedema development and to test the functional response of the lymphatic network to potential therapeutic mechanisms. Two pro-lymphangiogenic mechanisms, LTB_4 antagonism and epsin deletion, were shown to increase lymphatic function following lymphatic injury. Interestingly, metrics related to lymphatic pump capacity, such as contractile amplitude and transport, showed significant increase while frequency of contraction was unchanged for

both treatments. These therapeutic approaches only improved lymphatic function in the context of lymphatic injury, suggesting that their respective targets (LTB_4 and epsin) modulate lymphatic function only in the lymphedema microenvironment. Further analysis of the effect of LTB_4 and 5-LO signaling on lymphatic pump function through isolated lymphatic vessel tests *ex vivo* and adenovirus-induced overexpression of 5-LO *in vivo* showed no effect of these molecules directly on lymphatic function. Future studies should further investigate how the lymphedema microenvironment, including both the immune response and changes in lymphatic morphology, may influence the response of collecting lymphatics to potential therapeutic treatments.

CHAPTER 3
THE KINETICS OF LYMPHATIC DYSFUNCTION AND LEUKOCYTE EXPANSION IN THE DRAINING LYMPH NODE IN A MOUSE MODEL OF LYMPHEDEMA (AIM 2)

[1]

3.1 Overview

The mechanisms of lymphedema development are not well understood, but emerging evidence highlights the crucial role the immune system plays in driving its progression. It is well known that lymphatic function deteriorates as lymphedema progresses; however, the connection between this progressive loss of function and the immune-driven changes that characterize the disease has not been well established. In this study, we assess changes in leukocyte populations in lymph nodes within the lymphatic drainage basin of the tissue injury site (dLNs) using a mouse tail model of lymphedema in which a pair of draining collecting vessels are left intact. We additionally quantify lymphatic pump function using established NIR lymphatic imaging methods and lymph-draining NPs synthesized and employed by our team for lymphatic tissue drug delivery applications to measure lymphatic transport to and resulting NP accumulation within dLNs associated with swelling following surgery. When applied to assess the effects of the anti-inflammatory drug bestatin, which has been previously shown to be a possible treatment for lymphedema, we find lymph-draining NP accumulation within dLNs and lymphatic function to increase as lymphedema progresses, but no significant effect on leukocyte populations in dLNs or tail swelling. These results suggest that ameliorating this loss of lymphatic function is not sufficient to reverse swelling in this surgically induced disease model that better recapitulates the ex-

[1] Adapted from Cribb et al [128]

tent of lymphatic injury seen in human lymphedema. It also suggests that loss of lymphatic function during lymphedema may be driven by immune-mediated mechanisms coordinated in dLNs. Our work indicates that addressing both lymphatic vessel dysfunction and immune cell expansion within dLNs may be required to prevent or reverse lymphedema when partial lymphatic function is sustained.

3.2 Motivation and Background

Lymphedema is a debilitating disease that affects millions of people around the world and is characterized by tissue fibrosis, limb swelling, and recurrent soft tissue infections [50]. There are currently no pharmacological treatments for lymphedema; however, the immune response has been heavily implicated in lymphedema development. A variety of leukocytes, including T cells, macrophages, dendritic cells, and neutrophils, are increased in lymphedematous skin and have been shown to contribute to fibrogenesis, lymphatic hyperplasia, and lymphatic dysfunction [59, 75, 78, 79, 129, 130]. These leukocytes secrete cytokines and proteins, including TNF-α, TGF-β, iNOS, IL-1, and IL-6, which drive fibrosis and lymphatic dysfunction through their interactions with stromal cells and surrounding tissue [59, 84–87].

Previous reports have focused primarily on studying leukocyte infiltration into lymphedematous tissue to explain their effects on the existing lymphatic vasculature and the resultant swelling. Few studies have examined how leukocyte populations in downstream LNs respond during lymphedema. Garcia Nores et al. found that CD4+ T cells are activated by dendritic cells in regional LNs and migrate to the site of injury to initiate lymphedema [76]. Leukocyte populations within LNs draining the skin of mice lacking dermal lymphatic vessels were also previously reported in genetic models of disease [83, 94]. To our knowledge, no studies have investigated how multiple leukocyte populations in the dLNs change as swelling worsens during lymphedema progression, however, which is of key clinical importance since the onset of lymphedema is a delayed process and fluid at the site

of disease onset is continuously drained to downstream LNs [131].

Multiple studies have identified possible treatments for lymphedema that target various immune-mediated changes that characterize the disease [81, 101, 132]. One such possible treatment is bestatin, a drug which antagonizes the production of LTB_4, a lipid mediator of inflammation and a metabolite of arachidonic acid [133]. A previous study found that bestatin treatment reduced swelling and improved lymphatic function in a mouse model of lymphedema through the drug's antagonism of LTB_4, which is elevated in lymphedema both in mouse models and clinically and has strong anti-lymphangiogenic effects at high concentrations [111]. The culmination of these various studies strongly suggests that both impaired lymphangiogenesis and leukocytes, including T cells and macrophages, drive tissue fibrosis and lymphatic dysfunction during lymphedema development.

Many previous studies of lymphedema used the mouse tail double vessel ligation model where all initial and collecting lymphatics in the tail are blocked due to circumferential ligation of lymphatics encircling the tail [12, 61]. This model results in minimal fluid and leukocyte uptake to the dLNs after the injury due to the complete blockage of lymph outflow from the lymphedema site. However, in human lymphedema, many drainage pathways from the affected limb are still intact, suggesting that drainage does not need to be fully inhibited for lymphedema to develop. An adaptation of this lymphedema model developed previously by our lab, the single vessel ligation model, leaves a pair of collecting lymphatic vessels intact while ligating the other initial and collecting lymphatic vessels. This procedure leaves an intact drainage pathway on one side of the tail while the other pathway is completely blocked, but the progression of lymphedema in this model mirrors the typical mouse tail model even though an intact drainage pathway exists [110].

This study presents a detailed analysis of time-varying changes in LN leukocyte populations during lymphedema using this single vessel ligation model. In so doing, both the immune response within the dLN in lymphedema and how flow into the LN may modulate these changes were simultaneously delineated. Moreover, we utilize this model to

explore the kinetics of transport, swelling, and immune cell populations within the dLNs in the context of LTB_4 antagonism with bestatin. Our findings demonstrate that leukocyte populations extensively expand in dLNs following lymphedema induction, and this increase in LN leukocyte populations is correlated with accumulation of NPs draining the injury site within the dLNs. Additionally, we show that treatment with bestatin increases lymphatic contractile transport and NP accumulation during lymphedema progression but does not reduce the observed leukocyte expansion in the dLNs or the tail swelling response characteristic of lymphedema.

3.3 Methods

3.3.1 Surgical Lymphedema Model

We used the single vessel ligation model of lymphedema developed in our lab where a pair of collecting vessels on one side of the mouse tail were left intact while the remaining dermal initial lymphatics and collecting vessels were ligated and cauterized [110]. Eight-week-old male and female C57Bl/6 mice (Charles River Laboratories, Wilmington, MA, USA) were used for this study according to procedures approved by the Georgia Institute of Technology IACUC Review Board (Protocol # A100293 approved on 6 March 2019). All animals were first anesthetized using inhaled isoflurane (5% induction, 2% maintenance). All animals received incisions 1.6 cm from the base of the animal spanning 80–90% of the circumference of the tail with particular care to standardize the incisions as much as possible. All incisions were cauterized to prevent bleeding and fluid leakage. After the surgical procedures, both collecting vessels were checked with NIR imaging to ensure they were either severed or remained intact as appropriate. Previously, our group characterized the lymphatic physiology of the tail as having a dominant and a nondominant collecting vessel [33]. All surgeries done in this study involved ligation and cauterization of the dominant collecting vessel. In this manuscript, the LN downstream of the dominant collecting vessel is referred to as the injured vessel dLN while the LN downstream of the nondominant col-

lecting vessel is referred to as the intact vessel dLN. Mice were euthanized at 2 days (n = 14), 1 week (n = 16), 2 weeks (n = 21), and 3 weeks (n = 15) after surgery.

3.3.2 Flow Cytometry

Both the sacral LNs, which drain fluid from the tail, were harvested when mice were euthanized at 2 days, 1 week, 2 weeks, and 3 weeks after surgery. The LNs were stored in a 1 mg/mL Collagenase D solution (Sigma-Aldrich, St. Louis, MO, USA) and incubated at 37 °C for 1 h for disassociation. We then pushed the LNs through a 70 µm cell strainer to create a single cell suspension. A CD16/32 antibody blocking solution (Tonbo Biosciences, San Diego, CA, USA) was added for 5 min on ice. After spinning down for 5 min at 350xg and decanting the liquid, Zombie Green live/dead solution (BioLegend, San Diego, CA, USA) was added at room temperature for 30 min. Following a wash step, multiple antibodies conjugated to fluorophores were added to the suspensions for 30 min on ice. The antibodies used were APC anti-mouse F4/80 (1:40), APC/Cyanine7 anti-mouse Ly6G (1:100), Brilliant Violet 421 anti-mouse/human CD11b (1:33), Brilliant Violet 510 anti-mouse Ly6C (1:100), Brilliant Violet 605 anti-mouse CD3 (1:40), Brilliant Violet 711 anti-mouse CD64 (1:40), Brilliant Violet 785 anti-mouse CD19 (1:40), PE anti-mouse I-A/I-E (1:40), PE/Cy7 anti-mouse CD206 (MMR) (1:50), and PerCP anti-mouse CD11c (1:40) (Bio-Legend, San Diego, CA, USA). After labeling with antibodies, 2% PFA was added for 15 min on ice to fix the cells. The stained cells were then stored in FACS buffer (10 mg/mL BSA in PBS) for analysis. A BD Fortessa Flow Cytometer was used to run the samples. UltraComp eBeads (Thermo Fisher Scientific, Waltham, MA, USA) were used for single-stain compensation controls. BD FACSDiva was used to record results and FlowJo was used for all analysis of results. Our flow panel did not include a stain for CD45, so leukocytes were defined as CD3+/CD19+/CD11b+/CD11c+/Ly6C+. The gating strategy implemented in FlowJo is shown in Figure 3.1. Using these same methods, we analyzed T cell subpopulations using the following antibodies: APC anti-mouse CD4 (1:100) and PE

anti-mouse CD8a (1:100) (BioLegend, San Diego, CA, USA). The gating strategy for the analysis of T cell subpopulations is shown in Figure 3.2.

3.3.3 Tail Swelling

Tail swelling was measured prior to surgery and when mice were euthanized. Tail images were taken using an iPhone camera with a ruler adjacent to the tail to provide a measurement reference and ImageJ was used to quantify swelling. The diameter of the tail was measured at 5 mm to 10 mm increments along the tail starting at the site of injury. The truncated cone method was used to determine the total volume of the tail given the diameters along its length. Percent volume change was measured by comparing the tail volume at endpoint to the volume prior to surgery.

3.3.4 Nanoparticle Synthesis and Characterization

SH-NP were synthesized as previously described [134–138]. Briefly, 500 mg of Pluronic F127 (Sigma-Aldrich, St. Louis, MO, USA) was dissolved in 10 mL of MilliQ water to form micelles. Under argon, 400 µL of propylene sulfide (TCI, Tokyo, Japan) was added and stirred for 30 m before the addition of 14 mg of thiolated initiator activated for 15 m in 322 µL of sodium methoxide (Sigma-Aldrich, St. Louis, MO, USA) [47]. After 15 m, 64 µL of 1,8-diazabicyclo[5.4.0] undec-7-ene was added, and the solution was capped and reacted for 24 h while stirring at 1500 rpm. The reaction was then uncapped and exposed to air for 2 h, then dialyzed in a 100 kDa membrane (Spectrum Labs, New Brunswick, NJ, USA) against 5 L of MilliQ water for 3 d with 6 water changes. NP were dye labeled by overnight reaction with an excess of IRdye 680RD maleimide (LI-COR, Lincoln, NE, USA) in 1X PBS, and excess dye was removed by size exclusion chromatography using Sepharose CL-6B resin (GE Healthcare, Chicago, IL, USA). NP were concentrated by spin filtration and sterile filtered through a 0.2 µm filter. NP diameter was measured using a Malvern ZetaSizer instrument. Characterization of these NPs is shown in Figure 3.3.

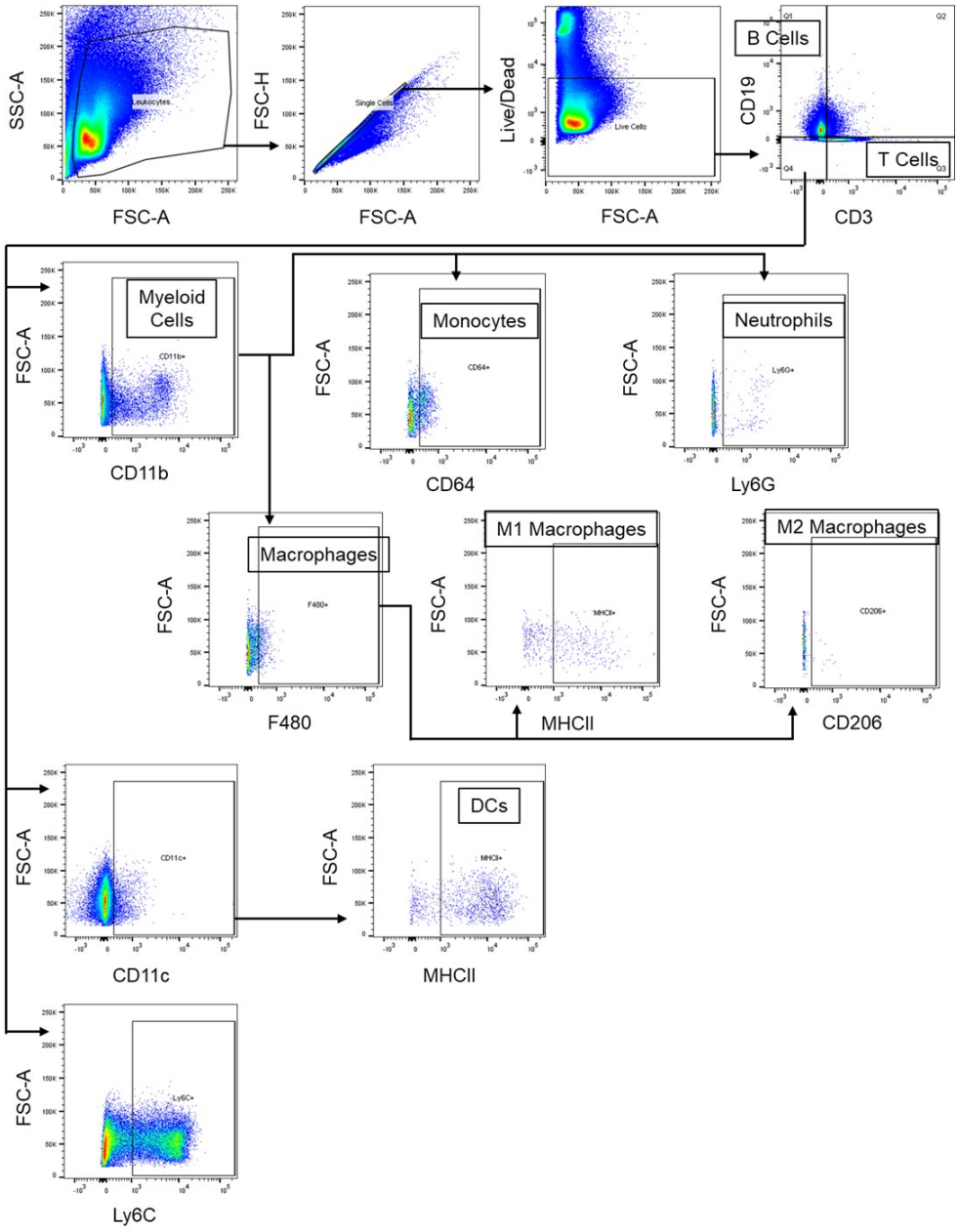

Figure 3.1: Gating strategy for flow cytometry analysis. The gating strategy to classify the following leukocyte subsets: T Cells (CD3+), B Cells (CD19+), Myeloid cells (CD11b+), Dendritic cells (CD11c+ MHCII+), Monocytes (CD11b+ CD64+), Macrophages (CD11b+ F480+) including M1 (MHCII+) and M2 (CD206+) polarization, and Neutrophils (CD11b+ Ly6G+).

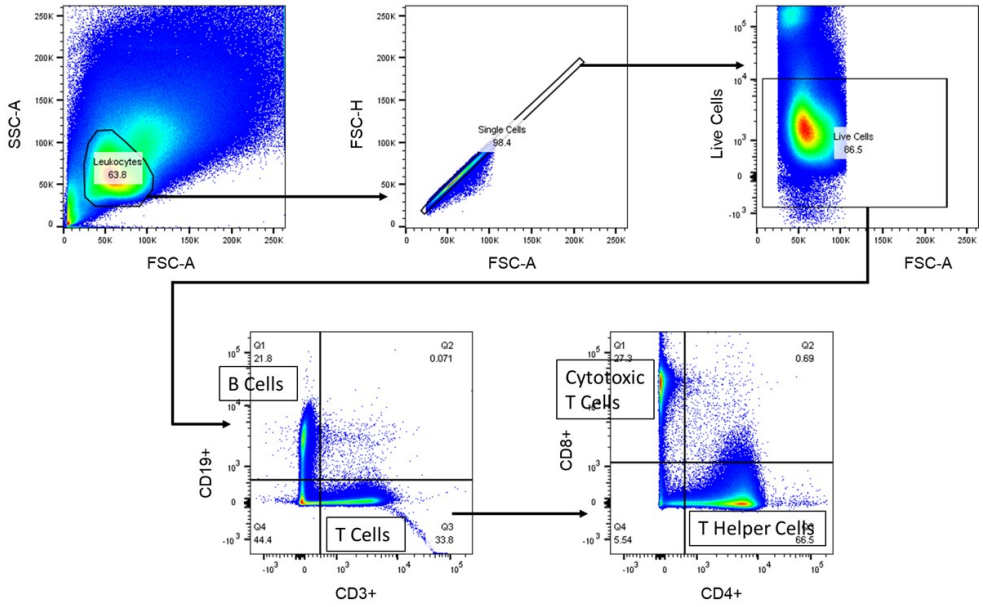

Figure 3.2: Gating strategy for flow cytometry analysis of T cell subpopulations. The gating strategy to classify T helper cells (CD3+ CD4+) and cytotoxic T cells (CD3+ CD8+).

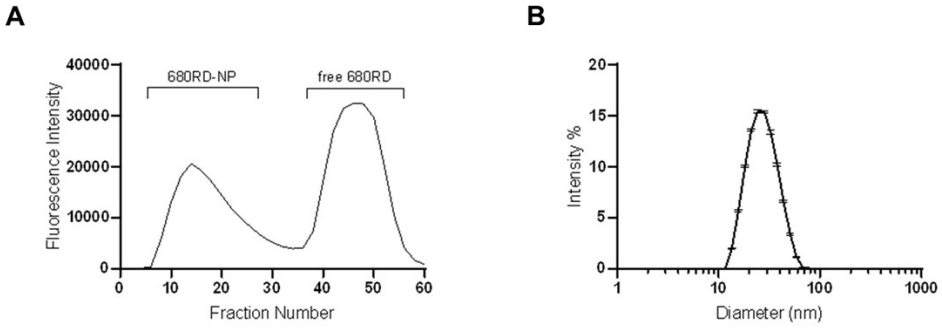

Figure 3.3: Characterization of NPs labeled with IRdye 680RD (680RD-NP). (A) Elution profile of 680RD-NP from a CL-6B size exclusion chromatography column. Separate peaks for 680RD-NP and unconjugated 680RD clearly emerge, allowing for cleaning and isolation of NP fractions. (B) NP diameter, measured by dynamic light scattering.

3.3.5 Nanoparticle NIR Functional Analysis

A total of 10 µL of 680-NPs were injected intradermally into the mouse tail tip while the mouse was under anesthesia 24 hrs prior to euthanasia. After euthanasia, the sacral LNs draining the mouse tail were harvested and placed into a black 96-well plate. The LNs were then imaged using a customized imaging system consisting of a Sutter Instrument Lambda LS Xenon arc lamp (Sutter Instrument, Novato, CA, USA), an Olympus MVX-ZB10 microscope (Olympus Life Science, Waltham, MA, USA), a 650 nm bandpass excitation filter (45 nm full-width half maximum, FWHM), a 720 nm bandpass emission filter (60 nm FWHM), and a 685 nm longpass dichroic mirror. Images were acquired with a Photometrics Evolve Delta 512 EM-CCD (Teledyne Photometrics, Tuscon, AZ, USA). The two LNs were imaged in the same field of view using 1x magnification and an exposure time of 50 ms.

Multiple metrics were used to quantify fluorescence in the LNs. The maximum fluorescence of the LN was quantified as the maximum fluorescence value within the LN. The normalized mean fluorescence was quantified as the mean fluorescence within the LN subtracted by the mean background fluorescence of a window 50 pixels by 50 pixels located away from the LN. The normalized sum of fluorescence was calculated as the normalized mean fluorescence multiplied by the area of the LN in pixels.

3.3.6 Bestatin Treatment

Bestatin treatment started at three days after surgery, as a previous study showed that beneficial effects of bestatin treatment were dependent on starting the treatment at this time [111]. To make bestatin stock, bestatin (Cayman Chemical, Ann Arbor, MI, USA) was first dissolved in DMSO at a 4 mg/mL concentration. Aliquots of 100 µL of this solution were stored in -20 °C. Aliquots were diluted with 900 µL of sterile saline per aliquot prior to injection. This bestatin solution was then administered through daily intraperitoneal injection at a concentration of 2 mg/kg. The control group received daily intraperitoneal injections of

equivalent volumes of sterile saline without DMSO. Bestatin-treated mice were euthanized at 1W (n = 15), 2W (n = 18), and 3W (n = 12) after surgery.

3.3.7 NIR Lymphatic Functional Analysis

NIR lymphatic imaging was performed according to previously published methods [32, 33, 110, 120]. LI-COR IRDye 800CW NHS Ester (LI-COR Biosciences, Lincoln, NE, USA) was conjugated to 20 kDa methoxypolyethylene glycol amine (Simga-Aldrich, St. Louis, MO, USA) and stored as lyophilized aliquots at -20 °C. After reconstitution in saline, 10 µL of this tracer was injected intradermally into the tip of the tail for fluorescence imaging. The injection was given at an entry angle of approximately 10 degrees to an approximate depth of 1 mm to specifically target the lymphatic vasculature. Care was taken to position the injection as close to the midline of the tail as possible to avoid favoring one collecting vessel over the other. Images were taken with a customized imaging system consisting of a Sutter Instrument Lambda LS Xenon arc lamp (Sutter Instrument, Novato, CA, USA), an Olympus MVX-ZB10 microscope (Olympus Life Science, Waltham, MA, USA), a 769 nm bandpass excitation filter (49 nm full-width half maximum, FWHM), an 832 nm bandpass emission filter (45 nm FWHM), and an 801.5 nm longpass dichroic mirror. Images were acquired with a Photometrics Evolve Delta 512 EM-CCD (Teledyne Photometrics, Tuscon, AZ, USA). The field of view was centered on the mouse's tail at the site of injury. This location ensured that both the intact collecting vessel and the injury site could be viewed. The small volume of fluid injection and the use of NIR to enhance tissue penetration ensured that only fluorescence in the deeper collecting lymphatics was visible downstream of the injection site. The animals were imaged continuously from the time of injection until 20 min post-injection with a 50 ms exposure time and a frame rate of 10 fps. Analysis of NIR functional metrics was performed during the steady-state period ranging from 5–20 min after injection, as defined previously [33]. Lymphatic contractile frequency, amplitude, transport, and pumping pressure were measured and recorded as previously published

[110].

3.3.8 Statistical Analysis

For comparison of leukocyte populations in the dLNs among the various timepoints analyzed, Kruskal–Wallis tests with Dunn's multiple comparisons tests were used. Spearman's rank correlation was used to calculate correlations between swelling percentage and various leukocyte populations. Fluorescent measurements from the 680IR NP experiments were transformed using the natural logarithm to create a normally distributed dataset. Ordinary one-way ANOVA tests with Tukey's multiple comparisons tests were then used to compare between timepoints. Kruskal–Wallis tests with Dunn's multiple comparisons tests were used to compare the normalized difference of leukocyte populations in intact versus injured vessel dLNs between timepoints. Linear regression was used to calculate correlations between normalized difference and fluorescent measurements. A mixed-effects model with Šídák's multiple comparisons test was used to compare normalized lymphatic fluorescence transport from the NIR imaging measurements between the timepoints analyzed. Two-way ANOVA test with Šídák's multiple comparisons tests were used to compare the natural logarithm of fluorescent measurements from the 680IR NP experiments between saline and bestatin-treated mice at each timepoint. The NP fluorescent measurements were transformed using the natural logarithm to create a normal distribution of the data. Multiple linear regression was also used to investigate how NP fluorescence metrics correlated with both treatment and timepoint. The multiple linear regression model used the natural logarithm of the NP fluorescence metric as the dependent variable, with treatment and timepoint as the independent variables. The least-squares regression included terms for both independent variables and the interaction between them. Multiple Mann–Whitney tests using the Holm–Šídák method were used to compare leukocyte populations in dLNs between saline and bestatin-treated mice at each timepoint. Multiple Mann–Whitney tests using the Holm–Šídák method were used to compare normalized difference between saline

and bestatin-treated mice at each timepoint. GraphPad Prism was used for all statistical analysis.

3.4 Results

3.4.1 Leukocyte populations expand in dLNs during lymphedema progression

To study how various immune cell populations in dLNs change during lymphedema progression, we used a single vessel ligation lymphedema mouse tail model developed by our group [110]. This model leaves one collecting vessel trunk intact, allowing for drainage from the site of injury to the LN downstream of the functioning vessel, referred to as the intact vessel dLN, while the LN downstream of the ligated vessel, referred to as the injured vessel dLN, experiences inhibited lymph inflow. Both sacral LNs (dLNs) that normally drain the mouse tail were harvested at multiple timepoints (2 days, 1, 2, and 3 weeks) following lymphedema induction, dispersed into single cell suspensions, stained with antibodies against a variety of leukocyte markers, and analyzed on a flow cytometer. We found that the sum of leukocyte populations in both dLNs significantly increased during the swelling following lymphedema induction. The number of various leukocyte populations were overall increased in summed dLNs three weeks post-surgery (3W), including T (CD3+) and B (CD19+) cells, myeloid cells (CD11b+), monocytes (CD11b+ CD64+), macrophages (CD11b+ F480+), M1 macrophages (CD11b+ F480+ MHCII+), M2 macrophages (CD11b+ F480+ CD206+), dendritic cells (CD11c+ MHCII+), and neutrophils (CD11b+ Ly6G+) (Figure 3.4A and Figure 3.5A). With respect to their distribution amongst total leukocytes, T cell frequencies decreased somewhat whereas B cells increased by 3W (Figure 3.4B). Frequencies of dendritic cells, monocytes, macrophages, M1 macrophages, M2 macrophages, and neutrophils also significantly increased by 3W (Figure 3.4B and Figure 3.5B). This data suggests that leukocytes expand extensively in the dLNs following lymphedema induction in a manner that is not specific to a particular leukocyte subset. Interestingly, the dLNs transition from a T cell majority composition to

a roughly equal number of T and B cells as swelling increases. It remains to be investigated the extent that this change in distribution is driven by differences in lymphocyte proliferation or migration.

3.4.2 T helper cells increase as a percentage of T cells in dLNs during lymphedema development

Previous studies have identified CD4+ T helper cells as key drivers of lymphedema progression, including their roles in increasing tissue fibrosis and reducing lymphatic function [75, 76]. To analyze how T cell subpopulations in the dLNs change during disease progression in our model, we used flow cytometry to again analyze cell populations in the dLNs, this time analyzing changes in T helper cells (CD3+ CD4+) and cytotoxic T cells (CD3+ CD8+). Given the observed changes in T cells shown in Figure 1, we quantified these T cell subpopulations only at 2W following lymphedema surgery, when the increase in T cells in the dLNs is first observed. Compared to an unoperated control, both T helper cells and cytotoxic T cells are increased in dLNs at the 2W timepoint (Figure 3.6A). However, we found that T helper cells as a percentage of T cells increased in dLNs at the 2W timepoint, while there was no measured change in cytotoxic T cells as a percentage of T cells (Figure 3.6B). We also found a positive correlation between change in tail volume and percentage of T cells for T helper cells ($p=0.1323$), while there was a negative correlation for cytotoxic T cells ($p=0.1150$) (Figure 3.6C). These results show that CD4+ T helper cells make up a larger proportion of T cells in the dLNs as swelling manifests during lymphedema progression. This data corresponds well with previous studies which have shown similar increases in CD4+ T helper cells in lymphedematous tissue and have implicated CD4+ T helper cell migration from dLNs to peripheral tissues as a key driver of lymphedema [75, 76].

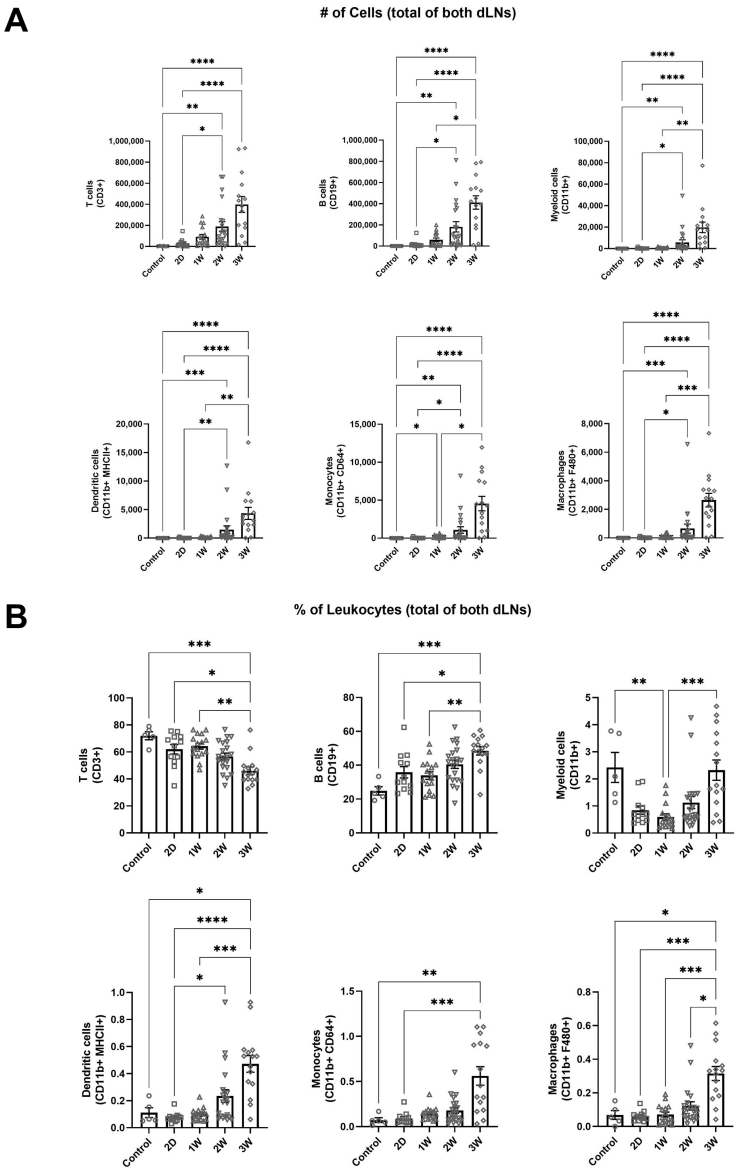

Figure 3.4: Leukocyte populations increase in dLNs during lymphedema progression. (A) Number of T cells, B cells, CD11b+ cells, dendritic cells, monocytes, and macrophages in dLNs for an unoperated control and after single vessel ligation lymphedema surgery at 2D, 1W, 2W, and 3W timepoints. Represented as the sum of the two dLNs. (B) T cell, B cell, CD11b+ cell, dendritic cell, monocyte, and macrophage frequencies of total leukocytes within dLNs for an unoperated control and after single vessel ligation lymphedema surgery at 2D, 1W, 2W, and 3W timepoints. Represented as the sum of the two dLNs for each leukocyte type divided by the sum of total leukocytes within the two dLNs. Kruskal-Wallis tests with Dunn's multiple comparisons were used to compare between timepoints for both number of cells and percentage of leukocytes. Control (n=6), 2D (n=14), 1W (n=16), 2W (n=21), 3W (n=15). Mean ± s.e.m. $^{*}(p < 0.05)$,$^{**}(p < 0.01)$,$^{***}(p < 0.001)$,$^{****}(p < 0.0001)$.

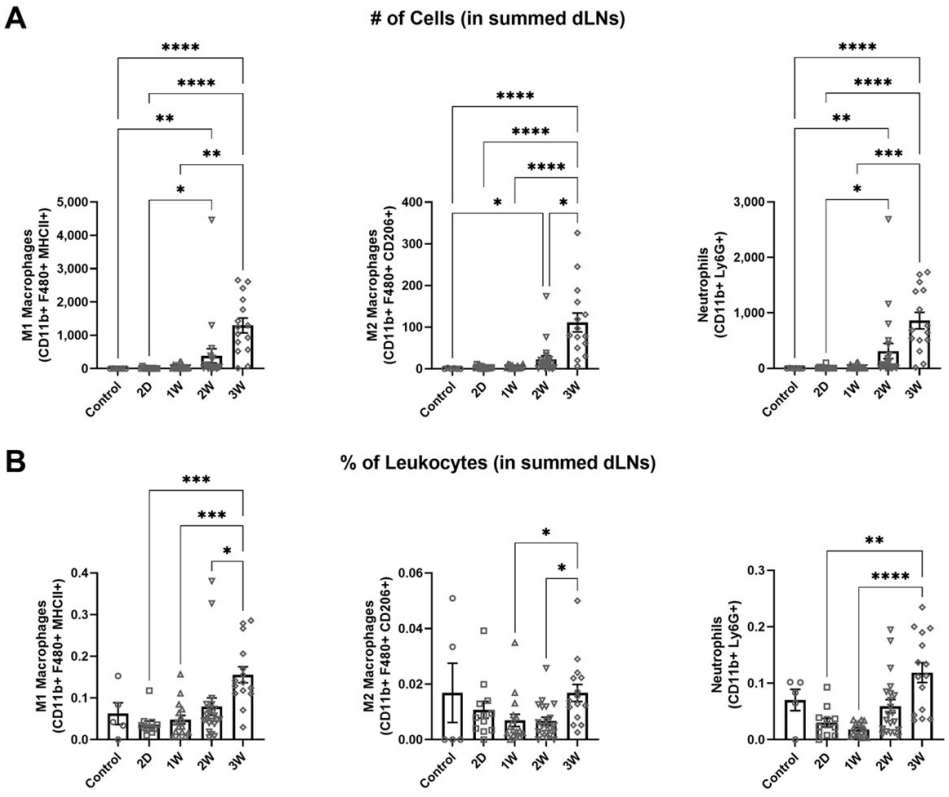

Figure 3.5: M1 and M2 macrophage and neutrophil populations increase in dLNs during lymphedema progression. (A) Number of M1 macrophages, M2 macrophages, and neutrophils in dLNs for an unoperated control and after single vessel ligation lymphedema surgery at 2D, 1W, 2W, and 3W timepoints. Represented as the sum of the two dLNs. (B) M1 macrophage, M2 macrophage, and neutrophil frequencies of total leukocytes within dLNs for an unoperated control and after single vessel ligation lymphedema surgery at 2D, 1W, 2W, and 3W timepoints. Represented as the sum of the two dLNs for each leukocyte type divided by the sum of total leukocytes within the two dLNs. Kruskal-Wallis tests with Dunn's multiple comparisons were used to compare between timepoints for both number of cells and percentage of leukocytes. Control (n=6), 2D (n=14), 1W (n=16), 2W (n=21), 3W (n=15). Mean ± s.e.m. $^{*}(p < 0.05),^{**}(p < 0.01),^{***}(p < 0.001),^{****}(p < 0.0001)$.

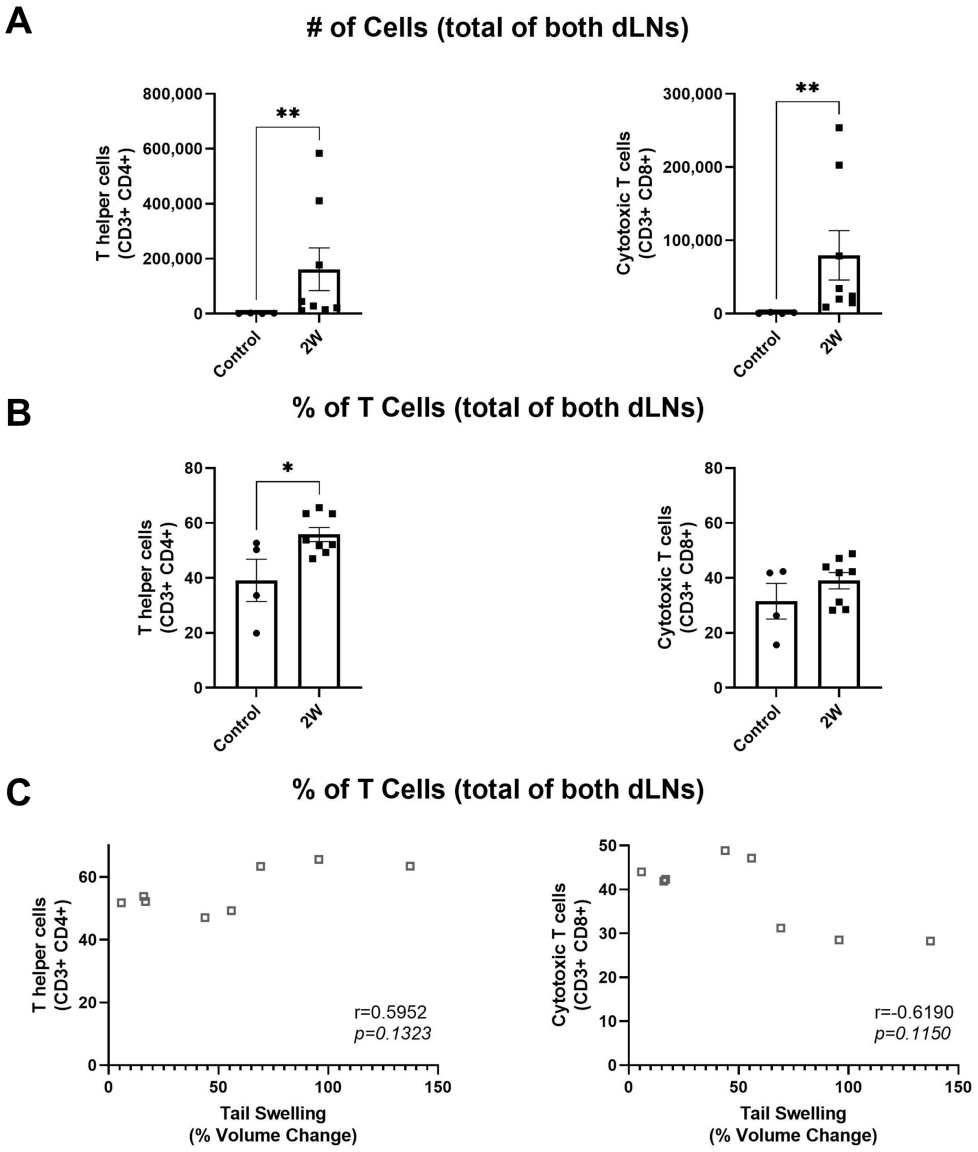

Figure 3.6: T helper cells increase as a percentage of T cells in dLNs during lymphedema development while cytotoxic T cells do not. (A) Number of T helper cells and cytotoxic T cells in dLNs for an unoperated control and after single vessel ligation lymphedema surgery at 2W timepoint. Represented as the sum of the two dLNs. Mann-Whitney tests were used for comparison between groups. (B) T helper cell and cytotoxic T cell percentages of T cells within dLNs for an unoperated control and after single vessel ligation lymphedema surgery at 2W timepoint. Represented as the sum of the two dLNs for T cell subtype divided by the sum of total T cells within the two dLNs. Unpaired T tests were used for comparison between groups. Control (n=4), 2W (n=8). Mean ± s.e.m. $^{*}(p < 0.05),^{**}(p < 0.01)$. (C) Spearman's rank correlation between percent of T cells and percent volume change following single vessel ligation lymphedema surgery for T helper cells and cytotoxic T cells.

3.4.3 B cells, but not T cells, proliferate in dLNs following single vessel ligation surgery

Following our observation that leukocytes expanded in dLNs following single vessel ligation surgery, we were interested in determining if this expansion occurred due to proliferation of leukocytes within the dLNs. To test this we added Ki67, a known proliferative marker, to our flow cytometry panel to both measure total proliferation of cells within the dLNs and specific proliferation of various leukocytes. Given that T and B cells make up the majority of leukocytes within the dLNs, we focused on analyzing the Ki67 expression of these cells. At two weeks following single vessel ligation surgery, we found that B cells expressed increased Ki67 expression in sacral LNs (dLNs) compared to popliteal LNs (non-draining LNs), measured by both total number of Ki67+ B cells (Figure 3.7A) and the percentage of B cells which are Ki67+ (Figure 3.7B). T cells showed no increased Ki67 expression in dLNs, either by total number (Figure 3.7C) or percentage (Figure 3.7D). We additionally quantified the ratio of the percentage of Ki67+ cells between the sacral LNs and the popliteal LNs for both lymphocyte subpopulations, finding that B cells showed a significantly higher ratio compared to T cells (Figure 3.7E). The sham surgery group showed no significant differences in Ki67 expression between the sacral and popliteal LNs for either B or T cells (Figure 3.7F-J). These results suggest that the increase in the B cell population is driven by increased proliferation of B cells within dLNs during lymphedema development, while this same proliferation is not observed in the T cell population.

3.4.4 Tail swelling correlates with changes in leukocyte populations in dLNs

Similar to the varied presentation of lymphedema clinically, the single vessel ligation lymphedema mouse tail model used in this study results in a swelling response of the tail that varies amongst animals in its severity as well as rate of progression. This allows how the extent of swelling impacts leukocyte populations in the intact vessel dLN to be studied. The swelling observed herein showed a similar increase in tail volume as observed in previous reports, with percent volume change reaching a maximum at 3W (Figure 3.8). Using

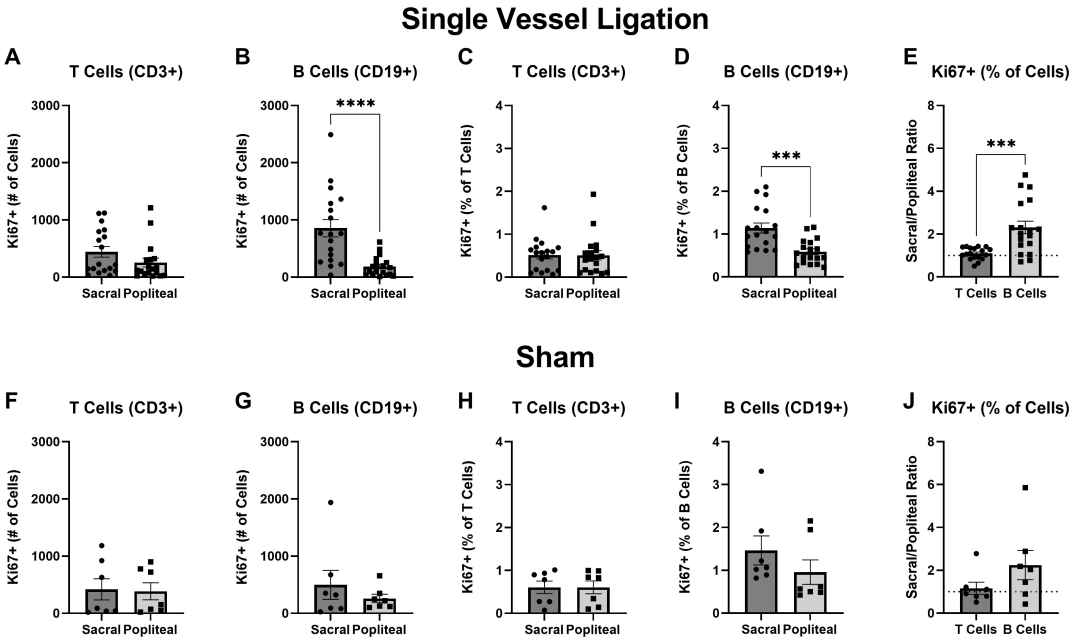

Figure 3.7: B cells in dLNs, but not T cells, significantly express Ki67 following single vessel ligation surgery to induce lymphedema. Lymphocytes in the dLNs were analyzed using flow cytometry and Ki67 staining was used to measure cell proliferation at 2W after surgery. Mice underwent either (A-E) single vessel ligation or (F-J) sham surgery. Number of Ki67+ (A,F) T cells and (B,G) B cells in the sacral (dLNs) and popliteal (non-dLNs). Represented as the sum of the two LNs. Percentage of (C,H) T cells and (D,I) B cells that express Ki67 in the sacral and popliteal LNs. Represented as the sum of the Ki67+ cells from the two LNs divided by the sum of the parent cells within the two LNs. (E,J) Sacral/Popliteal ratio for percentage of T and B cells that express Ki67. Mann-Whitney tests were used to compare between groups. Single Vessel Ligation (n = 18), Sham (n = 7). Mean ± s.e.m. $^{*}(p < 0.05)$,** $(p < 0.01)$,*** $(p < 0.001)$,**** $(p < 0.0001)$.

Spearman's rank correlation, we found that the numbers of T cells, B cells, dendritic cells, macrophages, M1 macrophages, monocytes, and neutrophils within the intact vessel dLN were all positively correlated with the percent change in volume of the tail (Figure 3.10A and Figure 3.9A). This result showed that leukocyte expansion in the intact vessel dLN was related to the extent of tail swelling observed in this lymphedema model. Additionally, we found that leukocyte populations as a fraction of total leukocytes in the intact vessel dLN correlated with swelling for a variety of cell types. T cell fraction negatively correlated with swelling, while B cell fraction positively correlated with swelling (Figure 3.10B). Other leukocyte populations, including dendritic cells, macrophages, M1 macrophages, monocytes, and neutrophils, also had positive correlations between swelling and frequency (Figure 3.10B and Figure 3.9B). These results follow from the changes observed in leukocyte populations in the dLNs over time as swelling also increases by the 3W timepoint in this model.

3.4.5 Increased accumulation of lymph-draining nanoparticles within intact vessel dLN compared to injured vessel dLN following single vessel ligation diminishes as swelling progresses

To measure transport to and NP accumulation within dLNs, we used a NP system that has been previously shown to preferentially drain into lymphatic vessels after injection and accumulate within dLNs [134–138]. These NPs were covalently conjugated to fluorophore IRdye 680RD (LI-COR Biotechnology, Lincoln, NE, USA) using an irreversible linker and intradermally injected into the tip of the tail one day prior to harvesting of the dLNs. After dissecting the LNs at various time points, we measured the fluorescence in the LNs at the 700 nm emission wavelength of the dye using an Olympus NIR imaging microscope. Using these images (Figure 3.11A), we calculated multiple metrics including maximum fluorescence intensity within the LN, mean fluorescence intensity within the LN (normalized to background fluorescence), and the sum of the fluorescence intensity within the LN (normal-

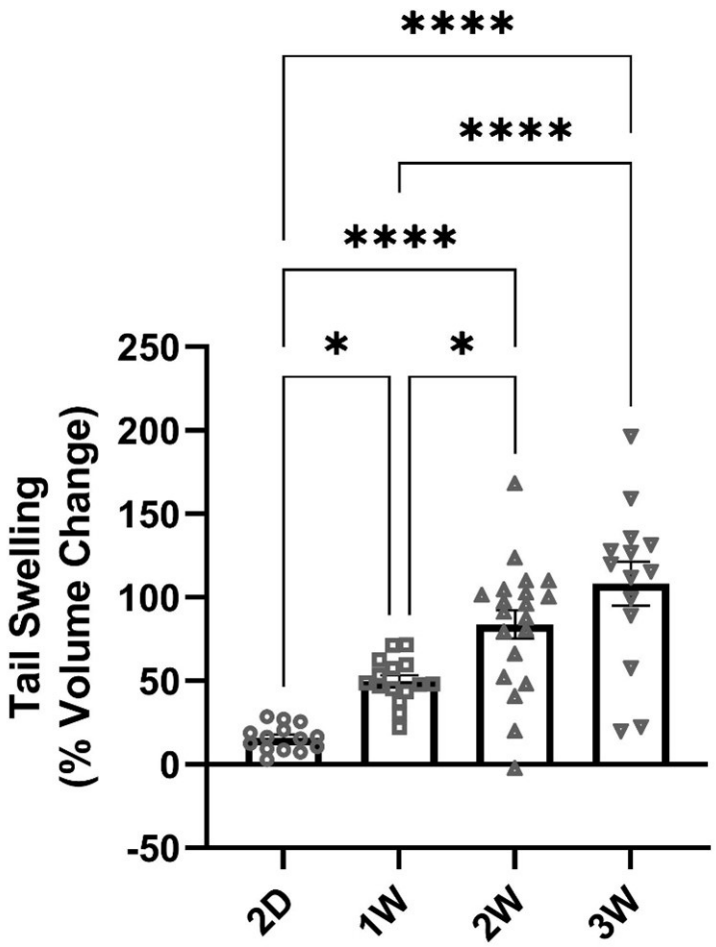

Figure 3.8: Tail swelling following single vessel ligation surgery. Tail swelling following single vessel ligation surgery measured as percent change in volume from presurgery baseline. Swelling was measured at endpoint, specifically at 2D, 1W, 2W, and 3W timepoints. One-way ANOVA tests with Tukey's multiple comparisons were used to compare between timepoints. Mean ± s.e.m. $^{*}(p < 0.05)$,**** $(p < 0.0001)$.

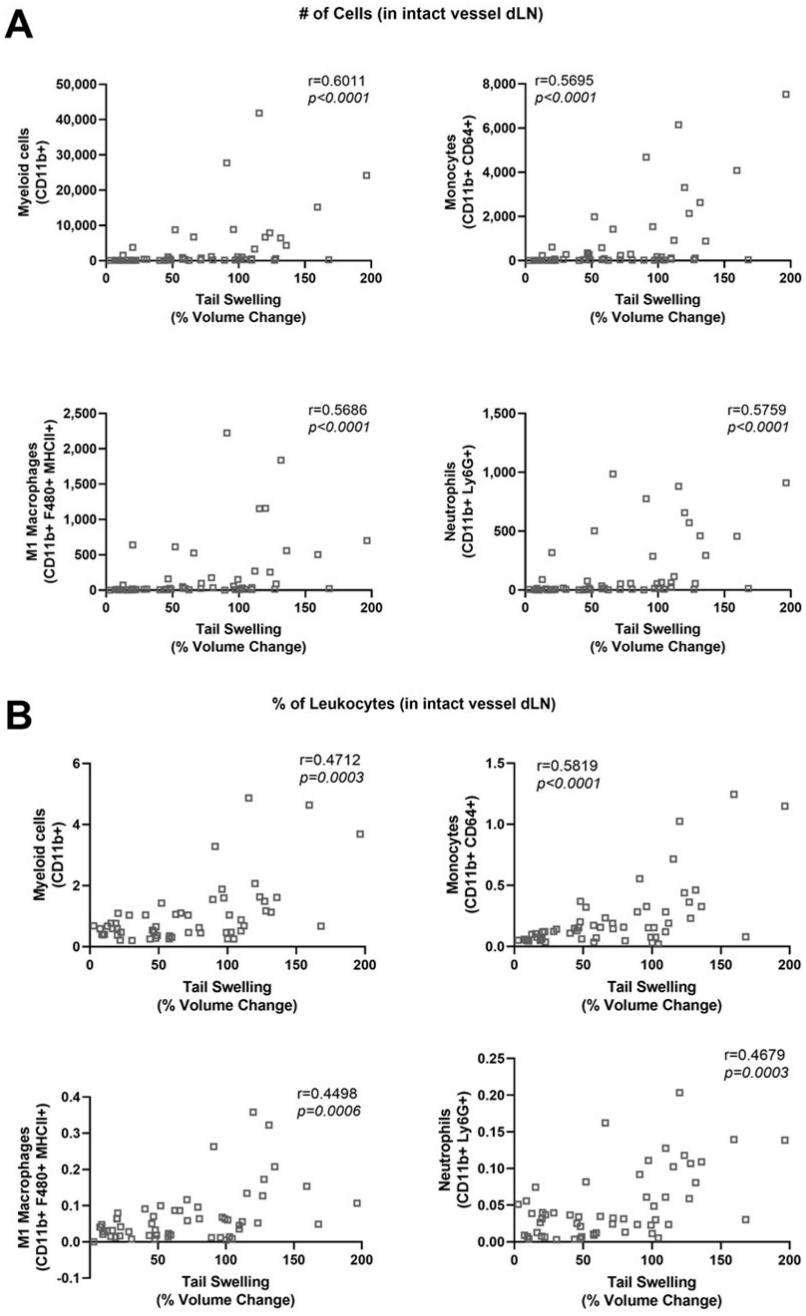

Figure 3.9: Myeloid cell expansion in dLNs correlates with increase in tail volume after lymphedema surgery. (A) Spearman's rank correlation between number of cells in intact vessel dLN and percent volume change following single vessel ligation lymphedema surgery for myeloid cells, monocytes, M1 macrophages, and neutrophils. (B) Spearman's rank correlation between fraction of leukocytes in intact vessel dLN and percent volume change following single vessel ligation lymphedema surgery for myeloid cells, monocytes, M1 macrophages, and neutrophils.

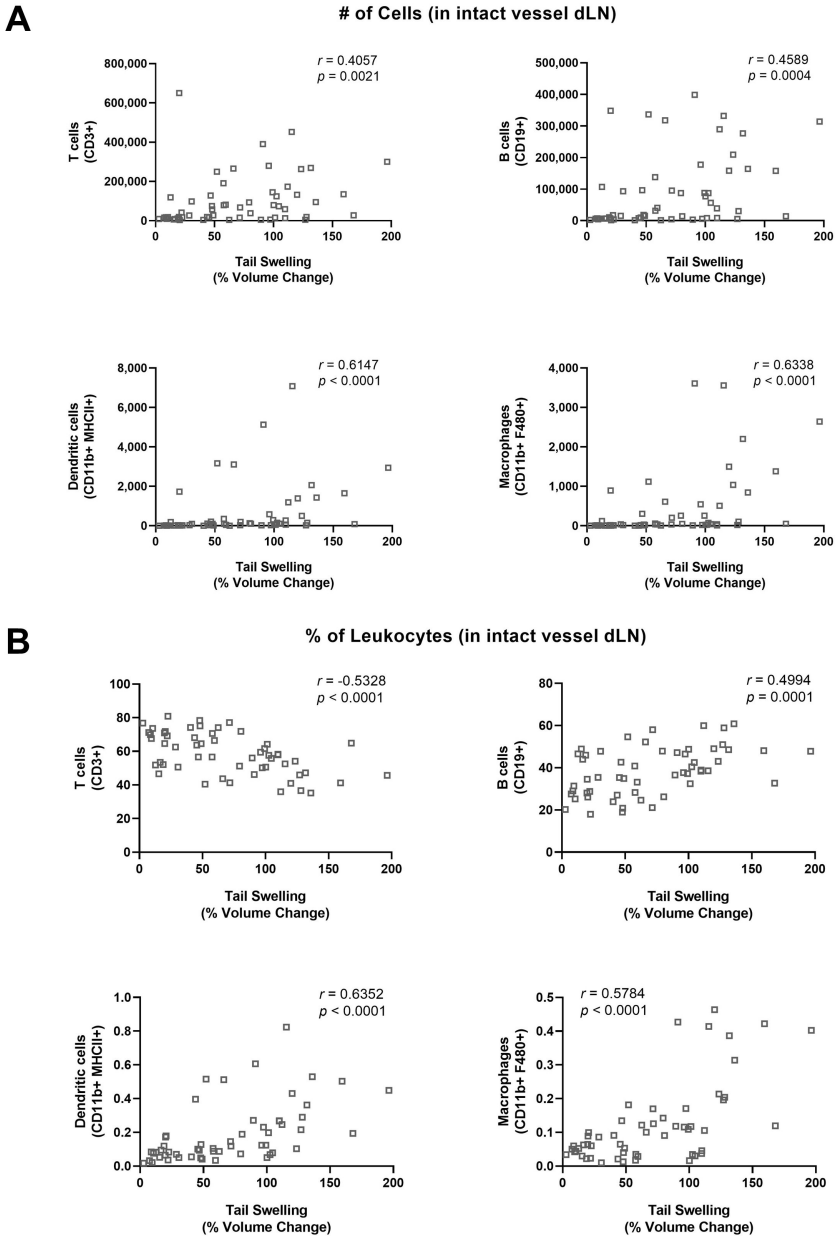

Figure 3.10: Leukocyte expansion in dLNs correlates with increase in tail volume after lymphedema surgery. (A) Spearman's rank correlation between number of cells in intact vessel dLN and percent volume change following single vessel ligation lymphedema surgery for T cells, B cells, dendritic cells, and macrophages. (B) Spearman's rank correlation between fraction of leukocytes in intact vessel dLN and percent volume change following single vessel ligation lymphedema surgery for T cells, B cells, dendritic cells, and macrophages.

ized to background fluorescence). The natural logarithm was used to transform each metric to form a normal distribution and allow for statistical analysis using parametric methods. NP fluorescence (both the maximum measured signal and normalized mean) within the intact vessel dLN decreased significantly at 2W compared to 2D, and at 3W compared to 2D and 1W (Figure 3.11B). The size of the intact vessel dLN also significantly increased between 2D and 3W, in alignment with the flow cytometrically measured cellular expansion of the intact vessel dLN leukocyte populations (Figure 3.11B). The normalized sum of fluorescence in the intact vessel dLN does not significantly change at any timepoint, possibly indicating that the reduction in mean and maximum fluorescence is due to the same amount of NP spread out over the increased LN area (Figure 3.11B). From the metrics used in our analysis, normalized sum of fluorescence best represents overall NP drainage to the dLN given that it represents the total fluorescent signal from NPs trafficked to the dLN. It is important to note that the increased LN area does not result in increased NP accumulation as measured by normalized sum of fluorescence, even though the capacity of the LN for NP accumulation likely increases with LN area. The normalized sum of fluorescence increases in the injured vessel dLN at 3W compared to 2D and 1W, suggesting that partial collateralization of the lymphatic network has occurred, and transport has been partially restored to the injured vessel dLN (Figure 3.11C). Additionally, the ratio of NP fluorescence in the intact vessel dLN to that in the injured vessel dLN was significantly increased at 2D and 1W compared to 3W and at 2D compared to 2W for maximum fluorescence. The ratio was also significantly increased at 2D and 1W compared to 2W and 3W for normalized mean fluorescence and at 2D and 1W compared to 3W for normalized sum of fluorescence (Figure 3.11D). The change in this ratio shows that NP accumulation in the intact vessel dLN is significantly higher than the injured vessel dLN within 1W of the surgery, while after 2W as swelling progresses the differences between the injured and intact vessel dLNs are diminished. Restoration of transport to the injured vessel dLN partially explains the loss of differences between the dLNs as lymphedema develops.

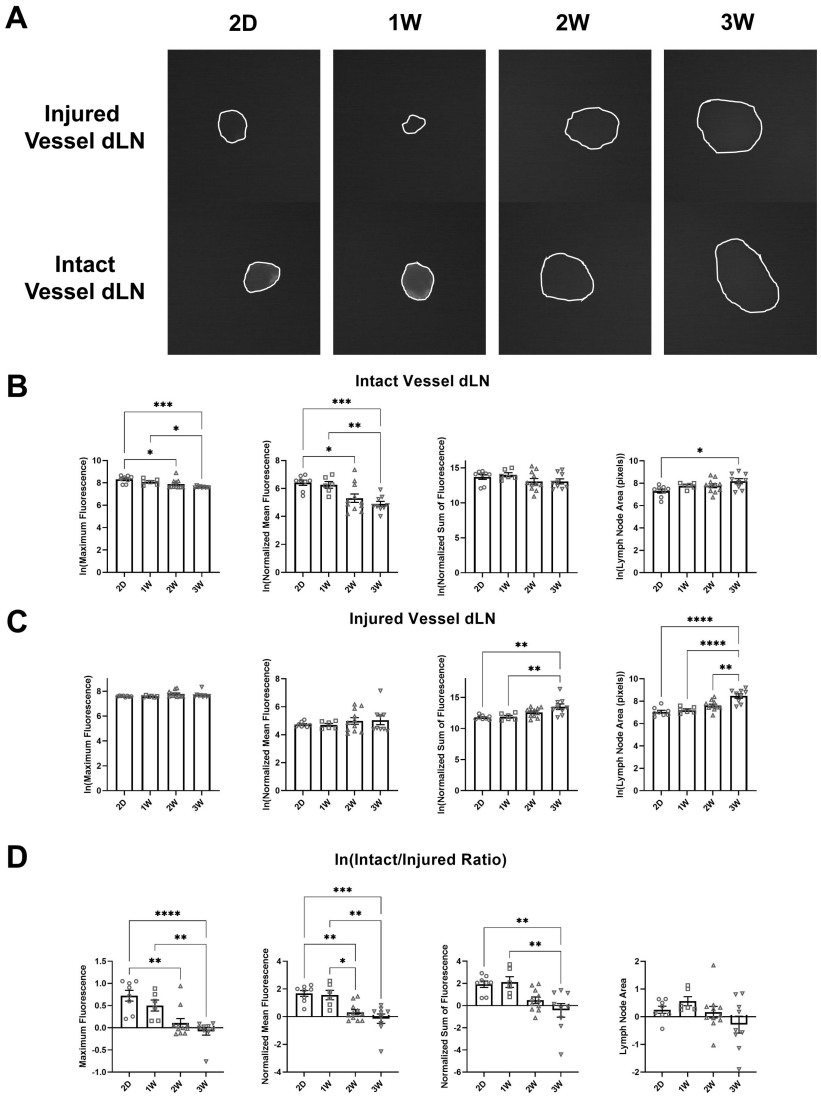

Figure 3.11: Lymph-draining NP accumulation within the intact vessel dLN decreases during lymphedema progression. (A) Fluorescent images of LNs harvested 24 hours after injection of NPs conjugated with 680 IR Dye at 2D, 1W, 2W, and 3W timepoints. (B) Natural logarithm of maximum fluorescence, normalized mean fluorescence, normalized sum of fluorescence, and LN area for the intact vessel dLN at 2D, 1W, 2W, and 3W timepoints. (C) Natural logarithm of maximum fluorescence, normalized mean fluorescence, normalized sum of fluorescence, and LN area for the injured vessel dLN at 2D, 1W, 2W, and 3W timepoints. (D) Natural logarithm of the intact/injured ratio for maximum fluorescence, normalized mean fluorescence, normalized sum of fluorescence, and LN area at 2D, 1W, 2W, and 3W timepoint. One-way ANOVA tests with Tukey's multiple comparisons were used to compare between timepoints for B, C, and D. 2D (n=8), 1W (n=6), 2W (n=11), 3W (n=9). Mean ± s.e.m. $^{*}(p < 0.05)$,** $(p < 0.01)$,*** $(p < 0.001)$,**** $(p < 0.0001)$.

3.4.6 Increased Leukocyte Expansion in the Intact Vessel dLN Following Single Vessel Ligation

Immune cell expansion in the intact vessel dLN was compared to that of the injured vessel dLN post injury. We found no significant differences between intact and injured vessel dLNs for any of the leukocyte populations we surveyed (Figure 3.12). However, certain trends were apparent, including an increase in number of cells in the intact vessel dLN compared to the injured vessel dLN at the 1W timepoint. Equation 3.1 shows the calculation for a metric we call normalized difference,

$$NormDiff = \frac{Cells(IntVesseldLN) - Cells(InjVesseldLN)}{Cells(IntVesseldLN) + Cells(InjVesseldLN)} \tag{3.1}$$

which is positive if more cells are in the intact vessel dLN, and negative if more cells are in the injured vessel dLN. Normalized difference was significantly increased at 1W compared to 3W for monocytes, macrophages, and M1 macrophages (Figure 3.13A). Additionally, a similar trend at 1W was observed for all other leukocyte populations. This indicates that a larger proportion of leukocytes were within the intact vessel dLN at 1W compared to the injured vessel dLN, but these differences were lost by 2W. Interestingly these differences were most pronounced in cell populations known to be highly migratory, including monocytes and macrophages. Previous studies in our lab have shown that contractile function in the intact lymphatic vessel in this model decreases significantly by the 2W timepoint [110]. The loss of preferential proliferation and migration in the intact vessel dLN may be due to loss of function in the intact vessel [110]. To analyze whether lymphatic transport to the dLNs as measured by NIR-labeled NP accumulation within the dLNs was correlated with local leukocyte expansion, we plotted normalized difference for the total number of live cells versus the intact/injured ratio for maximum, normalized mean, and normalized sum of fluorescence. We found that normalized difference was positively correlated with each of these metrics (Figure 3.13B). This indicates that the differential transport of NPs to the

dLNs was correlated with the differential expansion of cells within the dLNs. Normalized difference was also positively correlated with the intact/injured ratio for LN area, showing that the number of cells identified via flow cytometry correlated with the size of the dLN (Figure 3.13B).

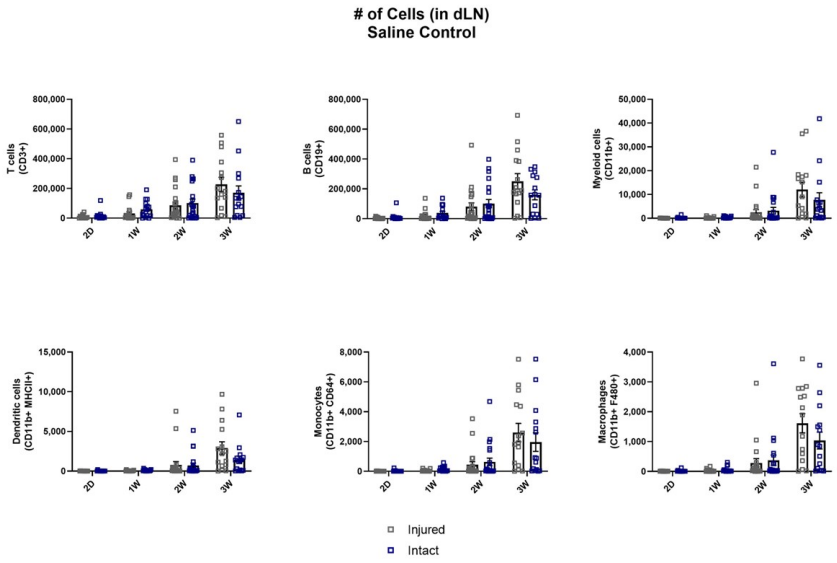

Figure 3.12: Leukocyte expansion in intact versus injured vessel dLNs during lymphedema progression. Number of T cells, B cells, CD11b+ cells, dendritic cells, monocytes, and macrophages in both injured and intact vessel dLNs after single vessel ligation lymphedema surgery at 2D, 1W, 2W, and 3W timepoints. Multiple Mann-Whitney tests using the Holm-Šídák method were used to compare between injured and intact vessel dLNs at each timepoint. Mean ± s.e.m.

3.4.7 Bestatin Treatment Increases Nanoparticle Accumulation within the Intact Vessel dLN during Later Stages of Lymphedema Progression

LTB_4 is a known chemoattractant and has been shown to play a bimodal role in lymphangiogenesis, with low concentrations being lymphangiogenic and high concentrations being anti-lymphangiogenic [111, 121, 139]. Previous studies suggest that LTB_4 levels increase during lymphedema, and these high levels of LTB_4 in lymphedema inhibit lymphangiogenesis and resolution of swelling, thus driving progression of the disease [111]. We were interested in studying how antagonism of LTB_4 may modulate lymphatic function during

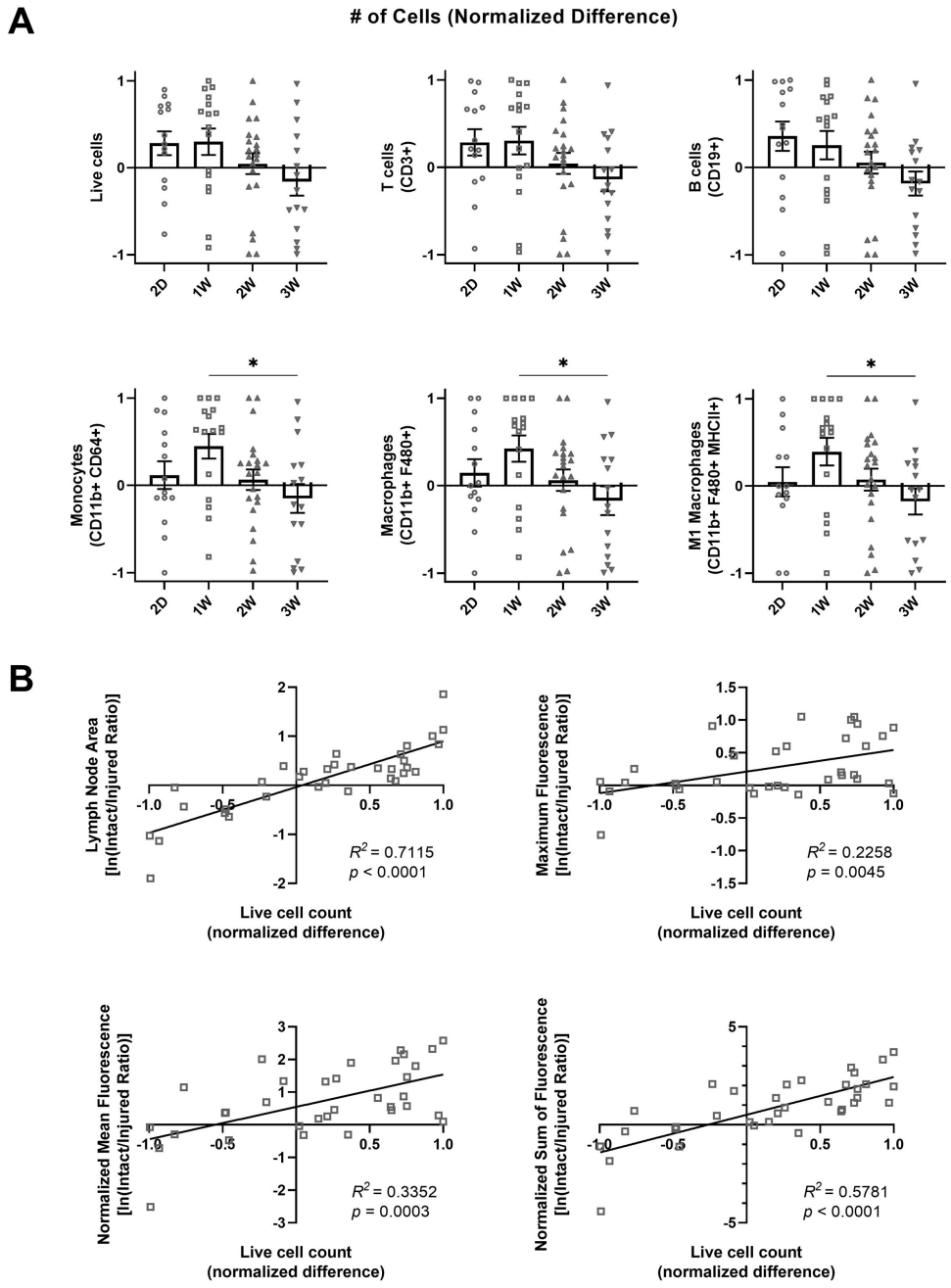

Figure 3.13: Differential leukocyte expansion between the dLNs is correlated with differential NP accumulation. (A) Normalized difference between intact and injured vessel dLNs for number of live cells, T cells, B cells, monocytes, macrophages, and M1 macrophages at 2D, 1W, 2W, and 3W timepoints. Kruskal–Wallis tests with Dunn's multiple comparisons were used to compare between timepoints. Mean ± s.e.m. $^{*}(p < 0.05)$. (B) Linear correlations and Pearson's correlation coefficient (R2) between normalized difference of number of live cells and the natural logarithm of intact/injured ratio for LN area, maximum fluorescence, normalized mean fluorescence, and normalized sum of fluorescence.

lymphedema progression. To approach this question, we treated mice with daily injections of bestatin, an LTB_4 antagonist, starting 3 days after surgery. Even with this measured change in lymphatic contractile function, bestatin did not reduce tail swelling compared to the saline group at any of the timepoints analyzed (Figure 3.14B). To measure NP uptake to and accumulation within the dLNs, we harvested the dLNs at 1W, 2W, and 3W after single vessel ligation surgery. As described previously, one day prior to LN harvest, NIR-labeled NPs were injected intradermally into the tail. After LN harvest, we again used our NIR imaging setup to take fluorescent images of the dLNs and quantify maximum, normalized mean, and normalized sum of fluorescence (Figure 3.14C). We found that bestatin-treated mice had increased NP accumulation in the intact vessel dLN at 3W compared to the saline control group, quantified through both normalized mean fluorescence and normalized sum of fluorescence (Figure 3.14D). We also used multiple linear regression to analyze how both treatment and time correlated with NP fluorescent measurements. The coefficient of the interaction term between treatment and time in the linear regression model was significantly correlated for normalized sum of fluorescence ($p = 0.0307$) and close to significant for normalized mean fluorescence ($p = 0.0509$), showing that the slopes of these NP fluorescent measurements in the intact vessel dLN versus time were different between treatment groups. However, fluorescence in the injured vessel dLN at 3W showed no difference between the bestatin and saline groups (Figure 3.15). Additionally, there were no significant differences in the intact/injured ratio for these fluorescence metrics between the bestatin and saline groups (Figure 3.14E). These results suggest that LTB_4 antagonism through bestatin treatment increases transport and accumulation of NPs to the intact vessel dLN during lymphedema progression. The return of fluid transport to the injured vessel dLN, however, was not significantly altered by bestatin treatment. Taken together, these results suggest that antagonism of LTB_4 through bestatin treatment increases transport and accumulation of NPs to the dLNs, specifically in the vessel left intact following single vessel ligation surgery.

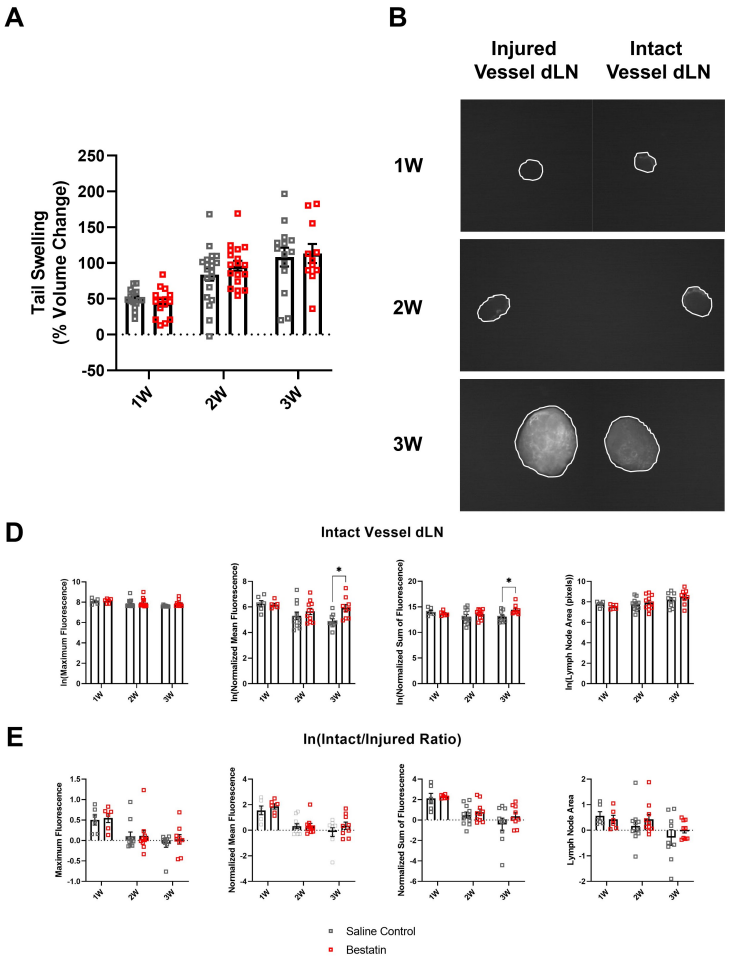

Figure 3.14: Bestatin treatment increases NP accumulation in the intact vessel dLN during lymphedema progression. (A) Lymphatic fluorescence transport measured from NIR imaging of in vivo lymphatic collecting vessel contraction at 1W, 2W, and 4W timepoints. A mixed-effects model with Šídák's multiple comparisons was used to compare between treatments for each timepoint. Saline Control: 1W (n = 11), 2W (n = 11), 4W (n = 7); Bestatin: 1W (n = 9), 2W (n = 9), 4W (n = 5). $^{*}(p < 0.05),^{**}(p < 0.01)$. (B) Tail swelling following single vessel ligation surgery measured as percent change in volume from presurgery baseline for both bestatin-treated and saline control groups. Swelling of bestatin-treated mice was measured at endpoint, specifically at 1W, 2W, and 3W timepoints. (C) Fluorescent images of LNs harvested from bestatin-treated mice 24 h after injection of NPs conjugated with 680 IR Dye at 1W, 2W, and 3W timepoints. (D) Natural logarithm of maximum fluorescence, normalized mean fluorescence, normalized sum of fluorescence, and LN area in the intact vessel dLN for the saline control group and the bestatin-treated group at 1W, 2W, and 3W timepoints. (E) Natural logarithm of the intact/injured ratio for maximum fluorescence, normalized mean fluorescence, normalized sum of fluorescence, and LN area for the saline control group and the bestatin-treated group at 1W, 2W, and 3W timepoint. Two-way ANOVA with Šídák's multiple comparisons to compare between treatments at each timepoint for C and D. 1W (n = 6), 2W (n = 11), 3W (n = 9). Mean ± s.e.m. $^{*}(p < 0.05)$.

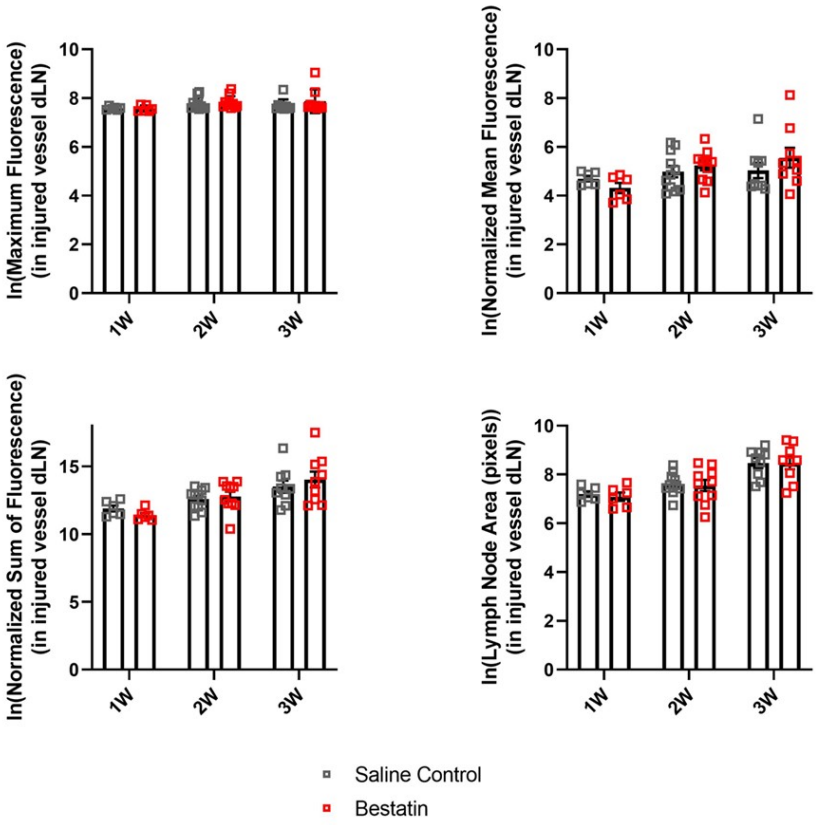

Figure 3.15: Bestatin treatment does not change NP uptake to the injured vessel dLN during lymphedema progression. Natural logarithm of maximum fluorescence, normalized mean fluorescence, normalized sum of fluorescence, and LN area in the injured vessel dLN for the saline control group and the bestatin-treated group at 1W, 2W, and 3W timepoints. Two-way ANOVA with Šídák's multiple comparisons to compare between treatments at each timepoint. 1W (n = 6), 2W (n = 11), 3W (n = 9). Mean ± s.e.m.

3.4.8 Bestatin Treatment Has No Significant Effect on Magnitude of Immune Response in dLNs during Lymphedema Progression

Given the observed increase in lymphatic function following bestatin treatment, we were interested in studying if LTB_4 mediated the observed immune cell expansion in the dLNs in the context of lymphedema. Using the flow cytometry protocol described earlier, we found that bestatin treatment had no significant effect on either number of leukocytes or frequency of leukocytes in the summed dLNs for the leukocyte subsets analyzed compared to the saline control group (Figure 3.16A,B). This data suggests that LTB_4 did not significantly modulate the increase in leukocytes in the dLNs observed during lymphedema progression. We also found that swelling correlated with both number and frequency of cells in the intact vessel dLN for bestatin-treated mice similarly to the correlations observed in untreated mice (Figure 3.17A,B). This result shows that in bestatin-treated mice the expansion of leukocytes in the dLNs was still directly correlated with the observed tail swelling.

3.4.9 Bestatin Treatment Leads to Leukocyte Expansion in the Intact Vessel dLN Compared to the Injured Vessel dLN

We also wanted to analyze how LTB_4 antagonism would differentially affect immune cell expansion in the intact vessel dLN versus the injured vessel dLN. We again analyzed the LNs separately at each timepoint, comparing total cell number between the intact and injured vessel dLNs for bestatin-treated mice. For bestatin-treated mice, the intact vessel dLNs had more T and B cells, myeloid cells, dendritic cells, monocytes, and macrophages than the injured vessel dLNs at 2W (Figure 3.18). Normalized difference was also significantly higher in the bestatin group compared to the control group at 2W for these leukocyte subsets (Figure 3.19A). Taken with the results from Figure 3.14A showing an increase in lymphatic contractile function following bestatin treatment at 2W after surgery, this data suggests that this increased lymphatic function may have been partially responsible for the differential leukocyte expansion between LNs at 2W following bestatin treatment. We

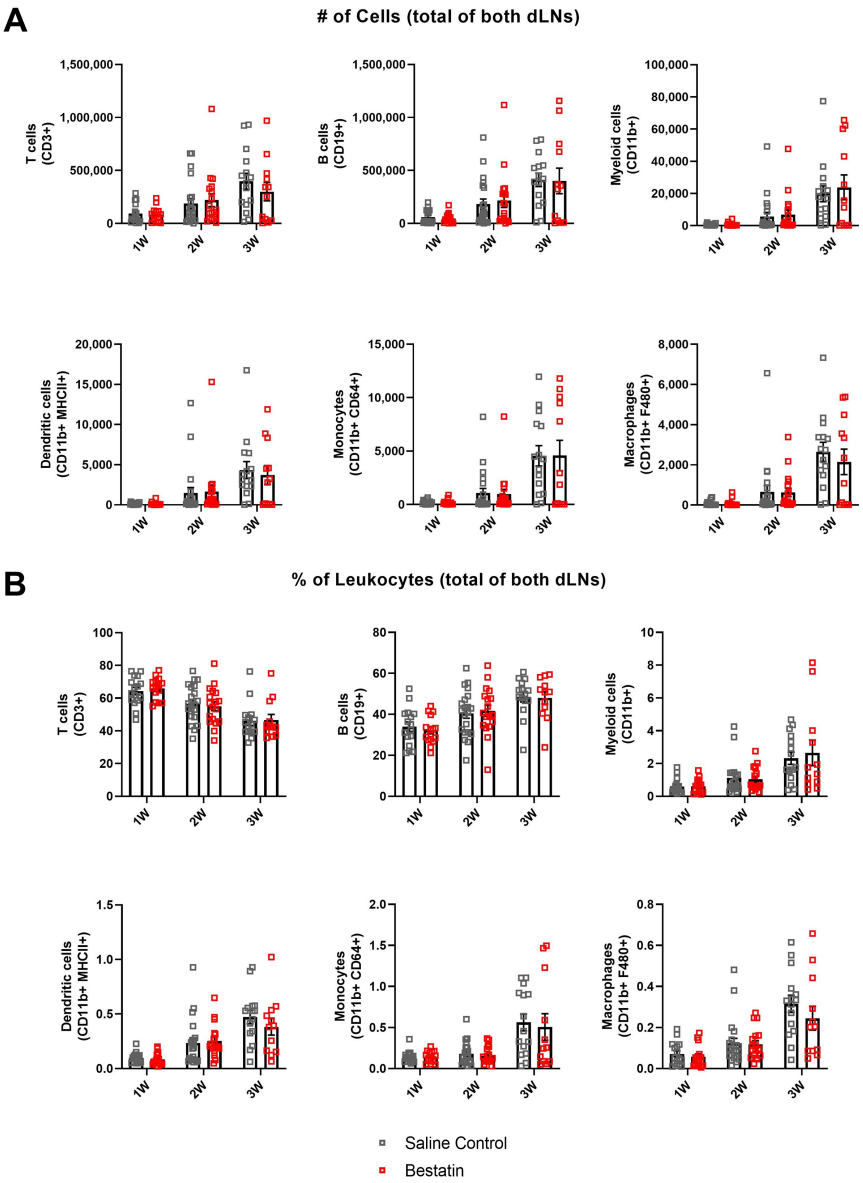

Figure 3.16: Bestatin treatment does not affect the overall leukocyte populations in the dLNs during lymphedema progression. (A) Number of T cells, B cells, CD11b+ cells, dendritic cells, monocytes, and macrophages in dLNs after single vessel ligation lymphedema surgery for the saline control group and the bestatin-treated group at 1W, 2W, and 3W timepoints. Represented as the sum within the two dLNs. (B) T cell, B cell, CD11b+ cell, dendritic cell, monocyte, and macrophage frequencies of total leukocytes within dLNs after single vessel ligation lymphedema surgery for the saline control group and the bestatin-treated group at 1W, 2W, and 3W timepoints. Represented as the sum within the two dLNs for each leukocyte type divided by the sum of overall leukocytes within the two dLNs. Multiple Mann–Whitney tests using the Holm–Šídák method were used to compare between treatments at each timepoint for both number of cells and percentage of leukocytes. 1W (n = 15), 2W (n = 18), 3W (n = 12). Mean ± s.e.m.

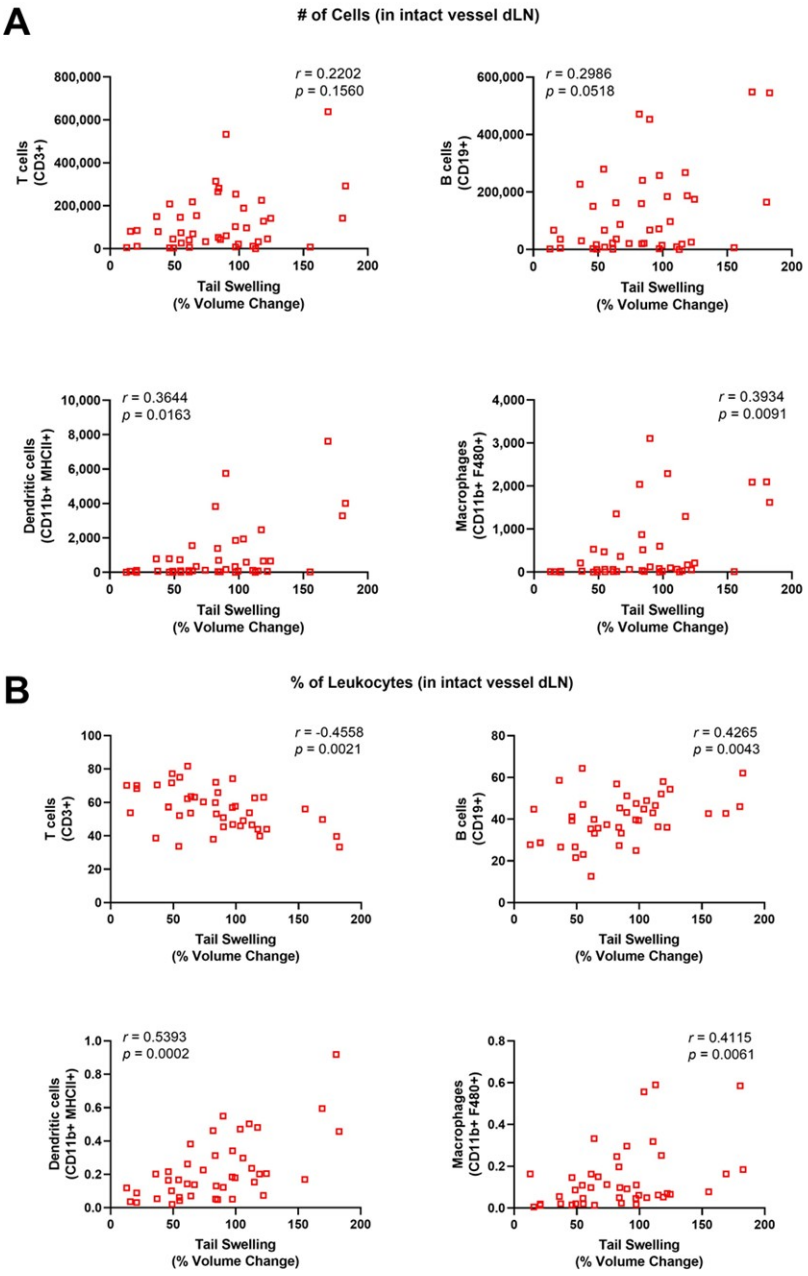

Figure 3.17: Leukocyte expansion in dLNs following bestatin treatment correlates with increase in tail volume after lymphedema surgery. (A) Spearman's rank correlation between number of cells in intact vessel dLN and percent volume change following single vessel ligation lymphedema surgery for T cells, B cells, dendritic cells, and macrophages. (B) Spearman's rank correlation between fraction of leukocytes in intact vessel dLN and percent volume change following single vessel ligation lymphedema surgery for T cells, B cells, dendritic cells, and macrophages. All data shown is from bestatin-treated mice.

also plotted NP fluorescence metrics versus normalized difference to determine if bestatin treatment altered the correlations observed between lymphatic function and dLN leukocyte expansion in the untreated group. For the bestatin-treated group, the intact/injured ratios of maximum fluorescence and normalized mean fluorescence showed no correlation with the normalized difference of cells in the dLNs, while the intact/injured ratio of normalized sum of fluorescence did show a positive correlation with normalized difference (Figure 3.19B). The intact/injured ratio of LN area was still positively correlated with normalized difference (Figure 3.19B). These results show that there was still a correlation between NP fluorescence in the dLNs and leukocyte expansion following bestatin treatment; however, the effects of bestatin treatment on normalized difference at 2W likely explain the loss of this correlation for maximum fluorescence and normalized mean fluorescence.

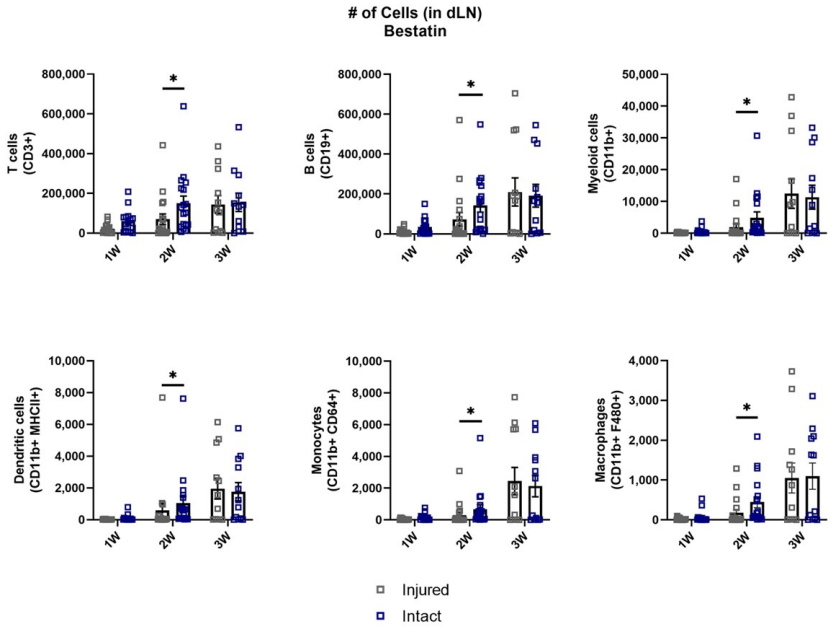

Figure 3.18: Leukocyte expansion in intact versus injured vessel dLNs following bestatin treatment during lymphedema progression. Number of T cells, B cells, CD11b+ cells, dendritic cells, monocytes, and macrophages in both injured and intact vessel dLNs following single vessel ligation lymphedema surgery and bestatin treatment at 1W, 2W, and 3W timepoints. Multiple Mann-Whitney tests using the Holm-Šídák method were used to compare between injured and intact vessel dLNs at each timepoint. Mean ± s.e.m. $^{*}(p < 0.05)$.

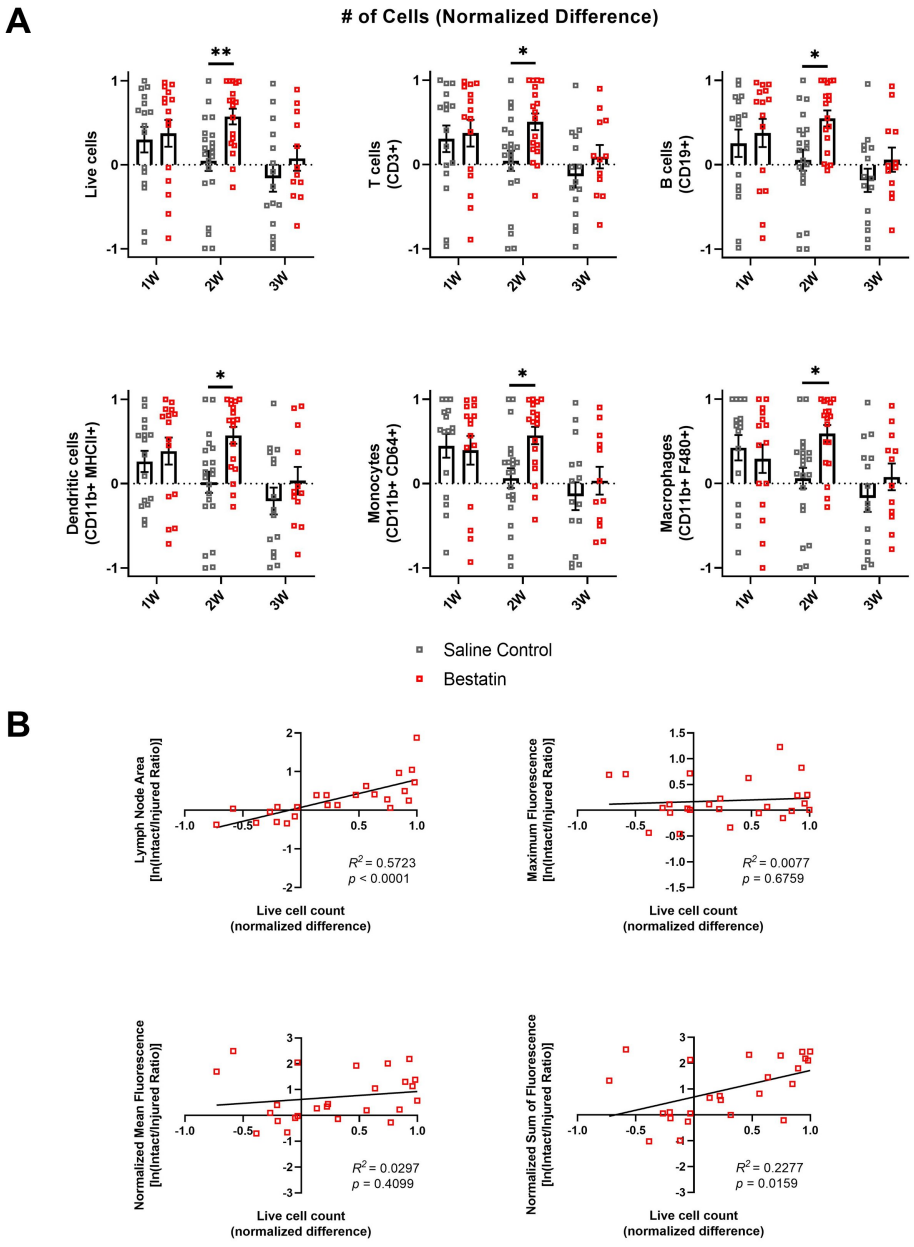

Figure 3.19: Bestatin treatment prolongs the differential leukocyte expansion of the intact compared to the injured vessel dLNs during lymphedema progression. (A) Normalized difference between intact and injured vessel dLNs number of total cells, T cells, B cells, dendritic cells, monocytes, and macrophages for the saline control group and the bestatin-treated group at 2D, 1W, 2W, and 3W timepoints. Multiple Mann–Whitney tests using the Holm–Šídák method were used to compare between treatments at each timepoint. Mean ± s.e.m. $^{*}(p < 0.05), ^{**}(p < 0.01)$. (B) Linear correlations and Pearson's correlation coefficient (R2) between normalized difference of number of live cells and the natural logarithm of intact/injured ratio for LN area, maximum fluorescence, normalized mean fluorescence, and normalized sum of fluorescence for the bestatin-treated group.

3.5 Discussion and Future Work

3.5.1 Leukocyte expansion is driven by B cell but not T cell proliferation

The immune response during lymphedema development has been previously well characterized in lymphedematous tissue [59, 75, 76, 78, 79, 81, 101, 111, 130, 132]. This study provides the first evidence that total levels of leukocytes within LNs draining the diseased tissue bed significantly increase during lymphedema progression (Figure 3.4A). Additionally, we show that B cell proliferation as quantified by Ki67 expression increases in dLNs following lymphedema development, but T cell proliferation is not significantly increased (Figure 3.7). We hypothesized that proliferation was at least partially responsible for the expansion of lymphocytes observed in dLNs as lymphocytes are not known to extensively traffic to LNs during inflammation [38, 140–143]. However, the lack of an increase in Ki67 expression by T cells was unexpected as T cells do expand in total number within the dLNs following lymphedema surgery. A previous study has suggested that CD4+ T cells migrate from dLNs to sites of injury during lymphedema development, although the mechanisms facilitating this migration remain unclear [76]. It is possible that proliferating T cells within dLNs exit the LNs during lymphedema development, potentially explaining why Ki67 expression by T cells within the LNs did not increase. This efflux of T cells from the dLNs may also counteract the expansion of LN resident T cells, possibly explaining why the frequency of T cells within the dLNs decreases during lymphedema progression, even as the overall number of T cells within the dLNs increases.

3.5.2 CD4+ T helper cells fraction in dLNs corresponds with swelling

Given previous studies which have implicated CD4+ T helper cells as key regulators of tissue fibrosis and lymphatic remodeling in lymphedema, we aimed to analyze the response of CD4+ T cells within dLNs [75–77, 79]. Our data suggests that CD4+ T cells increase as a percentage of T cells within the dLNs during lymphedema progression. Interestingly, the

mice with the most swollen tails at 2W following surgery also had the highest frequency of T helper cells within the dLNs (Figure 3.6C). Other studies which have analyzed T helper cell involvement in lymphedema have used the complete ligation mouse tail lymphedema model, which induces a larger swelling response than that seen in the single vessel ligation model used in our study [75, 76]. Taken together, it seems likely that T helper cells make up most T cells within both the dLNs and lymphedematous skin during significant tissue swelling. Our results show that the previously identified T helper cell response is present in the context of lymphedema development when lymphatic drainage from the lymphedema site remains intact and that dLNs are likely critical in facilitating this immune response.

3.5.3 Humoral immunity during lymphedema development

We have additionally identified that B cells increase in number during lymphedema development in the dLNs and overtake T cells as the predominant leukocyte subset within the dLNs (Figure 3.4A,B). The noted differences between T and B cell proliferation within dLNs as measured by Ki67 expression helps to explain why B cells become the largest leukocyte subpopulation as lymphedema and swelling progress (Figure 3.7). Previous studies investigating B cell changes in lymphedematous skin found no differences in B cell populations between control and lymphedema groups [77]. Additionally, humoral immunity was shown to be impaired following immunization in a genetic mouse model that lacked dermal lymphatic drainage, suggesting that cell trafficking to LNs along with passive antigen transport is required for strong humoral immunity [83]. The proliferation of B cells within the dLNs suggest that they are activated by antigen as lymphedema develops; however, we did not directly measure antibody titers and cannot directly comment on the activity of these B cells. There is also evidence that B cells in inflamed LNs may play a role in enhancing dendritic cell migration from distal tissue [144]. The role of humoral immunity and antibody production from B cells during lymphedema development has been understudied, and our data suggests that more research focused on elucidating the role of

B cells in this process is needed.

3.5.4 Single vessel ligation results in increased myeloid cell populations within intact vessel dLN compared to injured vessel dLN

Myeloid cells, primarily macrophages, have been suggested to play an important role in driving lymphatic failure and tissue fibrosis during lymphedema development [59, 78, 145]. Our data suggests that multiple myeloid cell subsets, including monocytes, macrophages, dendritic cells, and neutrophils increase in number within the dLNs during lymphedema development (Figure 3.4A). This increase is likely due to both migration of tissue-resident myeloid cells to the dLNs, and proliferation of LN resident myeloid cell populations [92, 146]. Interestingly, normalized difference between the intact and injured vessel dLNs was significantly increased at 1W compared to 3W for both monocytes and macrophages following lymphedema induction, while other leukocyte subsets did not show a significant increase (Figure 3.13A). Given that monocytes and macrophages are both migratory cell types, it is likely that their migratory capabilities are at least partially responsible for their observed increase in the dLNs. Future studies are needed to determine if migration of myeloid cells to the LNs following lymphedema surgery initiates the observed expansion of leukocytes, or whether this growth is independent of myeloid cell migration.

3.5.5 Insights gained from the immune response during chronic wound healing

It is well known that impaired immune responses contribute to chronic wound healing, which often can occur in diabetic and elderly patients. For proper wound healing, pro-inflammatory and anti-inflammatory responses are well-regulated and occur at established times. These same responses are dysregulated and imbalanced in chronic wound healing, leading to increased fibrosis, decreased reepithelialization, and ECM damage [67, 147]. The immune response during lymphedema mimics many of the characteristics of impaired wound healing responses. Our results show that many of the leukocyte populations in-

volved in wound healing also increase in dLNs during lymphedema progression. There are clear differences between these responses, as the important role of CD4+ T cells in driving tissue fibrosis and lymphatic dysfunction in lymphedema have not been observed in chronic wound healing [67]. Insights gained from studying the mechanisms of chronic wound development and the variety of leukocytes, cytokines, and growth factors involved can help identify future directions for the study of the immune response in lymphedema.

3.5.6 Inflammation-induced lymphangiogenesis within LNs during lymphedema progression

Inflammation has been previously shown to induce lymphangiogenesis within the LN [144]. Our results suggest that the dLNs become much larger as lymphedema progresses and we have also identified that many leukocyte populations increase greatly in number in the dLNs. From our flow cytometry data, we also found that the number of cells not identified as leukocytes (CD3-, CD19-, CD11b-, CD11c-, Ly6C-) increased (Figure 3.20). It is likely that these cells include stromal cells that form the structure of the LN and endothelial cells, including lymphatic endothelial cells. Thus, our data likely indicates that lymphedema progression induces lymphangiogenesis within the dLNs, contributing to the observed growth in LN size. Previous work by Angeli et al shows that B cells drive lymphangiogenesis in inflamed LNs following immunization, suggesting that one result of the increased B cell proliferation observed in dLNs is increased lymphangiogenesis [144]. Further study is needed to investigate if lymphangiogenesis within the dLNs may contribute to the inflammatory response of the lymph node during the progression of lymphedema.

3.5.7 Relationship between lymphatic functional changes and the immune response

One major question regarding the pathogenesis of lymphedema is whether the onset of swelling is due to a loss of lymphatic function, which initiates the resulting immune response, or whether this loss of lymphatic function is a byproduct of immune-mediated physiological changes. To begin to answer this question, we combined a detailed analysis

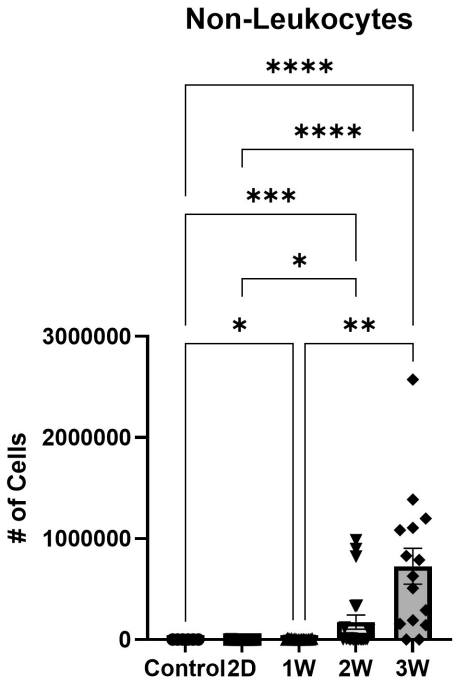

Figure 3.20: Non-leukocytes increase in dLNs during lymphedema progression. The number of non-leukocytes (CD3-CD19-CD11b-CD11c-Ly6c-) was quantified via flow cytometry. Data shown in unoperated control and at 2D, 1W, 2W, and 3W after single vessel ligation.

of immune cell composition in the dLNs during lymphedema development with experiments designed to track NP transport and uptake to the dLNs. Our novel single vessel ligation lymphedema model additionally allowed us to determine how differences in transport to the dLNs may impact the resultant expansion of LN resident leukocytes. We found that transport to and accumulation of NPs within the intact vessel dLN as measured by the normalized sum of fluorescence did not change significantly during lymphedema progression, while NP accumulation within the injured vessel dLN correspondingly increased (Figure 3.11B,C). This explains why differences in NP transport between the dLNs at 2D and 1W were diminished at later timepoints (Figure 3.11D). Given that lymphatic transport in the injured collecting vessel is not restored over this time frame [110], this suggests the formation of collaterals downstream that facilitate flow to the injured vessel dLN. Interestingly, this collateralization is sufficient to support leukocyte expansion in the injured vessel dLN through either direct immune cell migration or proliferation within the dLN. By also analyzing leukocyte populations within these LNs at these timepoints, we found that this loss in differential transport was accompanied by a loss in differential leukocyte composition. Normalized difference, a metric to describe differential leukocyte composition between the dLNs, was significantly positively correlated with the ratio between the intact and injured vessel dLNs of fluorescence metrics measuring NP accumulation within the LNs (Figure 3.13B). Taken together, these results show that differences in transport to the LNs are correlated with differences in leukocyte expansion within the LNs in the context of lymphedema. This study is the first that we know of to show that leukocyte proliferation in the dLNs during lymphedema varies depending on the magnitude of transport into the dLNs. These differences may be due to increased trafficking of migratory leukocytes and direct drainage of inflammatory factors to the intact vessel dLN, driving proliferation of LN resident leukocytes. It is important to note that even though transport of NPs to the intact vessel dLN did not increase during lymphedema progression, previous studies have shown that magnitude and speed of immune cell migration to dLNs through lymphatics

depends on factors other than bulk lymph flow [38]. It is likely that both increased cell migration and cell proliferation contribute to the observed increase in leukocyte expansion during lymphedema progression even without an increase in lymphatic drainage to the intact vessel dLN. Future work should more specifically identify the mechanisms driving the observed differential leukocyte proliferation.

3.5.8 Insights on the use of bestatin treatment for clinical lymphedema

To understand how anti-inflammatory treatment may affect the composition of leukocytes within the dLNs during lymphedema development, we treated mice with bestatin following surgery. Bestatin has previously been shown to ameliorate swelling through its pro-lymphangiogenic effects in the double vessel ligation mouse tail lymphedema while also partially rescuing lymphatic function [111]. Additionally, bestatin treatment in a contact dermatitis model showed potent anti-inflammatory effects, reducing skin infiltration of neutrophils and CD8+ T cells [122]. Surprisingly, we found that bestatin treatment did not reduce leukocyte expansion in the dLNs at any of the timepoints analyzed compared to a control group injected daily with saline (Figure 3.16A,B). Additionally, bestatin treatment did not resolve swelling at any of the timepoints (Figure 3.14B). These results differ from a previous report which had identified bestatin as a potential treatment for lymphedema [111]. Our single vessel ligation lymphedema model leaves a pair of intact collecting vessels on one side of the tail while the complete ligation model used in the previous study blocked all lymphatic flow from the tail. One explanation for the lack of improvement in swelling in our model is that the pro-lymphangiogenic mechanism of action for bestatin is most effective in preventing swelling in a model where all lymphatic flow is blocked and lymphangiogenesis is necessary to reconnect the lymphatic network along the tail. In the clinical context this would suggest that bestatin is perhaps most efficacious as a therapy in more advanced stages of lymphedema. In our model, the intact collecting vessel provides an existing drainage pathway and prevents complete fluid stagnation, so it is possible that

LTB_4 levels are not sufficiently high enough for antagonization of LTB_4 to affect swelling. It is worth noting, however, that the severity of swelling in the single vessel model and the complete ligation model are not markedly different.

Ketoprofen, a non-steroidal anti-inflammatory drug acting on the metabolism of arachidonic acid upstream of LTB_4, has been tested as a treatment for lymphedema in a clinical trial [132, 148]. Ketoprofen was shown to reduce skin thickness and improve histopathological characteristics of lymphedema but did not reduce limb volume in these patients [148]. In the case of chronic lymphedema, a primary source of excess volume is likely adipose hypertrophy, which seems to respond less to anti-inflammatory treatment [148]. In this study, we did not analyze histopathological changes in tail tissue following bestatin treatment but the observed increase in lymphatic function demonstrates the therapeutic efficacy of bestatin, even though changes in limb volume were limited, similar to what has been observed thus far clinically.

It is also important to note that bestatin is used clinically to treat patients with chronic lymphedema, while our mouse model of lymphedema presents acute disease which eventually resolves. Chronic lymphedema is characterized by extensive and prolonged swelling, sustained tissue fibrosis and hardening, and adipose hypertrophy. These aspects of the disease are difficult to reproduce in animal models of acute disease, so our single vessel ligation model only recapitulates some aspects of the clinical manifestation of lymphedema. Potential benefits of bestatin on lymphatic function observed in this study may thus provide additional benefits in clinical lymphedema given that our model does not fully reproduce the chronic disease characteristics.

While bestatin treatment did not reduce swelling or inhibit leukocyte expansion in the dLNs in our lymphedema model, it did increase NP accumulation within the intact vessel dLN as lymphedema progressed (Figure 3.14D). Through analysis of both NP uptake to the dLNs and in vivo imaging of lymphatic collecting vessel pumping we show that bestatin treatment increases lymphatic function as lymphedema progresses, suggesting that

LTB_4 mediates the decrease in lymphatic function that occurs during lymphedema development (Figure 3.14A,D). Further study is needed to determine the mechanism through which LTB_4 mediates these changes in lymphatic function, whether it is through direct action on collecting lymphatics or through activation of leukocytes and production of various cytokines known to regulate lymphatic contractility [149–153].

Interestingly, bestatin-treated mice showed significant differential leukocyte expansion between the dLNs at 2W compared to the saline control group (Figure 3.19A). Taken together with the NIR measurements of lymphatic function, this difference between the dLNs corresponded with increases in lymphatic contractile transport in bestatin-treated mice at 2W and in NP accumulation at 3W. It is likely that increased leukocyte migration and transport to the intact vessel dLN at 2W in bestatin-treated mice could explain the differential increase in leukocytes, but we did not directly measure cell migration in these experiments. It is important to note that the increase in lymphatic contractile transport was measured in the intact vessel and the increase in NP accumulation was measured in the intact vessel dLN. The intact vessel dLN will drive the immune response as it receives significantly more drainage from the injury site than the injured vessel dLN in the first week following surgery in this model. Additionally, the differential leukocyte expansion at 2W following bestatin treatment preceded the increase in NP accumulation at 3W in the intact vessel dLN. These results suggest that differences in LN leukocyte populations may precede changes in drainage to the LNs. The immune response may thus drive some of the observed changes in lymphatic function in this model.

3.5.9 Conclusion

Through combining flow cytometry analysis of leukocyte populations in dLNs with novel NIR imaging techniques to quantify lymphatic transport, our work has begun to uncover the relationship between fluid uptake and immune cell involvement during lymphedema development. We show that differential NP transport into the dLNs during lymphedema

development was correlated with differential leukocyte expansion in those dLNs (Figure 3.13B). Bestatin treatment increased NP transport to the intact vessel dLN in our model (Figure 3.14D). This increase in lymphatic function also extended the differential leukocyte development between the dLNs (Figure 3.19A). However, this improvement in functional lymphatic transport did not affect the swelling in these mice (Figure 3.14B). The growth of leukocyte populations in the dLNs was also not affected by the changes in lymphatic function (Figure 3.16A,B). These results suggest that improving transport from sites of lymphatic injury during lymphedema development is not sufficient to reverse the characteristic swelling or immune cell-mediated physiological changes. Additionally, differential leukocyte composition within the dLNs was measured at timepoints prior to later differences in transport to the intact vessel dLN, suggesting that changes in lymphatic function during lymphedema development may be mediated by the immune response rather than purely by changes in the mechanical properties of the collecting lymphatic vessels. Future treatments for lymphedema may need to target both lymphatic function and the immune system to fully reverse the swelling that characterizes the disease.

CHAPTER 4
CONCLUSIONS AND FUTURE DIRECTIONS

Lymphedema is a vastly understudied disease, and there are currently no pharmotherapeutic treatments for it used in the clinic. This lack of treatment options is partly due to incomplete understanding of the disease's development. Two areas of interest that have not been fully studied in the context of lymphedema development are the functional response of the lymphatic vasculature and the immune response within LNs that drain the site of lymphatic injury. Better characterization of how lymphatic function and the immune response change during disease and how potential therapies modulate these changes is needed. Our work aimed to improve understanding through two approaches: (1) Using *in vivo* and *ex vivo* approaches to measure lymphatic contractile function following lymphedema induction and quantifying the beneficial effect of potential lymphedema therapies on lymphatic function, and (2) Characterizing the kinetics of the leukocyte response in dLNs during lymphedema and determining the effect of LTB_4 antagonism on these changes.

Our results show that the progressive decrease in function of the intact lymphatic vasculature following lymphedema induction is closely correlated to the swelling response of the mouse tail in our model. This suggests that loss of lymphatic function in vessels undamaged during an initial injury to the lymphatic network is directly related to the swelling that occurs during lymphedema. We further show that LTB_4 antagonism and epsin deletion, pro-lymphangiogenic strategies that have showed promise in reducing lymphedema in animal models, also increase lymphatic contractile function during lymphedema development. The beneficial effects on function of these strategies reveal that their therapeutic potential may not solely depend on their pro-lymphangiogenic mechanisms.

By analyzing leukocyte populations in dLNs following lymphedema induction, we observed a general expansion of leukocyte subsets including T and B cells and myeloid cells

(macrophages, monocytes, dendritic cells and neutrophils). Interestingly, experiments to measure proliferation of these cells revealed that B cells in dLNs expressed more Ki67 than T cells, suggesting that B cells respond more strongly to the immunological microenvironment induced by lymphatic injury and tissue swelling. B cells also increased as a fraction of total leukocytes within dLNs during lymphedema development as T cell fraction decreased, corresponding with our proliferation measurements. This proliferative response specific to B cells has not been identified previously in the context of secondary lymphedema, and it is likely that antigens (potentially released due to tissue injury and remodeling) drive this reaction. Previous work investigating the role of CD4+ T cells in lymphedema progression showed that dendritic cells migrate from the extremities to LNs following lymphatic injury and activate CD4+ T cells. This process must also be antigen-mediated as dendritic cells present antigen to T cells for their activation. Future work is needed to understand the functional role that B cells may play in lymphedema development. This includes studying the mechanisms driving B cell proliferation (including if this is an antigen-mediated process) and the potential functional role of antibodies produced by activated B cells.

Our study of LTB_4 shows that antagonizing it using bestatin following lymphedema induction increases lymphatic function in a variety of contexts, including through measurement of lymphatic contraction *in vivo* using NIR imaging and through quantifying NP uptake to dLNs. However, bestatin treatment does not alter the immune response in dLNs or reduce tail swelling in our single vessel ligation model. It is possible that the pro-lymphangiogenic mechanisms of LTB_4 antagonism are less efficacious in reducing swelling when a lymphatic pathway is left intact. A previous study by Rutkowski *et al* showed that interstitial lymph flow is necessary to drive lymphangiogenesis and is mitigated when lymphatic vasculature is left intact [154]. These results urge caution in the potential use of bestatin as a treatment for clinical lymphedema, as the state of the lymphatic vasculature may determine the utility of the treatment.

This study has furthered understanding of both the lymphatic functional response and

leukocyte expansion and activation in dLNs during lymphedema development. Our results surprisingly showed that the beneficial effect of LTB_4 antagonism on lymphatic function in lymphedema is not due to a direct effect of LTB_4 or 5-LO signaling metabolites on lymphatic function. Given that overexpression of 5-LO *in vivo* did not affect lymphatic function, it is likely that the altered microenvironment of lymphedema provides additional cues (increased leukocyte infiltration and cytokine secretion) that mediate the effect of LTB_4 on lymphatic function. Our work attempts to bridge the gap between detailed analysis of lymphatic functional changes during lymphedema and a comprehensive evaluation of leukocyte response in dLNs. Further study is needed to more specifically examine the immune cell-mediated mechanisms driving changes in lymphatic function (such as cytokine secretion) and potentially reverse these changes through targeting these mechanisms.

Appendices

APPENDIX A

MATLAB CODE FOR QUANTIFICATION OF NIR FUNCTIONAL METRICS

```
clear
clc
threshold = 0.001;

%Packet Processing
%Intensity data will be imported from text files (tab delimited)
%and will be analyzed to determine the functional metrics.
%Browse for intensity file
[FileName, PathName] = uigetfile('*.txt','Select the intensity ...
    data');
%Full file names for the intensity file
intensityFile = strcat(PathName,FileName);

% filepath = '\\130.207.40.141\public\Matthew Cribb\Single Vessel ...
    Ligation Experiments\10 Weeks Post Surgery - 2.21.17\Mouse ...
    8\Mouse8_RightFunction\';
% filename = 'Right Vessel Average Intensity';
% extension = '.txt';
%
% fileloc= strcat(filepath, filename, extension);
x= dlmread(intensityFile, '\t');

%%x2=Wounded3(9573:9921,1);

y2=smooth(x,3);
y2=y2(100:end);
```

```
%y2=y2(800:end); changed
t=1:length(y2);
t=t.*(1/10).*(1/60);

[maxtab2, min2]=peakdet(y2,100); %Intensity change to be ...
    considered a peak

if maxtab2(1,1) < min2(1,1)
    maxtab2 = maxtab2(2:end,:);
end

if maxtab2(end,1) > min2(end,1)
    maxtab2 = maxtab2(1:end-1,:);
end

mintab2=min2(1,:);
for n=2:length(min2)-1
    index=min2(n);
    while y2(index) ≤ min2(n,2)*(1+threshold)
        index=index-1;
    end
    mintemp2(1,1)=index;mintemp2(1,2)=y2(index);
    index=min2(n);
    while y2(index) ≤ min2(n,2)*(1+threshold)
        index=index+1;
    end
    mintemp2(2,1)=index;mintemp2(2,2)=y2(index);
    mintab2 = [mintab2 ; mintemp2];
end
mintab2 = [mintab2 ; min2(end,:)];

packet_width2=[];
mean_packet_min2=[];
```

```
packet_integral2=zeros(1,length(maxtab2));
packet_boundary2=[];
for n=1:2:length(mintab2)-1
    packet_width2 = [packet_width2 mintab2(n+1,1)-mintab2(n,1)];
    mean_packet_min2 = [mean_packet_min2 mean([mintab2(n+1,2) ...
        mintab2(n,2)])];
end

integral_y2=[];
for n=1:length(maxtab2)
    packet_line_x2 = mintab2(n*2-1,1):mintab2(n*2,1);
    packet_slope2 = ...
        (mintab2(n*2,2)-mintab2(n*2-1,2))/(mintab2(n*2,1)-
    mintab2(n*2-1,1));
    packet_offset2 = mintab2(n*2-1,2) - packet_slope2 * ...
        mintab2(n*2-1,1);
    for index=1:length(packet_line_x2)
        packet_line_y2(index) = ...
            packet_line_x2(index)*packet_slope2 + packet_offset2;
    end
    packet_line2 = [packet_line_x2; packet_line_y2];
    packet_line2 = packet_line2';
    packet_boundary2 = [packet_boundary2;packet_line2];

    packet_amplitude2(n) = maxtab2(n,2) - mean_packet_min2(n);
    packet_amplitude_perdiff2(n) = ...
        packet_amplitude2(n)/mean_packet_min2(n);
for index = mintab2(n*2-1,1):mintab2(n*2,1)
        integral_y2=[integral_y2;y2(index)];
    end
    for index = 1:length(integral_y2)
    packet_integral2(n) = packet_integral2(n) + ...
        integral_y2(index)-packet_line_y2(index);
```

```
    end
    packet_integral_norm2(n) = ...
        packet_integral2(n)/mean_packet_min2(n);
    packet_line_y2=[];
    integral_y2=[];
end

fig2 = figure;
plot(t,y2, 'linewidth', 3)
hold on
plot(t(maxtab2(:,1)),maxtab2(:,2),'r.',t(mintab2(:,1)),mintab2(:,2),
'g.', 'markersize', 15)
plot(t(packet_boundary2(:,1)),packet_boundary2(:,2),'g.',
'markersize', 4)
box off
%axis([t(2000) t(end)])
set(gca,'fontsize',26)
xlabel('Time (minutes)','fontsize',28);ylabel('Normalized ...
    Intensity','fontsize',28);
title({strrep([FileName, PathName],'_','.');' '},'Fontsize',10);
% ax=gca;
% ax.YLim=[0.9 1.21];
% ax.XLim=[0 2];
% ax.LineWidth=3;

%print(fig2, '-dtiff', [filepath filename 'Plot2'])

%packets per min, assuming 10fps
packet_frequency2 = ...
    length(maxtab2)/(mintab2(end,1)-mintab2(2,1))*600;
avg_packet_width2 = mean(packet_width2);
avg_packet_amplitude2 = mean(packet_amplitude2);
avg_packet_amplitude_perdiff2 = mean(packet_amplitude_perdiff2);
```

```
113 avg_packet_integral2 = mean(packet_integral2);
114 avg_packet_integral_norm2 = mean(packet_integral_norm2);
115
116 %normalized per minute, assuming 10fps
117 packet_transport2 = ...
        sum(packet_integral2)/(mintab2(end,1)-mintab2(1,1))*600;
118 packet_transport_norm2 = ...
        sum(packet_integral_norm2)/(mintab2(end,1)-mintab2(1,1))*600;
119
120 output = [packet_frequency2; ...
        avg_packet_width2;avg_packet_amplitude2;avg_packet_integral2;
121 packet_transport2];
122
123 %find average packet min (baseline)
124
125 avgPackMin= mean(mean_packet_min2);
126
127 %filename
128
129 packet_frequency2
130 avg_packet_width2
131 avg_packet_amplitude2
132 avg_packet_amplitude_perdiff2
133 avg_packet_integral2
134 avg_packet_integral_norm2
135 packet_transport2
136 packet_transport_norm2
137
138 % dlmwrite([filepath filename 'Output' extension], output)
```

APPENDIX B

MATLAB CODE FOR ANALYSIS OF LYMPHATIC PUMPING PRESSURE

```
clear
clc

%%
%Pumping Pressure Measurement
%Pressure and intensity data will be imported from text files ...
    (tab delimited)
%and will be analyzed to determine the measured pumping pressure.
%Browse for pressure and intensity files
[pFileName, pPathName] = uigetfile('*.txt','Select the pressure ...
    data');
[iFileName, iPathName] = uigetfile('*.txt','Select the intensity ...
    data');
%Full file names for the pressure and intensity files
pressureFile = strcat(pPathName,pFileName);
intensityFile = strcat(iPathName,iFileName);
%Input frame where pumping pressure measurement started to adjust ...
    time data
%for pressure measurement
prompt = 'Which frame did the pumping pressure measurement start ...
    on?';
dlg_title = 'Input Frame';
num_lines = 1;
PressureFrameStart = inputdlg(prompt,dlg_title,num_lines,{'0'});
PressureFrameStartNum = str2double(PressureFrameStart{1});
```

```
%Read in data from pressure file, and separate out adjusted time ...
    data and
%the pressure data
PressureWksht = tdfread(pressureFile);
PressureFieldNames = fieldnames(PressureWksht);
PressureTimeData = ...
    PressureWksht.(PressureFieldNames{1})+PressureFrameStartNum;
PressureData = PressureWksht.(PressureFieldNames{2});
%Read in data from intensity file, and separate out time data and the
%intensity data
IntensityWksht = tdfread(intensityFile);
IntensityFieldNames = fieldnames(IntensityWksht);
% IntensityTimeData = IntensityWksht.(IntensityFieldNames{1});
% IntensityData = IntensityWksht.(IntensityFieldNames{2});
IntensityData = IntensityWksht.(IntensityFieldNames{1});
IntensityTimeData=zeros(1,length(IntensityData))';
for k=2:length(IntensityData)
    IntensityTimeData(k) = IntensityTimeData(k-1)+1;
end
%Filter Intensity Data using a moving average filter (averaging ...
    over 15
%points)
timeIntervalFilter = 15;
FilterMat = ones(1,timeIntervalFilter)/timeIntervalFilter;
IntensityDataFiltered = filter(FilterMat, 1, IntensityData);
% Code to view filtered data vs actual data:
% figure
% hold on
% plot(IntensityTimeData,IntensityData)
% plot(IntensityTimeData,IntensityDataFiltered)
% legend('Intensity Data','Intensity Data Filtered')

%%
```

```
%Determining Pumping Pressure Value
count = 0;
%Find time point where pressure first goes above 80 mmHg (t1) and ...
    when it
%decreases below 60 mmHg after holding the pressure at 80 mmHg (t2)
for i=1:length(PressureData)
    if PressureData(i)>80 && count==0
        t1_P = floor(PressureTimeData(i));
        [Val1, t1] = min(abs(IntensityTimeData-t1_P));
        count = 1;
    elseif PressureData(i)<60 && count==1
        t2_P = floor(PressureTimeData(i));
        [Val2, t2] = min(abs(IntensityTimeData-t2_P));
        count = 2;
    elseif PressureData(i)<1 && count==2
        t3_P = floor(PressureTimeData(i));
        [Val3, t3] = min(abs(IntensityTimeData-t3_P));
        break;
    end
end
%Find max intensity after t2 and find index of value in
%IntensityDataFiltered
[maxIntensity, maxIntIndex_NA] = max(IntensityDataFiltered(t2:t3));
maxIntIndex = length(IntensityDataFiltered) - ...
    length(IntensityDataFiltered(t2:end)) + maxIntIndex_NA;
%Find min intensity after t1 and find index of value in
%IntensityDataFiltered
[minIntensity, minIntIndex_NA] = ...
    min(IntensityDataFiltered(t2:maxIntIndex));
minIntIndex = length(IntensityDataFiltered) - ...
    length(IntensityDataFiltered(t2:end)) + minIntIndex_NA;
%Average min and max intensity to find the mid intensity
midIntensity = mean([minIntensity maxIntensity]);
```

```
%Find the index and time where the intensity data is closest to ...
    the mid
%intensity
% [midIntVal, midIntIndex_NA] = ...
    min(abs(IntensityDataFiltered(minIntIndex:maxIntIndex)-
midIntensity));
% midIntIndex = length(IntensityDataFiltered) - ...
    length(IntensityDataFiltered(minIntIndex:end)) + midIntIndex_NA;
for k=minIntIndex:maxIntIndex
    midIntIndex=k;
    if IntensityDataFiltered(k-1)≤midIntensity & ...
        IntensityDataFiltered(k)≥midIntensity
        break;
    end
end
midIntTime = IntensityTimeData(midIntIndex);
%Find the index and pumping pressure where the intensity data is ...
    closest to
%the mid intensity
if (maxIntensity-minIntensity)>50
    [pressPumpVal, pressPumpIndex] = ...
        min(abs(PressureTimeData-midIntTime));
    PumpingPressure = PressureData(pressPumpIndex);
else
    PumpingPressure = 0;
end
uiwait(msgbox(strcat('The Pumping Pressure ...
    is:',num2str(PumpingPressure),' mmHg')));
%%
%Emptying Rate
%Find how quickly the intensity decreases to its minimum value
[maxIntEmpRate, maxIntEmpRateIndex_NA] = ...
    max(IntensityDataFiltered(t1:t2));
```

```
105 maxIntEmpRateIndex = length(IntensityDataFiltered) - ...
        length(IntensityDataFiltered(t1:end)) + maxIntEmpRateIndex_NA;
106 minThreshold = 1.10*minIntensity;
107 for j=maxIntEmpRateIndex:t3
108     if IntensityDataFiltered(j)<minThreshold
109         threshIntIndex = j;
110         break;
111     end
112 end
113 EmpRate = round((maxIntEmpRate-minThreshold)./ ...
114 (IntensityTimeData(threshIntIndex)-IntensityTimeData ...
115 (maxIntEmpRateIndex)),1);
116 uiwait(msgbox(strcat('The Emptying Rate is:',num2str(EmpRate),' ...
        IU/s')));
117
118 %%
119 %Plotting Data
120 figure
121 hold on
122 title('Pumping Pressure Measurement')
123 yyaxis right
124 plot(PressureTimeData,PressureData)
125 axis([0 max(max(PressureTimeData),max(IntensityTimeData)) -5 90])
126 xlabel('Time (s)')
127 ylabel('Pumping Pressure (mmHg)')
128 yyaxis left
129 plot(IntensityTimeData,IntensityDataFiltered)
130 %Line to denote the pumping pressure on the graph
131 if PumpingPressure>0
132     line([PressureTimeData(pressPumpIndex) ...
            PressureTimeData(pressPumpIndex)], ...
133     [min(IntensityDataFiltered)-500 ...
            max(IntensityDataFiltered)+500], ...
```

```
134      'Marker','.','LineStyle','-','Color','k')
135  end
136  %Line for emptying rate
137  line([IntensityTimeData(maxIntEmpRateIndex) ...
        IntensityTimeData(threshIntIndex)],[maxIntEmpRate ...
        minThreshold],'Marker','.','LineStyle','-','Color','r')
138  axis([0 max(max(PressureTimeData),max(IntensityTimeData)) ...
        min(IntensityDataFiltered)-500 max(IntensityDataFiltered)+500])
139  ylabel('Average Intensity')
```

REFERENCES

[1] A. Aspelund, S. Antila, S. T. Proulx, T. V. Karlsen, S. Karaman, M. Detmar, H. Wiig, and K. Alitalo, "A dural lymphatic vascular system that drains brain interstitial fluid and macromolecules," *Journal of Experimental Medicine*, vol. 212, no. 7, pp. 991–999, Jun. 2015.

[2] A. Louveau, I. Smirnov, T. J. Keyes, J. D. Eccles, S. J. Rouhani, J. D. Peske, N. C. Derecki, D. Castle, J. W. Mandell, K. S. Lee, T. H. Harris, and J. Kipnis, "Structural and functional features of central nervous system lymphatic vessels," *Nature*, vol. 523, pp. 337–341, 2015.

[3] S. Da Mesquita, Z. Papadopoulos, T. Dykstra, L. Brase, F. G. Farias, M. Wall, H. Jiang, C. D. Kodira, K. A. de Lima, J. Herz, A. Louveau, D. H. Goldman, A. F. Salvador, S. Onengut-Gumuscu, E. Farber, N. Dabhi, T. Kennedy, M. G. Milam, W. Baker, I. Smirnov, S. S. Rich, B. A. Benitez, C. M. Karch, R. J. Perrin, M. Farlow, J. P. Chhatwal, D. M. Holtzman, C. Cruchaga, O. Harari, J. Kipnis, and D. I. A. Network, "Meningeal lymphatics affect microglia responses and anti-ab immunotherapy," *Nature*, vol. 593, pp. 255–260, 2021.

[4] Q. Ma, B. V. Ineichen, M. Detmar, and S. T. Proulx, "Outflow of cerebrospinal fluid is predominantly through lymphatic vessels and is reduced in aged mice," *Nature Communications*, vol. 8, p. 1434, 2017.

[5] S. Proulx, Q. Ma, D. Andina, J.-C. Leroux, and M. Detmar, "Quantitative measurement of lymphatic function in mice by noninvasive near-infrared imaging of a peripheral vein," *JCI Insight*, vol. 2, e90861, Jan. 2017.

[6] X. Liu, E. De la Cruz, X. Gu, L. Balint, M. Oxendine-Burns, T. Terrones, W. Ma, H.-H. Kuo, C. Lantz, T. Bansal, E. Thorp, P. Burridge, Z. Jakus, J. Herz, O. Cleaver, M. Torres, and G. Oliver, "Lymphoangiocrine signals promote cardiac growth and repair," *Nature*, vol. 588, pp. 705–711, 2020.

[7] A. Kaipainen, J. Korhonen, T. Mustonen, V. W. van Hinsbergh, G. H. Fang, D. Dumont, M. Breitman, and K. Alitalo, "Expression of the fms-like tyrosine kinase 4 gene becomes restricted to lymphatic endothelium during development," *Proceedings of the National Academy of Sciences*, vol. 92, no. 8, pp. 3566–3570, 1995.

[8] T. Mäkinen, T. Veikkola, S. Mustjoki, T. Karpanen, B. Catimel, E. Nice, L. Wise, A. Mercer, H. Kowalski, D. Kerjaschki, S. Stacker, M. Achen, and K. Alitalo, "Isolated lymphatic endothelial cells transduce growth, survival and migratory signals via the vegf-c/d receptor vegfr-3," *The EMBO journal*, vol. 20, pp. 4762–4763, 2001.

[9] K. Vaahtomeri, S. Karaman, T. Mäkinen, and K. Alitalo, "Lymphangiogenesis guidance by paracrine and pericellular factors," *Genes & Development*, vol. 31, no. 16, pp. 1615–1634, 2017. eprint: http://genesdev.cshlp.org/content/31/16/1615.full.pdf+html.

[10] G. A. Secker and N. L. Harvey, "Regulation of vegfr signalling in lymphatic vascular development and disease: An update," *International Journal of Molecular Sciences*, vol. 22, no. 14, 2021.

[11] Y. Deng, X. Zhang, and M. Simons, "Molecular controls of lymphatic vegfr3 signaling," *Arteriosclerosis, Thrombosis, and Vascular Biology*, vol. 35, no. 2, pp. 421–429, 2015.

[12] J. M. Rutkowski, M. Moya, J. Johannes, J. Goldman, and M. A. Swartz, "Secondary lymphedema in the mouse tail: Lymphatic hyperplasia, vegf-c upregulation, and the protective role of mmp-9," *Microvascular Research*, vol. 72, no. 3, pp. 161–171, 2006.

[13] E. Nakamura, K. Koizumi, M. Kobayashi, and I. Saiki, "Inhibition of lymphangiogenesis related properties of murine lymphatic endothelial cells and lymph node metastasis of lung cancer by the matrix metalloproteinase inhibitor mmi270," *Cancer Science*, vol. 95, pp. 25–31, 2004.

[14] J. E. Rundhaug, "Matrix metalloproteinases and angiogenesis," *Journal of Cellular and Molecular Medicine*, vol. 9, pp. 267–285, 2005.

[15] C. Cursiefen, L. Chen, L. P. Borges, D. Jackson, J. Cao, C. Radziejewski, P. A. D'Amore, M. R. Dana, S. J. Wiegand, and J. W. Streilein, "Vegf-a stimulates lymphangiogenesis and hemangiogenesis in inflammatory neovascularization via macrophage recruitment," *The Journal of Clinical Investigation*, vol. 113, pp. 1040–1050, 2004.

[16] R. Cao, H. Ji, N. Feng, Y. Zhang, X. Yang, P. Andersson, Y. Sun, K. Tritsaris, A. J. Hansen, S. Dissing, and Y. Cao, "Collaborative interplay between fgf-2 and vegf-c promotes lymphangiogenesis and metastasis," *Proceedings of the National Academy of Sciences*, vol. 109, pp. 15 894–15 899, 2012.

[17] F. Bruyère and A. Noël, "Lymphangiogenesis: In vitro and in vivo models," *The FASEB Journal*, vol. 24, pp. 8–21, 2010.

[18] J. Kazenwadel, G. A. Secker, K. L. Betterman, and N. L. Harvey, "In vitro assays using primary embryonic mouse lymphatic endothelial cells uncover key roles for fgfr1 signalling in lymphangiogenesis," *PLOS ONE*, vol. 7, no. 7, pp. 1–12, Jul. 2012.

[19] S. Nakao, K. Maruyama, S. Zandi, M. I. Melhorn, M. Taher, K. Noda, E. Nusayr, T. Doetschman, and H.-M. Ali, "Lymphangiogenesis and angiogenesis: Concurrence and/or dependence? studies in inbred mouse strains," *The FASEB Journal*, vol. 24, no. 2, pp. 504–513, 2010.

[20] D. Marino, Y. Angehrn, S. Klein, S. Riccardi, N. Baenziger-Tobler, V. I. Otto, M. Pittelkow, and M. Detmar, "Activation of the epidermal growth factor receptor promotes lymphangiogenesis in the skin," *Journal of Dermatological Science*, vol. 71, no. 3, pp. 184–194, 2013.

[21] L. Alderfer, E. Russo, A. Archilla, B. Coe, and D. Hanjaya-Putra, "Matrix stiffness primes lymphatic tube formation directed by vascular endothelial growth factor-c," *The FASEB Journal*, vol. 35, no. 5, e21498, 2021.

[22] K. T. Campbell, M. B. Curtis, J. M. Massey, K. Wysoczynski, D. J. Hadley, S. C. George, and E. A. Silva, "Isolating and characterizing lymphatic endothelial progenitor cells for potential therapeutic lymphangiogenic applications," *Acta Biomaterialia*, vol. 135, pp. 191–202, 2021.

[23] E. B. Peters, N. Christoforou, K. W. Leong, G. A. Truskey, and J. L. West, "Polyethylene glycol hydrogel scaffolds containing cell-adhesive and protease-sensitive peptides support microvessel formation by endothelial progenitor cells," *Cellular and Molecular Bioengineering*, vol. 9, pp. 38–54, 2016.

[24] J. Hooks, "The role of loading and the microenvironment on the regulation of lymphatic function and health," Ph.D. dissertation, Georgia Institute of Technology, 2019.

[25] E. M. Sevick-Muraca, S. Kwon, and J. C. Rasmussen, "Emerging lymphatic imaging technologies for mouse and man," *The Journal of Clinical Investigation*, vol. 124, pp. 905–914, 2014.

[26] S. Modi, A. Stanton, W. Svensson, A. Peters, P. Mortimer, and J. Levick, "Human lymphatic pumping measured in healthy and lymphoedematous arms by lymphatic congestion lymphoscintigraphy," *The Journal of Physiology*, vol. 583, pp. 271–285, 2007.

[27] T. Avraham, A. Yan, J. C. Zampell, S. V. Daluvoy, A. Haimovitz-Friedman, A. P. Cordeiro, and B. J. Mehrara, "Radiation therapy causes loss of dermal lymphatic vessels and interferes with lymphatic function by tgf-β1-mediated tissue fibrosis," *American Journal of Physiology-Cell Physiology*, vol. 299, no. 3, pp. C589–C605, 2010.

[28] C. Blatter, E. F. J. Meijer, T. P. Padera, and B. J. Vakoc, "Simultaneous measurements of lymphatic vessel contraction, flow and valve dynamics in multiple lym-

phangions using optical coherence tomography," *Journal of Biophotonics*, vol. 11, no. 8, e201700017, 2018.

[29] V. Pamarthi, W. M. Pabon-Ramos, V. Marnell, and L. M. Hurwitz, "Mri of the central lymphatic system: Indications, imaging technique, and pre-procedural planning," *Topics in Magnetic Resonance Imaging*, vol. 26, pp. 175–180, 2017.

[30] J. C. Rasmussen, I.-C. Tan, M. V. Marshall, C. E. Fife, and E. M. Sevick-Muraca, "Lymphatic imaging in humans with near-infrared fluorescence," *Current Opinion in Biotechnology*, vol. 20, pp. 74–82, 2009.

[31] I.-C. Tan, E. A. Maus, J. C. Rasmussen, M. V. Marshall, K. E. Adams, C. E. Fife, L. A. Smith, W. Chan, and E. M. Sevick-Muraca, "Assessment of lymphatic contractile function after manual lymphatic drainage using near-infrared fluorescence imaging," *Archives of Physical Medicine and Rehabilitation*, vol. 92, no. 5, 756–764.e1, 2011.

[32] M. Weiler, T. Kassis, and J. B. Dixon, "Sensitivity analysis of near-infrared functional lymphatic imaging," *Journal of Biomedical Optics*, vol. 17, no. 6, pp. 1–11, 2012.

[33] M. Weiler and J. B. Dixon, "Differential transport function of lymphatic vessels in the rat tail model and the long-term effects of indocyanine green as assessed with near-infrared imaging," *Frontiers in Physiology*, vol. 4, p. 215, 2013.

[34] H. R. Hampton and T. Chtanova, "Lymphatic migration of immune cells," *Frontiers in Immunology*, vol. 10, p. 1168, 2019.

[35] G. F. Debes, C. N. Arnold, A. J. Young, S. Krautwald, M. Lipp, J. B. Hay, and E. C. Butcher, "Chemokine receptor ccr7 required for t lymphocyte exit from peripheral tissues," *Nature Immunology*, vol. 6, pp. 889–894, 2005.

[36] S. Noor, A. S. Habashy, J. P. Nance, R. T. Clark, K. Nemati, M. J. Carson, and E. H. Wilson, "Ccr7-dependent immunity during acute *Toxoplasma gondii* infection," *Infection and Immunity*, vol. 78, no. 5, pp. 2257–2263, 2010.

[37] Y. Xiong, W. Piao, C. C. Brinkman, L. Li, J. M. Kulinski, A. Olivera, A. Cartier, T. Hla, K. L. Hippen, B. R. Blazar, S. R. Schwab, and J. S. Bromberg, "Cd4 t cell sphingosine 1-phosphate receptor (s1pr)1 and s1pr4 and endothelial s1pr2 regulate afferent lymphatic migration," *Science Immunology*, vol. 4, no. 33, eaav1263, 2019.

[38] A. Teijeira, M. C. Hunter, E. Russo, S. T. Proulx, T. Frei, G. F. Debes, M. Coles, I. Melero, M. Detmar, A. Rouzaut, and C. Halin, "T cell migration from inflamed skin to draining lymph nodes requires intralymphatic crawling supported by icam-1/lfa-1 interactions," *Cell Reports*, vol. 18, no. 4, pp. 857–865, 2017.

[39] M. C. Hunter, A. Teijeira, R. Montecchi, E. Russo, P. Runge, F. Kiefer, and C. Halin, "Dendritic cells and t cells interact within murine afferent lymphatic capillaries," *Frontiers in Immunology*, vol. 10, p. 520, 2019.

[40] E. Vokali, S. S. Yu, S. Hirosue, M. Rinçon-Restrepo, F. V. Duraes, S. Scherer, P. Corthésy-Henrioud, W. W. Kilarski, A. Mondino, D. Zehn, S. Hugues, and M. A. Swartz, "Lymphatic endothelial cells prime naïve cd8+ t cells into memory cells under steady-state conditions," *Nature Communications*, vol. 11, p. 538, 2020.

[41] S. Hirosue and J. Dubrot, "Modes of antigen presentation by lymph node stromal cells and their immunological implications," *Frontiers in Immunology*, vol. 6, p. 446, 2015.

[42] R. M. Kedl, R. S. Lindsay, J. M. Finlon, E. D. Lucas, R. S. Friedman, and B. A. J. Tamburini, "Migratory dendritic cells acquire and present lymphatic endothelial cell-archived antigens during lymph node contraction," *Nature Communications*, vol. 8, p. 2034, 2017.

[43] B. A. Tamburini, M. A. Burchill, and R. M. Kedl, "Antigen capture and archiving by lymphatic endothelial cells following vaccination or viral infection," *Nature Communications*, vol. 5, p. 3989, 2014.

[44] E. D. Lucas and B. A. J. Tamburini, "Lymph node lymphatic endothelial cell expansion and contraction and the programming of the immune response," *Frontiers in Immunology*, vol. 10, p. 36, 2019.

[45] I. Mondor, M. Baratin, M. Lagueyrie, L. Saro, S. Henri, R. Gentek, D. Suerinck, W. Kastenmuller, J. X. Jiang, and M. Bajénoff, "Lymphatic endothelial cells are essential components of the subcapsular sinus macrophage niche," *Immunity*, vol. 50, 1453–1466.e4, 2019.

[46] A. Takeda, M. Hollmén, D. Dermadi, J. Pan, K. F. Brulois, R. Kaukonen, T. Lönnberg, P. Boström, I. Koskivuo, H. Irjala, M. Miyasaka, M. Salmi, E. C. Butcher, and S. Jalkanen, "Single-cell survey of human lymphatics unveils marked endothelial cell heterogeneity and mechanisms of homing for neutrophils," *Immunity*, vol. 51, no. 3, 561–572.e5, 2019.

[47] S. Jalkanen and M. Salmi, "Lymphatic endothelial cells of the lymph node," *Nature Reviews Immunology*, vol. 20, pp. 566–578, 2020.

[48] S. Bennuru and T. B. Nutman, "Lymphatics in human lymphatic filariasis: In vitro models of parasite-induced lymphatic remodeling," *Lymphatic Research and Biology*, vol. 7, pp. 215–219, 2009.

[49] S. Chakraborty, M. Gurusamy, D. C. Zawieja, and M. Muthuchamy, "Lymphatic filariasis: Perspectives on lymphatic remodeling and contractile dysfunction in filarial disease pathogenesis," *Microcirculation*, vol. 20, pp. 349–364, 2013.

[50] S. G. Rockson, V. Keeley, S. Kilbreath, A. Szuba, and A. Towers, "Cancer-associated secondary lymphoedema," *Nature Reviews Disease Primers*, vol. 5, no. 22, pp. 1–16, 2019.

[51] J. N. Cormier, R. L. Askew, K. S. Mungovan, Y. Xing, M. I. Ross, and J. M. Armer, "Lymphedema beyond breast cancer," *Cancer*, vol. 116, no. 22, pp. 5138–5149, 2010.

[52] S. C. Teunissen, W. Wesker, C. Kruitwagen, H. C. de Haes, E. E. Voest, and A. de Graeff, "Symptom prevalence in patients with incurable cancer: A systematic review," *Journal of Pain and Symptom Management*, vol. 34, pp. 94–104, 2007.

[53] P. Brouillard, L. Boon, and M. Vikkula, "Genetics of lymphatic anomalies," *The Journal of Clinical Investigation*, vol. 124, no. 3, pp. 898–904, Mar. 2014.

[54] S. Wiegand, G. Wichmann, and A. Dietz, "Treatment of lymphatic malformations with the mtor inhibitor sirolimus: A systematic review," *Lymphatic Research and Biology*, vol. 16, no. 4, pp. 330–339, 2018, PMID: 29924669.

[55] D. Kaigler, P. H. Krebsbach, P. J. Polverini, and D. J. Mooney, "Role of vascular endothelial growth factor in bone marrow stromal cell modulation of endothelial cells," *Tissue Engineering*, vol. 9, no. 1, pp. 95–103, 2003, PMID: 12625958.

[56] J. Rehman, D. Traktuev, J. Li, S. Merfeld-Clauss, C. J. Temm-Grove, J. E. Bovenkerk, C. L. Pell, B. H. Johnstone, R. V. Considine, and K. L. March, "Secretion of angiogenic and antiapoptotic factors by human adipose stromal cells," *Circulation*, vol. 109, no. 10, pp. 1292–1298, 2004.

[57] S. P. Hong, M. J. Yang, H. Cho, I. Park, H. Bae, K. Choe, S. H. Suh, R. H. Adams, K. Alitalo, D. Lim, and G. Y. Koh, "Distinct fibroblast subsets regulate lacteal integrity through yap/taz-induced vegf-c in intestinal villi," *Nature Communications*, vol. 11, p. 4102, 2020.

[58] R. Wei, M. Lv, F. Li, T. Cheng, Z. Zhang, G. Jiang, Y. Zhou, R. Gao, X. Wei, J. Lou, X. Wu, D. Luo, X. Ma, J. Jiang, D. Ma, and L. Xi, "Human cafs promote lymphangiogenesis in ovarian cancer via the hh-vegf-c signaling axis," *Oncotarget*, vol. 8, no. 40, pp. 67 315–67 328, 2017.

[59] F. Ogata, K. Fujiu, S. Matsumoto, Y. Nakayama, M. Shibata, Y. Oike, I. Koshima, T. Watabe, R. Nagai, and I. Manabe, "Excess lymphangiogenesis cooperatively

induced by macrophages and cd4+ t cells drives the pathogenesis of lymphedema," *Journal of Investigative Dermatology*, vol. 136, no. 3, pp. 706–714, 2016.

[60] E. Gousopoulos, S. T. Proulx, S. B. Bachmann, L. C. Dieterich, J. Scholl, S. Karaman, R. Bianchi, and M. Detmar, "An important role of vegf-c in promoting lymphedema development," *Journal of Investigative Dermatology*, vol. 137, no. 9, pp. 1995–2004, 2017.

[61] Y.-s. Yoon, T. Murayama, E. Gravereaux, T. Tkebuchava, M. Silver, C. Curry, A. Wecker, R. Kirchmair, C. S. Hu, M. Kearney, A. Ashare, D. G. Jackson, H. Kubo, J. M. Isner, and D. W. Losordo, "Vegf-c gene therapy augments postnatal lymphangiogenesis and ameliorates secondary lymphedema," *The Journal of Clinical Investigation*, vol. 111, no. 5, pp. 717–725, Mar. 2003.

[62] D. Szöke, G. Kovács, É. Kemecsei, L. Bálint, K. Szoták-Ajtay, P. Aradi, A. Styevkóné Dinnyés, B. L. Mui, Y. K. Tam, T. D. Madden, K. Karikó, R. P. Kataru, M. J. Hope, D. Weissman, B. J. Mehrara, N. Pardi, and Z. Jakus, "Nucleoside-modified vegfc mrna induces organ-specific lymphatic growth and reverses experimental lymphedema," *Nature Communications*, vol. 12, p. 3460, 2021.

[63] M. T. Visuri, K. M. Honkonen, P. Hartiala, T. V. Tervala, P. J. Halonen, H. Junkkari, N. Knuutinen, S. Ylä-Herttuala, K. K. Alitalo, and A. M. Saarikko, "Vegf-c and vegf-c156s in the pro-lymphangiogenic growth factor therapy of lymphedema: A large animal study," *Angiogenesis*, vol. 18, pp. 313–326, 2015.

[64] M. Lähteenvuo, K. Honkonen, T. Tervala, T. Tammela, E. Suominen, J. Lähteenvuo, I. Kholová, K. Alitalo, S. Ylä-Herttuala, and A. Saaristo, "Growth factor therapy and autologous lymph node transfer in lymphedema," *Circulation*, vol. 123, no. 6, pp. 613–620, 2011.

[65] A. Szuba, M. Skobe, M. J. Karkkainen, W. S. Shin, D. P. Beynet, N. B. Rockson, N. Dakhil, S. Spilman, M. L. Goris, H. W. Strauss, T. Quertermous, K. Alitalo, and S. G. Rockson, "Therapeutic lymphangiogenesis with human recombinant vegf-c," *The FASEB Journal*, vol. 16, no. 14, pp. 1985–1987, 2002.

[66] R. P. Kataru, J. E. Baik, H. J. Park, C. L. Ly, J. Shin, N. Schwartz, T. T. Lu, S. Ortega, and B. J. Mehrara, "Lymphatic-specific intracellular modulation of receptor tyrosine kinase signaling improves lymphatic growth and function," *Science Signaling*, vol. 14, no. 695, eabc0836, 2021.

[67] J. Larouche, S. Sheoran, K. Maruyama, and M. M. Martino, "Immune regulation of skin wound healing: Mechanisms and novel therapeutic targets," *Advances in Wound Care*, vol. 7, no. 7, pp. 209–231, 2018.

[68] H. N. Wilkinson and M. J. Hardman, "Wound healing: Cellular mechanisms and pathological outcomes," *Open Biology*, vol. 10, no. 9, p. 200 223, 2020.

[69] J. C. Brazil, M. Quiros, A. Nusrat, and C. A. Parkos, "Innate immune cell–epithelial crosstalk during wound repair," *The Journal of Clinical Investigation*, vol. 129, no. 8, pp. 2983–2993, Aug. 2019.

[70] W. L. Havran and J. M. Jameson, "Epidermal t cells and wound healing," *Journal of Immunology*, vol. 184, pp. 5423–5428, 2010.

[71] J. Li, J. Tan, M. M. Martino, and K. O. Lui, "Regulatory t-cells: Potential regulator of tissue repair and regeneration," *Frontiers in Immunology*, vol. 9, p. 585, 2018.

[72] X. Wang, S. Balaji, E. H. Steen, H. Li, M. M. Rae, A. J. Blum, Q. Miao, M. J. Butte, P. L. Bollyky, and S. G. Keswani, "T lymphocytes attenuate dermal scarring by regulating inflammation, neovascularization, and extracellular matrix remodeling," *Advances in Wound Care*, vol. 8, pp. 527–537, 2019.

[73] A. Takeuchi and T. Saito, "Cd4 ctl, a cytotoxic subset of cd4+ t cells, their differentiation and function," *Frontiers in Immunology*, vol. 8, p. 194, 2017.

[74] U. Hofmann, N. Beyersdorf, J. Weirather, A. Podolskaya, J. Bauersachs, G. Ertl, T. Kerkau, and S. Frantz, "Activation of cd4¡sup¿+¡/sup¿ t lymphocytes improves wound healing and survival after experimental myocardial infarction in mice," *Circulation*, vol. 125, no. 13, pp. 1652–1663, 2012.

[75] T. Avraham, J. C. Zampell, A. Yan, S. Elhadad, E. S. Weitman, S. G. Rockson, J. Bromberg, and B. J. Mehrara, "Th2 differentiation is necessary for soft tissue fibrosis and lymphatic dysfunction resulting from lymphedema," *The FASEB Journal*, vol. 27, no. 3, pp. 1114–1126, 2013. eprint: https://faseb.onlinelibrary.wiley.com/doi/pdf/10.1096/fj.12-222695.

[76] G. D. García Nores, C. L. Ly, D. A. Cuzzone, R. P. Kataru, G. E. Hespe, J. S. Torrisi, J. J. Huang, J. C. Gardenier, I. L. Savetsky, M. D. Nitti, J. Z. Yu, S. Rehal, and B. J. Mehrara, "Cd4+ t cells are activated in regional lymph nodes and migrate to skin to initiate lymphedema," *Nature Communications*, vol. 9, no. 1970, 2018.

[77] J. C. Zampell, A. Yan, S. Elhadad, T. Avraham, E. Weitman, and B. J. Mehrara, "Cd4+ cells regulate fibrosis and lymphangiogenesis in response to lymphatic fluid stasis," *PLOS ONE*, vol. 7, no. 11, pp. 1–16, Nov. 2012.

[78] S. Ghanta, D. A. Cuzzone, J. S. Torrisi, N. J. Albano, W. J. Joseph, I. L. Savetsky, J. C. Gardenier, D. Chang, J. C. Zampell, and B. J. Mehrara, "Regulation of inflammation and fibrosis by macrophages in lymphedema," *American Journal*

of Physiology-Heart and Circulatory Physiology, vol. 308, no. 9, H1065–H1077, 2015, PMID: 25724493. eprint: https://doi.org/10.1152/ajpheart.00598.2014.

[79] E. Gousopoulos, S. T. Proulx, J. Scholl, M. Uecker, and M. Detmar, "Prominent lymphatic vessel hyperplasia with progressive dysfunction and distinct immune cell infiltration in lymphedema," *The American Journal of Pathology*, vol. 186, no. 8, pp. 2193–2203, 2016.

[80] Y. Yuan, V. Arcucci, S. M. Levy, and M. G. Achen, "Modulation of immunity by lymphatic dysfunction in lymphedema," *Frontiers in Immunology*, vol. 10, p. 76, 2019.

[81] E. Gousopoulos, S. T. Proulx, S. B. Bachmann, J. Scholl, D. Dionyssiou, E. Demiri, C. Halin, L. C. Dieterich, and M. Detmar, "Regulatory t cell transfer ameliorates lymphedema and promotes lymphatic vessel function," *JCI Insight*, vol. 1, no. 16, pp. 1–15, Oct. 2016.

[82] G. D. García Nores, C. L. Ly, I. L. Savetsky, R. P. Kataru, S. Ghanta, G. E. Hespe, S. G. Rockson, and B. J. Mehrara, "Regulatory t cells mediate local immunosuppression in lymphedema," *The Journal of investigative dermatology*, vol. 138, pp. 325–335, 2018.

[83] S. N. Thomas, J. M. Rutkowski, M. Pasquier, E. L. Kuan, K. Alitalo, G. J. Randolph, and M. A. Swartz, "Impaired humoral immunity and tolerance in k14-vegfr-3-ig mice that lack dermal lymphatic drainage," *The Journal of Immunology*, vol. 189, no. 5, pp. 2181–2190, 2012. eprint: https://www.jimmunol.org/content/189/5/2181.full.pdf.

[84] D. A. Cuzzone, E. S. Weitman, N. J. Albano, S. Ghanta, I. L. Savetsky, J. C. Gardenier, W. J. Joseph, J. S. Torrisi, J. F. Bromberg, W. L. Olszewski, S. G. Rockson, and B. J. Mehrara, "Il-6 regulates adipose deposition and homeostasis in lymphedema," *American journal of physiology. Heart and circulatory physiology*, vol. 306, H1426–H1434, 2014.

[85] G. Arango Duque and A. Descoteaux, "Macrophage cytokines: Involvement in immunity and infectious diseases," *Frontiers in Immunology*, vol. 5, p. 491, 2014.

[86] C. M. Scull, W. D. Hays, and T. H. Fischer, "Macrophage pro-inflammatory cytokine secretion is enhanced following interaction with autologous platelets," *Journal of Inflammation*, vol. 7, p. 53, 2010.

[87] J. L. Stow, P. Ching Low, C. Offenhäuser, and D. Sangermani, "Cytokine secretion in macrophages and other cells: Pathways and mediators," *Immunobiology*, vol. 214, no. 7, pp. 601–612, 2009.

[88] T. Junt, E. A. Moseman, M. Iannacone, S. Massberg, P. A. Lang, M. Boes, K. Fink, S. E. Henrickson, D. M. Shayakhmetov, N. C. Di Paolo, N. van Rooijen, T. R. Mempel, S. P. Whelan, and U. H. von Andrian, "Subcapsular sinus macrophages in lymph nodes clear lymph-borne viruses and present them to antiviral b cells," *Nature*, vol. 450, pp. 110–114, 2007.

[89] C. Shi and E. G. Pamer, "Monocyte recruitment during infection and inflammation," *Nature Reviews Immunology*, vol. 11, pp. 762–774, 2011.

[90] R. M. Kratofil, P. Kubes, and J. F. Deniset, "Monocyte conversion during inflammation and injury," *Arteriosclerosis, Thrombosis, and Vascular Biology*, vol. 37, no. 1, pp. 35–42, 2017.

[91] W. A. Muller, "New mechanisms and pathways for monocyte recruitment," *The Journal of experimental medicine*, vol. 194, F47–F51, 2001.

[92] C. Jakubzick, E. L. Gautier, S. L. Gibbings, D. K. Sojka, A. Schlitzer, T. E. Johnson, S. Ivanov, Q. Duan, S. Bala, T. Condon, N. van Rooijen, J. R. Grainger, Y. Belkaid, A. Ma'ayan, D. W. Riches, W. M. Yokoyama, F. Ginhoux, P. M. Henson, and G. J. Randolph, "Minimal differentiation of classical monocytes as they survey steady-state tissues and transport antigen to lymph nodes," *Immunity*, vol. 39, no. 3, pp. 599–610, 2013.

[93] S. R. Larson, S. M. Atif, S. L. Gibbings, S. M. Thomas, M. G. Prabagar, T. Danhorn, S. M. Leach, P. M. Henson, and C. V. Jakubzick, "Ly6c+ monocyte efferocytosis and cross-presentation of cell-associated antigens," *Cell Death & Differentiation*, vol. 23, pp. 997–1003, 2016.

[94] A. M. Platt, J. M. Rutkowski, C. Martel, E. L. Kuan, S. Ivanov, M. A. Swartz, and G. J. Randolph, "Normal dendritic cell mobilization to lymph nodes under conditions of severe lymphatic hypoplasia," *The Journal of Immunology*, vol. 190, no. 9, pp. 4608–4620, 2013. eprint: https://www.jimmunol.org/content/190/9/4608.full.pdf.

[95] M. Stephens and S. Liao, "Neutrophil–lymphatic interactions during acute and chronic disease," *Cell and Tissue Research*, vol. 371, pp. 599–606, 2018.

[96] H. Hampton and T. Chtanova, "The lymph node neutrophil," *Seminars in Immunology*, vol. 28, Mar. 2016.

[97] A. Bogoslowski, S. Wijeyesinghe, W.-Y. Lee, C.-S. Chen, S. Alanani, C. Jenne, D. A. Steeber, C. Scheiermann, E. C. Butcher, D. Masopust, and P. Kubes, "Neutrophils recirculate through lymph nodes to survey tissues for pathogens," *The Journal of Immunology*, vol. 204, no. 9, pp. 2552–2561, 2020.

[98] O. Kamenyeva, C. Boularan, J. Kabat, G. Y. C. Cheung, C. Cicala, A. J. Yeh, J. L. Chan, S. Periasamy, M. Otto, and J. H. Kehrl, "Neutrophil recruitment to lymph nodes limits local humoral response to staphylococcus aureus," *PLOS Pathogens*, vol. 11, no. 4, pp. 1–31, Apr. 2015.

[99] H. R. Hampton, J. Bailey, M. Tomura, R. Brink, and T. Chtanova, "Microbe-dependent lymphatic migration of neutrophils modulates lymphocyte proliferation in lymph nodes," *Nature Communications*, vol. 6, p. 7139, 2015.

[100] S. D. Castell, M. F. Harman, G. Morón, B. A. Maletto, and M. C. Pistoresi-Palencia, "Neutrophils which migrate to lymph nodes modulate cd4+ t cell response by a pd-l1 dependent mechanism," *Frontiers in Immunology*, vol. 10, p. 105, 2019.

[101] J. C. Gardenier, R. P. Kataru, G. E. Hespe, I. L. Savetsky, J. S. Torrisi, G. D. García Nores, D. K. Jowhar, M. D. Nitti, R. C. Schofield, D. C. Carlow, and B. J. Mehrara, "Topical tacrolimus for the treatment of secondary lymphedema," *Nature Communications*, vol. 8, no. 14345, 2017.

[102] N. Unno, M. Nishiyama, M. Suzuki, H. Tanaka, N. Yamamoto, D. Sagara, Y. Mano, and H. Konno, "A novel method of measuring human lymphatic pumping using indocyanine green fluorescence lymphography," *Journal of Vascular Surgery*, vol. 52, pp. 946–952, 2010.

[103] T. S. Nelson, Z. Nepiyushchikh, J. S. T. Hooks, M. S. Razavi, T. Lewis, C. C. Clement, M. Thoresen, M. T. Cribb, M. K. Ross, R. L. Gleason, L. Santambrogio, J. F. Peroni, and J. B. Dixon, "Lymphatic remodelling in response to lymphatic injury in the hind limbs of sheep," *Nature Biomedical Engineering*, vol. 4, pp. 649–661, 2020.

[104] M. Mihara, H. Hara, Y. Hayashi, M. Narushima, T. Yamamoto, T. Todokoro, T. Iida, N. Sawamoto, J. Araki, K. Kikuchi, N. Murai, T. Okitsu, I. Kisu, and I. Koshima, "Pathological steps of cancer-related lymphedema: Histological changes in the collecting lymphatic vessels after lymphadenectomy," *PLOS ONE*, vol. 7, no. 7, pp. 1–10, Jul. 2012.

[105] F. Ogata, K. Fujiu, I. Koshima, R. Nagai, and I. Manabe, "Phenotypic modulation of smooth muscle cells in lymphoedema," *British Journal of Dermatology*, vol. 172, no. 5, pp. 1286–1293, 2015.

[106] A. W. Caulk, Z. V. Nepiyushchikh, R. Shaw, J. B. Dixon, and R. L. Gleason, "Quantification of the passive and active biaxial mechanical behaviour and microstructural organization of rat thoracic ducts," *Journal of The Royal Society Interface*, vol. 12, no. 108, p. 20 150 280, 2015.

[107] A. W. Caulk, J. B. Dixon, and R. L. Gleason, "A lumped parameter model of mechanically mediated acute and long-term adaptations of contractility and geometry in lymphatics for characterization of lymphedema," *Biomechanics and Modeling in Mechanobiology*, vol. 15, pp. 1601–1618, 2016.

[108] M. S. Razavi, T. S. Nelson, Z. Nepiyushchikh, R. L. Gleason, and J. B. Dixon, "The relationship between lymphangion chain length and maximum pressure generation established through in vivo imaging and computational modeling," *American Journal of Physiology-Heart and Circulatory Physiology*, vol. 313, no. 6, H1249–H1260, 2017, PMID: 28778909.

[109] C. Contarino and E. F. Toro, "A one-dimensional mathematical model of collecting lymphatics coupled with an electro-fluid-mechanical contraction model and valve dynamics," *Biomechanics and Modeling in Mechanobiology*, vol. 17, pp. 1687–1714, 2018.

[110] M. J. Weiler, M. T. Cribb, Z. Nepiyushchikh, T. S. Nelson, and J. B. Dixon, "A novel mouse tail lymphedema model for observing lymphatic pump failure during lymphedema development," *Scientific Reports*, vol. 9, no. 10405, 2019.

[111] W. Tian, S. G. Rockson, X. Jiang, J. Kim, A. Begaye, E. M. Shuffle, A. B. Tu, M. Cribb, Z. Nepiyushchikh, A. H. Feroze, R. T. Zamanian, G. S. Dhillon, N. F. Voelkel, M. Peters-Golden, J. Kitajewski, J. B. Dixon, and M. R. Nicolls, "Leukotriene b4 antagonism ameliorates experimental lymphedema," *Science Translational Medicine*, vol. 9, no. 389, 2017.

[112] T. Tammela, A. Saaristo, T. Holopainen, J. Lyytikkä, A. Kotronen, M. Pitkonen, U. Abo-Ramadan, S. Ylä-Herttuala, T. V. Petrova, and K. Alitalo, "Therapeutic differentiation and maturation of lymphatic vessels after lymph node dissection and transplantation," *Nature Medicine*, vol. 13, pp. 1458–1466, 2007.

[113] H. Chen, S. Fre, V. I. Slepnev, M. R. Capua, K. Takei, M. H. Butler, P. P. Di Fiore, and P. De Camilli, "Epsin is an eh-domain-binding protein implicated in clathrin-mediated endocytosis," *Nature*, vol. 394, pp. 793–797, 1998.

[114] C. E. Oldham, R. P. Mohney, S. L. Miller, R. N. Hanes, and J. P. O'Bryan, "The ubiquitin-interacting motifs target the endocytic adaptor protein epsin for ubiquitination," *Current Biology*, vol. 12, no. 13, pp. 1112–1116, 2002.

[115] A. Sen, K. Madhivanan, D. Mukherjee, and R. C. Aguilar, "The epsin protein family: Coordinators of endocytosis and signaling," *BioMolecular Concepts*, vol. 3, no. 2, pp. 117–126, 2012.

[116] M. Kazazic, V. Bertelsen, K. W. Pedersen, T. T. Vuong, M. V. Grandal, M. S. Rødland, L. M. Traub, E. Stang, and I. H. Madshus, "Epsin 1 is involved in re-

cruitment of ubiquitinated egf receptors into clathrin-coated pits," *Traffic*, vol. 10, no. 2, pp. 235–245, 2009.

[117] S. Pasula, X. Cai, Y. Dong, M. Messa, J. McManus, B. Chang, X. Liu, H. Zhu, R. S. Mansat, S.-J. Yoon, S. Hahn, J. Keeling, D. Saunders, G. Ko, J. Knight, G. Newton, F. Luscinskas, X. Sun, R. Towner, F. Lupu, L. Xia, O. Cremona, P. D. Camilli, W. Min, and H. Chen, "Endothelial epsin deficiency decreases tumor growth by enhancing vegf signaling," *The Journal of Clinical Investigation*, vol. 122, no. 12, pp. 4424–4438, Dec. 2012.

[118] H. Wu, H. A. Rahman, Y. Dong, X. Liu, Y. Lee, A. Wen, K. H. To, L. Xiao, A. E. Birsner, L. Bazinet, S. Wong, K. Song, M. L. Brophy, M. R. Mahamud, B. Chang, X. Cai, S. Pasula, S. Kwak, W. Yang, J. Bischoff, J. Xu, D. R. Bielenberg, J. B. Dixon, R. J. D'Amato, R. S. Srinivasan, and H. Chen, "Epsin deficiency promotes lymphangiogenesis through regulation of vegfr3 degradation in diabetes," *The Journal of Clinical Investigation*, vol. 128, no. 9, pp. 4025–4043, Aug. 2018.

[119] J. A. Kornuta and J. Brandon Dixon, "Ex vivo lymphatic perfusion system for independently controlling pressure gradient and transmural pressure in isolated vessels," *Annals of Biomedical Engineering*, vol. 42, pp. 1691–1704, 2014.

[120] T. S. Nelson, R. E. Akin, M. J. Weiler, T. Kassis, J. A. Kornuta, and J. B. Dixon, "Minimally invasive method for determining the effective lymphatic pumping pressure in rats using near-infrared imaging," *American Journal of Physiology-Regulatory, Integrative and Comparative Physiology*, vol. 306, no. 5, R281–R290, 2014, PMID: 24430884.

[121] T. Lämmermann, P. V. Afonso, B. R. Angermann, J. M. Wang, W. Kastenmüller, C. A. Parent, and R. N. Germain, "Neutrophil swarms require ltb4 and integrins at sites of cell death in vivo," *Nature*, vol. 498, pp. 371–375, 2013.

[122] J. Lv, L. Zou, L. Zhao, W. Yang, Y. Xiong, B. Li, and R. He, "Leukotriene b4 leukotriene b4 receptor axis promotes oxazolone-induced contact dermatitis by directing skin homing of neutrophils and cd8+ t cells," *Immunology*, vol. 146, no. 1, pp. 50–58, 2015. eprint: https://onlinelibrary.wiley.com/doi/pdf/10.1111/imm.12478.

[123] X. Liu, S. Pasula, H. Song, K. L. Tessneer, Y. Dong, S. Hahn, T. Yago, M. L. Brophy, B. Chang, X. Cai, H. Wu, J. McManus, H. Ichise, C. Georgescu, J. D. Wren, C. Griffin, L. Xia, R. S. Srinivasan, and H. Chen, "Temporal and spatial regulation of epsin abundance and vegfr3 signaling are required for lymphatic valve formation and function," *Science Signaling*, vol. 7, no. 347, ra97–ra97, 2014.

[124] T. Saito, N. Unno, N. Yamamoto, K. Inuzuka, H. Tanaka, M. Sano, R. Sugisawa, K. Katahashi, and H. Konno, "Low lymphatic pumping pressure in the legs is as-

sociated with leg edema and lower quality of life in healthy volunteers," *Lymphatic Research and Biology*, vol. 13, no. 2, pp. 154–159, 2015, PMID: 26091410.

[125] V. Cintolesi, A. W. Stanton, S. K. Bains, E. Cousins, A. M. Peters, A. D. Purushotham, J. R. Levick, and P. S. Mortimer, "Constitutively enhanced lymphatic pumping in the upper limbs of women who later develop breast cancer-related lymphedema," *Lymphatic Research and Biology*, vol. 14, no. 2, pp. 50–61, 2016, PMID: 27309032.

[126] A. Hagura, J. Asai, K. Maruyama, H. Takenaka, S. Kinoshita, and N. Katoh, "The vegf-c/vegfr3 signaling pathway contributes to resolving chronic skin inflammation by activating lymphatic vessel function," *Journal of dermatological science*, vol. 73, pp. 135–141, 2014.

[127] J. W. Breslin, N. Gaudreault, K. D. Watson, R. Reynoso, S. Y. Yuan, and M. H. Wu, "Vascular endothelial growth factor-c stimulates the lymphatic pump by a vegf receptor-3-dependent mechanism," *American Journal of Physiology-Heart and Circulatory Physiology*, vol. 293, no. 1, H709–H718, 2007, PMID: 17400713.

[128] M. T. Cribb, L. F. Sestito, S. G. Rockson, M. R. Nicolls, S. N. Thomas, and J. B. Dixon, "The kinetics of lymphatic dysfunction and leukocyte expansion in the draining lymph node during ltb4 antagonism in a mouse model of lymphedema," *International Journal of Molecular Sciences*, vol. 22, no. 9, 2021.

[129] C. L. Ly, R. P. Kataru, and B. J. Mehrara, "Inflammatory manifestations of lymphedema," *International Journal of Molecular Sciences*, vol. 18, no. 1, 2017.

[130] R. Tabibiazar, L. Cheung, J. Han, J. Swanson, A. Beilhack, A. An, S. S. Dadras, N. Rockson, S. Joshi, R. Wagner, and S. G. Rockson, "Inflammatory manifestations of experimental lymphatic insufficiency," *PLOS Medicine*, vol. 3, no. 7, null, Jul. 2006.

[131] J. Armer and B. Stewart, "Post-breast cancer lymphedema: Incidence increases from 12 to 30 to 60 months," *Lymphology*, vol. 43, pp. 118–127, 2010.

[132] K. Nakamura, K. Radhakrishnan, Y. M. Wong, and S. G. Rockson, "Anti-inflammatory pharmacotherapy with ketoprofen ameliorates experimental lymphatic vascular insufficiency in mice," *PLOS ONE*, vol. 4, no. 12, pp. 1–7, Dec. 2009.

[133] T. Yokomizo, T. Izumi, and T. Shimizu, "Leukotriene b4: Metabolism and signal transduction," *Archives of Biochemistry and Biophysics*, vol. 385, no. 2, pp. 231–241, 2001.

[134] A. Schudel, L. F. Sestito, and S. N. Thomas, "S-nitrosated poly(propylene sulfide) nanoparticles for enhanced nitric oxide delivery to lymphatic tissues," *Journal*

of Biomedical Materials Research Part A, vol. 106, no. 6, pp. 1463–1475, 2018. eprint: https://onlinelibrary.wiley.com/doi/pdf/10.1002/jbm.a.36348.

[135] L. F. Sestito and S. N. Thomas, "Lymph-directed nitric oxide increases immune cell access to lymph-borne nanoscale solutes," *Biomaterials*, vol. 265, p. 120 411, 2021.

[136] S. T. Reddy, A. Rehor, H. G. Schmoekel, J. A. Hubbell, and M. A. Swartz, "In vivo targeting of dendritic cells in lymph nodes with poly(propylene sulfide) nanoparticles," *Journal of Controlled Release*, vol. 112, no. 1, pp. 26–34, 2006.

[137] S. N. Thomas, E. Vokali, A. W. Lund, J. A. Hubbell, and M. A. Swartz, "Targeting the tumor-draining lymph node with adjuvanted nanoparticles reshapes the anti-tumor immune response," *Biomaterials*, vol. 35, no. 2, pp. 814–824, 2014.

[138] A. Schudel, A. P. Chapman, M.-K. Yau, C. J. Higginson, D. M. Francis, M. P. Manspeaker, A. R. C. Avecilla, N. A. Rohner, M. Finn, and S. N. Thomas, "Programmable multistage drug delivery to lymph nodes," *Nature Nanotechnology*, vol. 15, pp. 491–499, 2020.

[139] K. Goodarzi, M. Goodarzi, A. M. Tager, A. D. Luster, and U. H. von Andrian, "Leukotriene b4 and blt1 control cytotoxic effector t cell recruitment to inflamed tissues," *Nature Immunology*, vol. 4, pp. 965–973, 2003.

[140] M. C. Hunter, A. Teijeira, and C. Halin, "T cell trafficking through lymphatic vessels," *Frontiers in Immunology*, vol. 7, p. 613, 2016.

[141] C.-Y. Yang, T. K. Vogt, S. Favre, L. Scarpellino, H.-Y. Huang, F. Tacchini-Cottier, and S. A. Luther, "Trapping of naive lymphocytes triggers rapid growth and remodeling of the fibroblast network in reactive murine lymph nodes," *Proceedings of the National Academy of Sciences*, vol. 111, no. 1, E109–E118, 2014. eprint: https://www.pnas.org/content/111/1/E109.full.pdf.

[142] K. W. Tan, K. P. Yeo, F. H. S. Wong, H. Y. Lim, K. L. Khoo, J.-P. Abastado, and V. Angeli, "Expansion of cortical and medullary sinuses restrains lymph node hypertrophy during prolonged inflammation," *The Journal of Immunology*, vol. 188, no. 8, pp. 4065–4080, 2012. eprint: https://www.jimmunol.org/content/188/8/4065.full.pdf.

[143] C. D. Buckley, F. Barone, S. Nayar, C. Bénézech, and J. Caamaño, "Stromal cells in chronic inflammation and tertiary lymphoid organ formation," *Annual Review of Immunology*, vol. 33, no. 1, pp. 715–745, 2015, PMID: 25861980.

[144] V. Angeli, F. Ginhoux, J. Llodrà, L. Quemeneur, P. S. Frenette, M. Skobe, R. Jessberger, M. Merad, and G. J. Randolph, "B cell-driven lymphangiogenesis in in-

flamed lymph nodes enhances dendritic cell mobilization," *Immunity*, vol. 24, no. 2, pp. 203–215, 2006.

[145] J. S. Torrisi, G. E. Hespe, D. A. Cuzzone, I. L. Savetsky, M. D. Nitti, J. C. Gardenier, G. D. García Nores, D. Jowhar, R. P. Kataru, and B. J. Mehrara, "Inhibition of inflammation and inos improves lymphatic function in obesity," *Scientific Reports*, vol. 6, no. 19817, 2016.

[146] S. Ivanov and G. J. Randolph, "Myeloid cells pave the way for lymphatic system development and maintenance," *Pflügers Archiv - European Journal of Physiology*, vol. 469, pp. 465–472, 2017.

[147] P. J. Muire, L. H. Mangum, and J. C. Wenke, "Time course of immune response and immunomodulation during normal and delayed healing of musculoskeletal wounds," *Frontiers in Immunology*, vol. 11, p. 1056, 2020.

[148] S. G. Rockson, W. Tian, X. Jiang, T. Kuznetsova, F. Haddad, J. Zampell, B. Mehrara, J. P. Sampson, L. Roche, J. Kim, and M. R. Nicolls, "Pilot studies demonstrate the potential benefits of antiinflammatory therapy in human lymphedema," *JCI Insight*, vol. 3, no. 20, Oct. 2018.

[149] N. Miyahara, H. Ohnishi, S. Miyahara, K. Takeda, S. Matsubara, H. Matsuda, M. Okamoto, J. E. Loader, A. Joetham, M. Tanimoto, A. Dakhama, and E. W. Gelfand, "Leukotriene b4 release from mast cells in ige-mediated airway hyperresponsiveness and inflammation," *American Journal of Respiratory Cell and Molecular Biology*, vol. 40, no. 6, pp. 672–682, 2009, PMID: 19029019.

[150] R. Sun, X. Ba, L. Cui, Y. Xue, and X. Zeng, "Leukotriene b4 regulates proliferation and differentiation of cultured rat myoblasts via the blt1 pathway," *Molecules and Cells*, vol. 27, pp. 403–408, 2009.

[151] X. Liu, T. Yang, L. Miao, Y.-A. Mei, and C. Hu, "Leukotriene b4 inhibits l-type calcium channels via p38 signaling pathway in vascular smooth muscle cells," *Cellular Physiology and Biochemistry*, vol. 37, pp. 1903–1913, 2015.

[152] M. G. Johnston, A. Kanalec, and J. L. Gordon, "Effects of arachidonic acid and its cyclo-oxygenase and lipoxygenase products on lymphatic vessel contracility in vitro," *Prostaglandins*, vol. 25, no. 1, pp. 85–98, 1983.

[153] M. K. Ferguson, H. K. Shahinian, and F. Michelassi, "Lymphatic smooth muscle responses to leukotrienes, histamine and platelet activating factor," *Journal of Surgical Research*, vol. 44, no. 2, pp. 172–177, 1988.

[154] J. Rutkowski, K. Boardman, and M. Swartz, "Characterization of lymphangiogenesis in a model of adult skin regeneration," *American journal of physiology. Heart and circulatory physiology*, vol. 291, H1402–10, Oct. 2006.